U.PORTO

FEUP **FACULDADE DE ENGENHARIA**
UNIVERSIDADE DO PORTO

Thesis for the Degree of Doctor of Philosophy

DEVELOPMENT OF A COHESIVE ZONE MODEL FOR ADHESIVE JOINTS THAT INCLUDES HUMIDITY AND FATIGUE DEGRADATION

Submitted by

Marcelo Bruno Serrão Fontes Parente da Costa

Supervised by

Lucas Filipe Martins da Silva

Co-Supervised by

Raul Duarte Salgueiral Gomes Campilho

October 2017

Abstract

Adhesive joints in critical structures of industries such as aeronautical and automotive are exposed to environmental degradation agents such as humidity, which should be carefully considered as they will reduce the mechanical properties of said joints in the long term. Furthermore, cyclic loadings will also degrade the joint, so the combined effect of moisture degradation and fatigue on adhesive bonds should be understood.

To that effect, this work combines extensive experimental testing under various moisture degradation levels to determine the influence of humidity in the properties of adhesive joints under mode I. Firstly, specimens with reduced dimensions are proposed and validated which allow for faster saturation times, the possibility of being tested in an in-house environmental chamber and also increased speed in the manufacture process of all needed specimens: bulk tensile and double cantilever beam. Fick's law is determined for each studied adhesive, followed by immersion of the developed specimens in containers with distilled water. The specimens are then removed from the container at different time steps, which translates to different levels of average moisture content in the joint, and tested in both static and cyclic conditions. This allows for the relevant properties to be determined as a function of moisture content. Relationships are then determined for the evolution of each property as a function of moisture, so that the value of the property for any moisture concentration may be estimated. Finally, a finite element is created which encompasses all the previously determined relationships, allowing for an otherwise unaged adhesive joint to be simulated under both moisture and fatigue conditions. The element was studied for various types of conditions against experimental data and was found to accurately model stages of moisture degradation under static and fatigue conditions, thus has proved itself as a robust tool for modelling ageing in adhesive joints under mode I.

Resumo

Aplicações de juntas adesivas em estruturas críticas de indústrias tais como a aeronáutica e automóvel estão expostas a fatores de degradação ambiental como a humidade, que deverão ser cuidadosamente considerados pois irão afetar as propriedades mecânicas das juntas a longo termo. Além disso, solicitações cíclicas também irão degradar a junta, e como tal o efeito combinado da degradação por humidade e fadiga em juntas adesivas deve ser compreendido.

Para esse efeito, este trabalho combina uma forte componente de testes experimentais para vários níveis de degradação por humidade para determinar a influência desta nas propriedades da junta adesiva solicitada em modo I. Em primeiro lugar, provetes de dimensões reduzidas são propostos e validados que permitem atingir a saturação por humidade do adesivo mais rapidamente, podem ser testados numa estufa existente no laboratório local, e permitem acelerar o processo de fabrico de todos os provetes necessários: maciços de tração e também do tipo *double cantilever beam*. A lei de Fick é determinada para cada adesivo estudado, seguindo-se a imersão dos provetes em recipientes com água destilada. Os provetes são depois removidos do recipiente em instantes de tempo distintos e testados, o que se traduz em diferentes níveis do conteúdo médio de humidade na junta, e testados em condições estáticas e cíclicas. Isto permite que as propriedades relevantes sejam determinadas em função da quantidade de humidade. São depois encontradas relações para a evolução de cada propriedade em função da quantidade de humidade na junta, tal que o valor de cada propriedade para qualquer nível de concentração de humidade possa ser estimado. Finalmente, é criado um elemento finito que inclui todas as relações préviamente determinadas, permitindo que uma junta não degradada seja simulada em condições de humidade e fadiga. O elemento foi estudado para vários tipos de condições e comparado com dados experimentais, tendo modelado com sucesso os estágios de degradação por humidade em condições estáticas e cíclicas, sendo assim uma ferramenta robusta para modelar a degradação de juntas adesivas em modo I.

Acknowledgments

I would like to thank, from a professional point of view:

- My supervisor Professor Lucas Filipe Martins da Silva, without whom this thesis would not be possible, for his expertise, guidance, always being available to solve any problem necessary and for all the opportunities made available;

- My co-supervisor Prof. Raul Duarte Salgueiral Gomes Campilho, for his help through the thesis and in solving all numerical simulation doubts;

- The adhesives group AdFEUP, a team where every member works together towards a goal, making it much easier and faster to overcome any difficulties, and where valuable discussions took place that allowed for various improvements to this work;

- Everyone from INEGI Floor 6, formerly IdMEC Floor 7, whom, although not affiliated with adhesion research, provided valuable insight and companionship throughout all these years.

From a personal point of view:

- My parents, which made it possible for this step to be reached through all their sacrifices and patience;

- My friends, which hovered between being supportive and making fun of me for studying glues, have provided support and distractions when needed;

- My girlfriend, Carla, for all her patience and support. I love you.

Contents

List of publications

Papers

1. **Costa, M**, Viana, G, da Silva, LFM, Campilho, RDSG, "Environmental effect on the fatigue degradation of adhesive joints: a review" *The Journal of Adhesion* 93 (2017): 127-146

2. **Costa, M**, Viana, G, Canto, C, da Silva, LFM, Banea, MD, Chaves, F, Campilho, RDSG, Fernandes, AA, "Effect of the size reduction on the bulk tensile and double cantilever beam specimens used in cohesive zone models" *Proceedings of the Institution of Mechanical Engineers, Part L: Journal of Materials: Design and Applications* 230 (2016): 968-982

3. **Costa, M**, Viana, G, da Silva, LFM, Campilho, RDSG, "Effect of humidity on the mechanical properties of adhesively bonded aluminium joints" *Proceedings of the Institution of Mechanical Engineers, Part L: Journal of Materials: Design and Applications* (2016): 1464420716645263

4. **Costa, M**, Viana, G, da Silva, LFM, Campilho, RDSG, "Effect of humidity on the fatigue behaviour of adhesively bonded aluminium joints" *Latin American Journal of Solids and Structures* 14 (2017): 174-187

5. **Costa, M**, Viana, G, Créac'hcadec, R, da Silva, LFM, Campilho, RDSG, "A cohesive zone element for mode I modelling of adhesives degraded by humidity and fatigue" *International Journal of Fatigue* (2017) - Submitted

6. **Costa, M**, Carbas, R, Marques, E, Viana, G, da Silva, LFM, "An apparatus for mixed-mode fracture characterization of adhesive joints" *Theoretical and Applied Fracture Mechanics* (2017):

7. **Costa, M**, Carbas, R, Benedita, M, Marques, E, Viana, G, da Silva, LFM, Yokoi, E, Nakada, S, Furusawa, T, "Static assessment of the mixed-mode behaviour of three epoxy adhesives" *Engineering Fracture Mechanics* (2017):

8. Viana, G, **Costa, M**, Banea, MD, Da Silva, LFM, "Behaviour of environmentally degraded epoxy adhesives as a function of temperature" *The Journal of Adhesion* 93 (2017): 95-112

9. Viana, G, **Costa, M**, Banea, MD, da Silva, LFM, "A review on the temperature and moisture degradation of adhesive joints" *Proceedings of the Institution of Mechanical Engineers, Part L: Journal of Materials: Design and Applications* 231 (2017): 488-501

10. Viana, G, **Costa, M**, Banea, MD, da Silva, LFM, "Water diffusion in double cantilever beam adhesive joints" *Latin American Journal of Solids and Structures* 14 (2017): 188-201

11. Viana, G, **Costa, M**, Banea, MD, da Silva, LFM, "Moisture and temperature degradation of double cantilever beam adhesive joints" *Journal of Adhesion Science and Technology* 31 (2017): 1824-1838

12. Viana, G, **Costa, M**, Banea, MD, da Silva, LFM, "Cohesive Properties of Environmentally Degraded Epoxy Adhesives" *U. Porto Journal of Engineering* 3 (2017)tania: 49-56

13. Fernandes, P, Viana, G, Carbas, RJC, **Costa, M**, da Silva, LFM, Banea, MD, "The influence of water on the fracture envelope of an adhesive joint" *Theoretical and Applied Fracture Mechanics* 89 (2017): 1-15

14. de Sousa, CCRG, Campilho, RDSG, Marques, EAS, **Costa, M**, da Silva, LFM, "Overview of different strength prediction techniques for single-lap bonded joints" *Proceedings of the Institution of Mechanical Engineers, Part L: Journal of Materials: Design and Applications* 231 (2017): 210-223

15. Rodrigues, T, Chaves, F, da Silva, LFM, **Costa, M**, Barbosa, AQ, "Determination of the fracture envelope of an adhesive joint as a function moisture" *Materialwissenschaft und Werkstofftechnik* (2017) - Accepted for publication

16. Avendaño, R, Carbas, RJC, Chaves, FJP, **Costa, M**, da Silva, LFM, Fernandes, AA, "Impact loading of single lap joints of dissimilar lightweight adherends bonded with a crash-resistant epoxy adhesive" *Journal of Engineering Materials and Technology* 138 (2016): 041019

Book chapters

1. da Silva, LFM, **Costa, M**, Viana, G, Campilho, RDSG, "Analytical Modelling for the Single-Lap Joint" *Strength Prediction of Adhesively-Bonded Joints* (2017). ISBN: 9781498722469

2. Campilho, RDSG, **Costa, M**, Viana, G, da Silva, LFM, "Parameter Identification in Cohesive Zone Modelling" *Strength Prediction of Adhesively-Bonded Joints* (2017). ISBN: 9781498722469

3. **Costa, M**, Carbas, R, Marques, E, Viana, G, da Silva, LFM, "Adhesion bonding techniques" *Advances in manufacturing and processing of materials and structures* (2018). ISBN: 9781138035959

Chapter 1

Introduction

1.1 Background and motivation

Adhesives have been used as joining materials throughout history, but only recently has serious interest in this type of joining technique started to emerge as a true and valid replacement to conventional joining techniques such as bolting, riveting and welding. Coupling the attractive strength to weight ratio, reduction in weight, cost and emissions of adhesive joints with additional weight reduction techniques such as using lightweight materials for structural applications (i.e. aluminium and composite) is naturally of interest to various industries such as the automotive, aeronautical and railway. Because such distinct industries use adhesives, the requirements they must withstand vary, but one key consideration is the effect that environmental agents (such as moisture, temperature, radiation and gases) have on the properties of adhesives. Cars, planes and trains are examples of structures which go through varying temperatures and moisture during their use (as they move between cities and countries) and, as such, their bonds must withstand such functional requirements.

Environmental degradation of adhesive joints is therefore an important topic, and interest in this research field led to a scholarship for two students (financed by the Portuguese Science Foundation (FCT), grant number EXCL/EMS-PRO/0084/2012, in partnership with ALSTOM and Sika) to delve into the topic: one which focuses on the combined degradation of humidity and temperature, and other where the focus is on the combination of humidity and fatigue, both with the final objective of developing a finite element capable of simulating such degrading characteristics. This thesis targets the latter, which, although studying a unique combination of factors, shares some work with the thesis on humidity and temperature, which will be pointed out when appropriate through the text of this thesis.

Some of the project requirements are:

- Use of aluminium specimens (requested by ALSTOM), of an alloy similar to those used in the railway industry, and thus 6082-T6 was chosen together with the partner;

- Study of one Sika adhesive (requested by Sika), and because of this SikaPower 4720 was selected for this study together with Sika.

Based on these requirements, the material of the adherends is then defined, as is one of the adhesives to study. Another adhesive was selected, Nagase XNR 6852-1, due to the fact that the group has an ongoing relationship with Nagase Chemtex to study some of their adhesives, and also based on the fact that Nagase's XNR 6852-1 behaviour is expected to be very different from SikaPower 4720, which due to the scope of this thesis (study as much distinct situations as possible), is an important factor.

1.2   Objectives and methodology

The objectives and methodology of this thesis may be summarised as follows:

- Selection of two distinct adhesives that allow for dissimilar behaviour and more generalised degradation formulas to be determined;

- Determination of the moisture uptake characteristics of each adhesive by defining Fick's law;

- Optimisation of specimens such that moisture saturation may be reached faster than with conventional specimens;

- Determination of the evolution of all properties needed to calculate the mode I cohesive zone model as a function of moisture;

- Determination of mode I fatigue crack propagation curves for both adhesives as a function of moisture;

- Finding formulas that include all static and fatigue phenomena such that the element may degrade the numerical properties accordingly;

- Create a working finite element code that is capable of modelling degradation by moisture and fatigue under mode I.

Figure 1.1 represents the work flow of the thesis and how the experimental and numerical sections intertwine to reach the final goal.
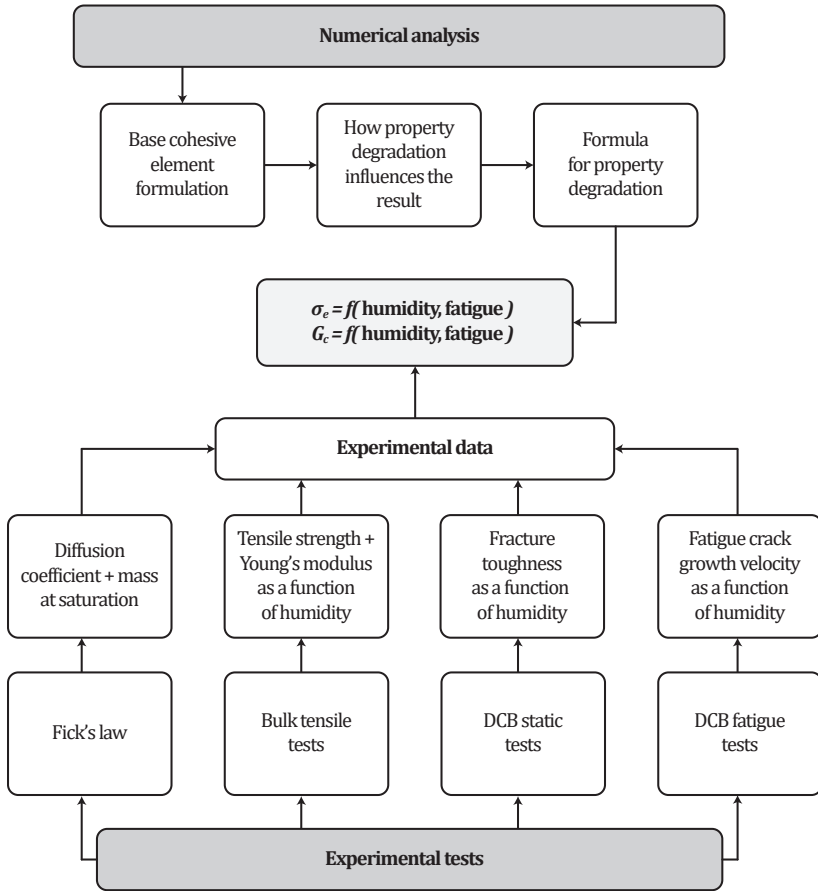
Figure 1.1: Thesis workflow.

1.3 Thesis outline

This thesis is structured in the following way:

- Introductory chapter where the motivation and research methodology to fulfil the set objectives is laid out;

- Summary of the appended papers where the main objectives and conclusions of each consecutive work is explained;

- Concluding remarks are then made and future work is suggested as possible improvements for the presented work.

Chapter 2

Summary of appended papers

The purpose of each appended paper, main results and some considerations are explained in this section.

2.1 Paper A

Because this work focuses on developing a numerical methodology to model adhesive joints subjected to environmental degradation and fatigue, the first step is understanding the current knowledge related to the topic. Because of this, **Paper A** is a literature review on the consequences of environmental degradation on the fatigue response of adhesive joints. Key details drawn from this paper include:

- Surface preparation is very important when dealing with fatigue in adhesive joints, and is of added importance if the joints are degraded by the environment. Phosphoric acid anodizing (PAA) is shown to be the most effective surface treatment for aluminium bonding;

- It was shown that, although moisture and temperature decrease the joint strength, temperature has a higher toll on the strength of adhesive joints than moisture;

- Hygrothermal ageing generally results in a decrease in the threshold fracture toughness (effectively meaning that the fatigue crack will start propagating sooner in wet conditions), and that the slope of the crack growth curve (the velocity of crack propagation) tends to be maintained or decreases with moisture.

This feedback is important because it acts as a starting point on what to expect from the experimental results and also in defining testing characteristics such as surface preparation. The variability of effects present in the literature is also important to understand as different adhesive formulations tested in this thesis may exhibit different behaviour, which may occur due to the different characteristics of both tested adhesives.

2.2 Paper B

When dealing with moisture degradation, the ingress of water into the joint must be studied, which means that the time until saturation is directly related to the slowest direction in which water travels inside the adhesive. Double cantilever beams (DCB), defined by standard ASTM D3433 and shown in Figure 2.1, will only have a small fraction of the adhesive exposed (the thickness), thus water ingress will take much longer than if all adhesive faces were exposed, and in such case the critical direction is the width.
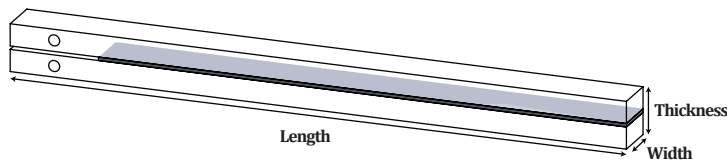
Figure 2.1: Double cantilever beams defined by standard ASTM D3433.

It is thus necessary to reduce the dimension of the necessary specimens so that manageable times to accomplish saturation inside the thesis time frame are possible. The objectives of **Paper B** include:

- Reduction of the DCB specimen dimensions so that saturation of bonded joints may occur in a timely fashion;

- Reduction of the DCB specimen dimensions so that the bonded joints may be tested inside the environmental chamber available in our laboratory;

- Reduction of the bulk specimen dimensions so that manufacture of all specimens for all testing conditions (various stages of humidity and various test temperatures) occurs faster.

It should be noted that some of the objectives are related to temperature, which is not studied in this thesis, but is studied in the other thesis associated with this research project, and thus requirements for both separated works were considered when developing the reduced specimens.

2.3 Paper C

Paper C focuses on investigating the mechanical properties of the studied adhesives as a function of moisture content, specifically the properties required for the modelling of the cohesive zone model: Young's modulus, tensile strength and fracture toughness.

Furthermore, relationships for determining the value of each degraded property as a function of moisture content were determined. Each bulk property may be estimated using the relationship shown in the manuscript, while the relationship for determining the fracture toughness was not included due to its complexity, but is presented here:

$$G_{Ic}(x) = C_1 x^5 + C_2 x^4 + C_3 x^3 + C_4 x^2 + C_5 x^1 + G_0$$

$$C_1 = G_0 D E_0 + G_0 D m_\infty \exp(G_0) + G_0 D \sigma_0^2$$

$$C_2 = \frac{G_0}{G_0 \sigma_0 - G_0 \sigma_0^2 - E_0 m_\infty^2 \exp(G_0)}$$

$$C_3 = \frac{G_0 \exp(G_0) + m_\infty G_0^2}{E_0^2}$$

$$C_4 = \frac{G_0 \sigma_0}{G_0 \sigma_0 - G_0 E_0 - m_\infty^3 - G_0^3 m_\infty^2}$$

$$C_5 = \frac{G_0 + m_\infty + G_0^5}{G_0 E_0 - G_0}$$

$$(2.1)$$

where G_0, E_0 and σ_0 are the fracture toughness, Young's modulus and tensile strength without ageing, respectively. These relationships are the basis behind the degradation routines incorporated into the cohesive zone element code, and allow the element to estimate the value for any degraded property necessary to build the CZM traction-separation law. It should be noted that the chosen process of testing various intermediate moisture steps was selected due to the fact that various real world applications in structures mentioned before, such as cars, planes and trains, are subjected to temporary variations in temperature and humidity. That is, when a plane travels from one hot and dry location to a cold and humid one, it is not at the new location for several years, and as such will only suffer partial joint degradation, such that moisture will only ingress slightly into the joint, producing a certain average moisture percentage that is more concentrated at the edges. Because of this phenomena, the same procedure was selected for the experimental process, which leads to results more related to real world applications. In any case, total saturation is also studied, so the result of the selected methodology is the best of both worlds: we test the worst case scenario (full saturation), but also various intermediate steps, which are the ones that real world joints experience.

2.4 Paper D

Following the determination of how humidity influences the mechanical properties, the influence of moisture on the fatigue behaviour is needed, which is the purpose of **Paper D**. In this paper, the fatigue

crack growth curves are determined as a function of relative humidity, and the Paris Law constants for the linear crack propagation zone are determined as a function of moisture content.

Furthermore, following the methodology set in **Paper C** of defining relationships that allow the degraded property values to be estimated, the Paris Law constants can be deduced using a proposed equation.

2.5 Paper E

Paper E concludes all preceding work by including all the determined relationships in a custom cohesive zone based finite element coded in FORTRAN for use in ABAQUS. The proposed finite element includes several important features:

- Humidity degradation of the adhesive may be modelled for any geometry;

- Fatigue degradation of the adhesive may be modelled for any geometry;

- Various types of traction-separation laws are included;

- A MATLAB interface was developed to facilitate the creation of the geometry, mesh, boundary conditions, files for running the simulation, files for extracting relevant simulation results and presenting them to the user.

Chapter 3

Conclusions and future work

The aim of this thesis was to improve the current knowledge and simulation possibilities of adhesive joints used in real work structures subjected to environmental degradation and fatigue.

To accomplish that goal, extensive experimental testing was performed to determine the influence of moisture degradation on various static properties, necessary to build the traction-separation law that dictates the physical meaning of the simulated adhesive joint: the Young's modulus, tensile strength and fracture toughness were determined for various stages of moisture content, from the dry to a fully saturated stage. Furthermore, fatigue testing was performed and the fatigue crack growth curves of each adhesive for each stage of moisture degradation were determined. Finally, a custom finite element based on the cohesive zone model approach was created which incorporated the experimental testing results and allows for the modelling of adhesive joints degraded by moisture in both static and fatigue conditions, and expands on those advantages by also incorporating various traction-separation relationships and a user-friendly interface to make it easier for the end user to perform said numerical simulations using the coded element.

With this, the objective of the thesis is accomplished, and a robust tool is created that allows for an engineer to model several characteristics of joints used in real world structures.

3.1 Future work

The presented work may be improved upon by studying additional topics, such as:

- All presented work focuses on mode I loads which, although being critical, do not fully represent how most real joints behave. Therefore the work that has been accomplished for mode I should also be performed for mode II, using appropriate specimens and experimental setups, such that mode II shear and fracture properties as a function of humidity are found for static and fatigue conditions;

- The finite element formulation only encompasses the finite element code for mode I modelling, so even if the degradation relationships for mode II are not incorporated, the base static code for mode II simulation should be added. In reality, the triangular traction-separation law has already been modified to incorporate both mode I and mode II considerations, although that is not present in the published paper as it was only built to test the single lap joint geometry and was not fully validated;

- Mixed-mode contributions may also be incorporated after mode I and mode II being implemented, which will widen the applicability of this element to virtually any possible situation;

- Studying more adhesives would probably lead to refinements in the degradation formulas and improve the methodology for use in a wider array of situations;

- Real joints should also be studied to validate the methodology and apply it to real word scenarios;

- Although a parallel thesis also studies temperature, the resulting finite element is different from the current one, thus it would be interesting to merge all code inside a single finite element, which could model temperate + humidity + fatigue.

Appendices

Paper A

Taylor & Francis
Taylor & Francis Group

Environmental effect on the fatigue degradation of adhesive joints: A review

M. Costa[a], G. Viana[a], L. F. M. da Silva [b], and R. D. S. G. Campilho[c]

[a]INEGI, Rua Dr. Roberto Frias 400, Porto, Portugal; [b]Departamento de Engenharia Mecânica, Faculdade de Engenharia da Universidade do Porto (FEUP), Rua Dr. Roberto Frias, Porto, Portugal; [c]Departamento de Engenharia Mecânica, Instituto Superior de Engenharia do Porto (ISEP), Instituto Politécnico do Porto, Rua Dr. António Bernardino de Almeida 431, Porto, Portugal

ABSTRACT

Environmental factors, such as temperature and moisture, are known to have a degrading effect on the mechanical properties and performance of adhesive joints, which may be perceived as a non-problem because various works have shown that the static response of an adhesive is normally unaffected by slight moisture and temperature variations that occur in real-world applications. While this may be true, performance under purely static conditions is rarely found in commercial uses and most adhesive joints are subjected to cyclic loadings throughout their life. Interestingly, not much work has been done on the effects of the environment on cyclically loaded adhesive joints, but the consensus is that the fatigue response is much more affected by environmental changes than the static response, which is arguably the most important analysis. The general trend is that hygrothermal ageing decreases the number of cycles the joint can withstand and also decreases the threshold fracture toughness value, which translates to cracks initiating sooner, but exceptions to these behaviours also exist.

1. Introduction

Adhesive joints are increasingly being used for commercial applications thanks to their optimal mechanical performance and better understanding of the mechanics of failure. Several industries are interested in the advantages of adhesives, such as the automotive manufacturers [1], where adhesion technology is increasingly used both in the assembly of supplementary elements (windows, windscreens, rubber joints, and inside cladding) and in structural applications. The aeronautical industry [2] is also interested in the structural and sealing scope of adhesives, and has remained so for some time as they are the pioneers in the study and application of adhesive bonds, resulting in aircrafts with levels of structural efficiency and durability that could not have been accomplished using conventional riveted structures. Aerospace [3] concerns

for adhesives are divided in two parts as follows: launch constrains where the bonds must withstand both static and dynamic loads of high intensities over a short period of time, and space environment requirements that subject the adhesive to thermo-mechanical solicitations over a long period, where, for example, temperatures ranging from −200°C to +200°C, depending on sun exposure, may be experienced for telecom satellites. The marine industry's [4] most evident requirement is resistance to moisture and temperature, with ASTM D1183 [5] defining a test cycle for exterior marine exposure that encompasses temperature fluctuations from −57°C to 71°C and relative humidity (RH) levels from <10% to 100% as well as full immersion in artificial sea water, complementing fatigue requirements of 10^7 cycles for the approval of marine adhesives, as defined in ASTM D3166 [6]. Special situations also exist, for example, the case of an adhesive used to bond a data recorder to live sea lions in order to study their behaviour, where resistance to scratching, hitting rocks, constant immersion in water, and strong sun radiation were successfully solved through a modified epoxy adhesive [4]. Adhesives for civil construction [7] do not have such extreme requirements, but must nonetheless provide high strength (60–70 MPa) and good adhesion on dry and wet concrete, while maintaining performance at different temperatures and weather conditions. Another area interested in the performance of adhesive joints subjected to environment is the railway industry [8], where various types of adhesives can be used for different parts of a train's body structure. Bonding heat-insulating materials to the roof sheets is one of the needs, where outside temperatures can range from −30°C to 80°C, which are mostly transferred to the adhesive due to the roof material being an aluminium alloy. One thing that is evident in all these industries are the vast temperature and moisture conditions adhesives need to withstand, all while being subjected to both static and fatigue solicitations, which can reach the frequency value of 8,000 Hz [3]. Therefore, it seems necessary to understand the effect that environmental conditions have on the fatigue response of adhesive joints. To achieve this, this paper is divided into the following sections: a review of key factors relevant to adhesive joints and fatigue (such as surface treatments to improve the bond's interface strength and diffusion tests to characterize moisture), followed by a review on the effects of environmental factors on S–N curves, and ending with the effects of temperature and moisture on the fatigue crack growth behaviour (Paris Law) of adhesive joints.

2. Adhesive Joints and Fatigue

One of the main advantages of adhesives is their weight-reduction capabilities, which is then combined with other weight-reduction techniques such as bonding aluminium or composite materials to achieve optimal results. Bonding aluminium sheets is a technique used in various industries, with

the pioneers being the aircraft manufacturers, which have been studying adhesive bonds since the 1940s [2]. The early aircraft structures used phenolic adhesives over chromic-acid-anodized surfaces, which were studied extensively by de Bruyne [9] and Schliekelmann [10] and were proven safe. Unfortunately, during the late 1960s and early 1970s, when materials and processes were changed to simplify manufacturing, whole fleets of aircrafts saw their bonded structures debond with disastrous consequences. Upon investigation, it was found that the chromic acid anodization was not an appropriate surface preparation for the newly used cured epoxy adhesives; however, with an anodized surface the problem would be solved. This goes to show that not only must the adhesive be correctly selected, but the surface preparation as well.

2.1 *Surface Treatments*

A multitude of surface treatments exist, ranging from simple abrasion of the adherend to complicated chemical procedures applied to improve adhesion. The first developed test procedure to determine properly prepared bonded surfaces was the simple wedge-crack test, defined in ASTM D3762 [11], developed by Bethune at Boeing. The test equipment consists of a simple wedge, which is inserted into the middle of a pre-cracked joint, and the measures of the crack length evolution are performed throughout time. By plotting the crack length versus time plots for different surface treatments and environments, one can detect the best surface preparation procedures, which are the ones that provide a smaller crack length variation over time. In 1984, Kinloch showed [12] that the optimal surface preparation procedure for an epoxy adhesive bonded to an aluminium alloy submerged in water at 60°C was phosphoric acid anodizing (PAA), maintaining a crack length of 11 mm over time. The crack length for chromic acid anodizing (CAA) stabilized at 18 mm, and chromic acid etching (CAE) presented a final crack length of 22 mm. Further studies have shown that PAA is the optimal surface preparation procedure for aluminium-bonded joints, a trend even more evident in fatigue results. In 2000 [13], Briskham and Smith analysed different surface treatments for distinct temperature and moisture conditions in both static and fatigue set-ups. For the initial conditions under static conditions, they showed that the surface treatment had little effect on the lap shear strength, with PAA presenting a strength of 25 MPa versus the simple abrading and degrease that resulted in a strength of 21 MPa. This small difference grew when the specimens were exposed to 100% RH at 42°–48°C, and even more when they were immersed in 55°C water for 1,500 hr. Notably, PAA exhibited a slight reduction in strength under these conditions, while an amino silane treatment actually saw an increase in strength after the immersion. The fatigue results have far more drastic and

important repercussions. The joints were submerged in water at 55°C and tested under a stress cycle of 0.15–1.2 MPa at 2 Hz, resulting in a resistance of less than 100 hr for the simple abrading and degrease procedure, while the PAA-treated joint lasted almost 1,100 hr, an increase of roughly 11 times in resistance. Lefebvre [14] reached similar conclusions in 2002, where five different surface treatments were studied (base acid treatment, P2 etch, PAA, sulphuric acid anodization, and sol–gel reaction), and again PAA proved the best by a fair margin. The second-best treatment was the P2 etch, which presented a number of cycles until failure of less than 10^2 cycles, while for the same stress amplitude the PAA-treated joints exhibited 10^5 cycles. More recently, a study [15] of purely mechanical surface treatments analysed the changes in fatigue resistance due to surface preparation, in terms of total number of cycles, further confirming that the adherend surface needs to be carefully prepared prior to bonding. Another measure of surface treatment usefulness in fatigue set-up, besides cycles to failure, is the threshold strain-energy release rate (G_{th}), which is used in fatigue tests where the crack velocity is measured using the Paris Law. G_{th} measures an energy value at which the crack starts to propagate, so it would be of interest to study the effect that applying a surface treatment would have on the G_{th}. Some authors have done so, such as Fernando et al. [16] who studied the effect of CAE, PAA, and PAA with a primer (PAAP) on the fatigue performance of adhesively bonded aluminium-alloy joints, and found that CAE presented the worst results, while PAA and PAAP joints exhibited much improved and identical performance. Kinloch et al. [17] studied the same surface treatments and compared them with the basic grit blasting followed by degreasing (GBD), and also with grit blasting followed by degrease and followed by silane primer (GBS) [18]. The conclusions were similar for PAA and PAAP but different for CAE, as they found that CAE exhibited the same resistance as PAA, while Fernando et al. [16] concluded that CAE was inferior to PAA. Nonetheless, PAA continues to prove itself the optimal surface treatment, with Hadavina et al. [19] confirming the same trend as shown in [17], and Abel et al. [20] also found that applying a surface treatment leads to better performance when compared with the basic GBD. Figure 1 provides a comparison between the most relevant results of these papers, exhibiting the adequateness of PAA and also the importance of carefully preparing the surface to create lasting bonds. It should be noted that the different papers referenced in Fig. 1 have different joints and conditions, and therefore should not be compared between each other; the comparison should only be made for the results of each reference, which show the evolution in resistance for the conditions of each paper.
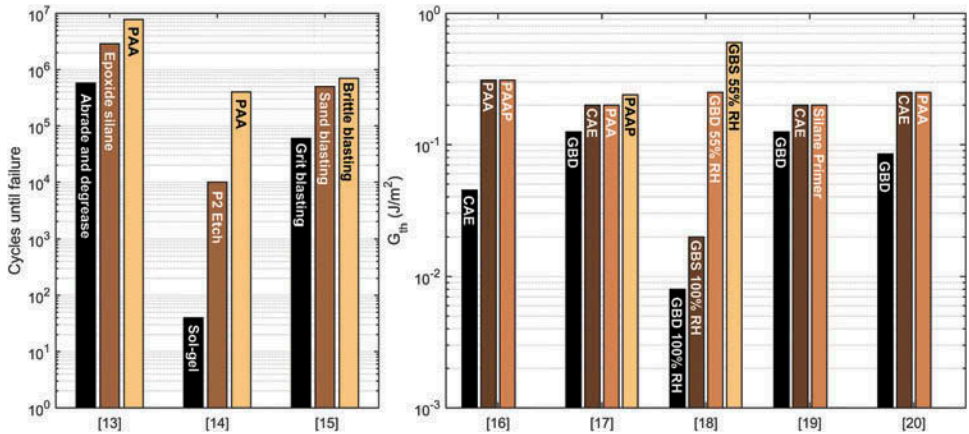
Figure 1. Effect of different surface treatments on the fatigue behaviour of aluminium-bonded joints: influence on the number of cycles until failure (left), and in the threshold fracture toughness (right). [13–20].

2.2 Environment

"Environment" is a broad term that encompasses various effects such as temperature, moisture, pressure, radiation, air quality, etc. [21]. Although most variables should impact the behaviour of an adhesive joint, this study focuses on the effects of temperature and moisture, because they are the most relevant when considering the distinct locations and industries where adhesive joints can be used all over the world, a notion further aggravated by climate prediction models stating a rise in global average temperature of up to 6°C until the year 2100 [22].

2.2.1. Temperature

Due to their polymeric nature, adhesives have limited resistance to temperature, which poses a problem due to the broad temperature ranges needed for some industries [23]. Even so, the maximum service temperature of adhesives has been rising steadily since the 1940s [1] when vinyl-phenolic adhesives could withstand approximately 80°C up until recently where polybenzothiazoles were found to withstand approximately 500°C. One of the key concerns, when dealing with temperature, is the glass-transition temperature (T_g) of the adhesive, the temperature above which a massive change in mechanical properties occurs, as shown by Harris and Fay [24] in 1992, where a test temperature above T_g led to a drastic decrease in the fatigue resistance of the joint, thus proving that such situations should be avoided. This problem directly influences the fact that different types of adhesives behave differently when in contact with moisture and temperature: adhesives whose T_g is below room temperature (for example polyurethanes or the polybutadiene studied in [24]), contrasting with adhesives with T_g

above room temperature (for example epoxies). The viscoelastic effects must also be equated, as evidence [25-27] has shown that the loading frequency is considerably temperature dependent in the case of adhesives with prominent viscoelastic behaviour and a higher loading frequency translates to a higher temperature in the joint as it reaches failure [27].

2.2.2. Moisture

Moisture may affect an adhesive joint in several ways [28]: it can penetrate the bond interface between adhesive and adherend, penetrate the adhesive itself leading to plasticization and chemical degradation of interfacial bonds, and lastly the adherends themselves may absorb some water and have their mechanical properties altered. Regarding bond interface penetration, surface treatments are used to improve the bond strength and have extremely positive effects when applied correctly (Fig. 1). Penetration of the adhesive itself is one of the biggest concerns, because the polymeric nature of the material inherently allows water particles to migrate through the molecules and interfere with the chemical composition. Water absorption is character-ized by Fick's law as a measure of the mass increase of the adhesive due to water exposure over time. Using Fick's law the percentage of total mass gain until saturation can be determined, as well as the time it takes to achieve saturation, and also the coefficient of diffusion (D) which represents a measure of the speed at which water penetrates a specific adhesive [29]. This behaviour is also influenced by temperature, so for example an adhesive with a specific D at room temperature will exhibit a higher value for D at a higher temperature. Figure 2 shows the increase in the value of D for higher temperatures when compared with room temperature.
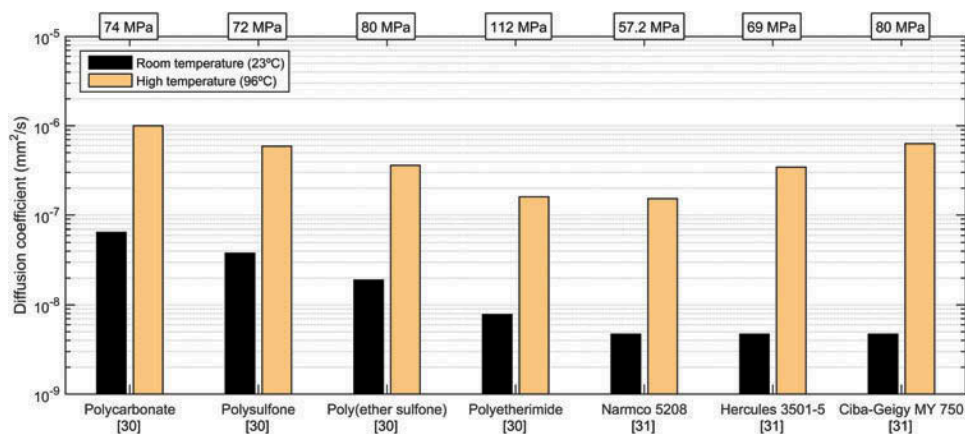

Figure 2. Influence of temperature in the coefficient of diffusion for different adhesives. Values for the tensile strength of each adhesive are displayed above the graph [30,31].

2.2.3. *Hygrothermal Effect*

While temperature and moisture considerations were separately discussed, their combined effect should also be mentioned. Effectively, combining both leads to further degradation of the joint due to the different degradation mechanisms of each separate effect, and the combined degradation due to these mechanisms is designated hygrothermal effect. Moisture in the adhesive also influences T_g, where a higher RH level has been reported to decrease T_g of the adhesive by various studies [32–37]. A separate concern when dealing with hygrothermal effects is the coefficient of thermal expansion differences between adhesive and adherend, where further care is needed when dealing with moisture, due to the fact that extra expansion occurs due to moisture (swelling due to water uptake into the adhesive), thus giving rise to a "coefficient of hygrothermal expansion". This swelling effect may greatly reduce the fatigue performance of a joint. A distinct effect that should be considered is the ratcheting behaviour of the adhesive, which experiences variable strain recovery due to the number of loading cycles, and such strain recovery is influenced by environmental effects. This ratcheting effect can have no detrimental effect on the fatigue life of an adhesive joint [38], but it should be considered nonetheless. Studies have shown that the accumulated ratcheting strain decreases to a stabilized value over time [39], and an increase in temperature was shown to greatly increase the ratcheting effect of adhesive joints while moisture was found to lower the ratcheting strain [40].

3. *S–N curves*

$S–N$ curves measure the number of cycles a joint can withstand when subjected to specific levels of stress. The idea is to determine the stress under which a joint can safely perform its duty, whatever that duty may be. For example, a specific requirement may be that the joint performs optimally until 10^4 cycles, and thus $S–N$ curves must be determined for that joint to determine the maximum stress at which such requirements can be fulfilled.

If the environment degrades an adhesive joint, then naturally that degradation must be evident in the $S–N$ curves, as the degrading effect should translate to a lower number of cycles for the same stress level. There is extensive evidence of this, as we will see next, but also some cases where the opposite happened.

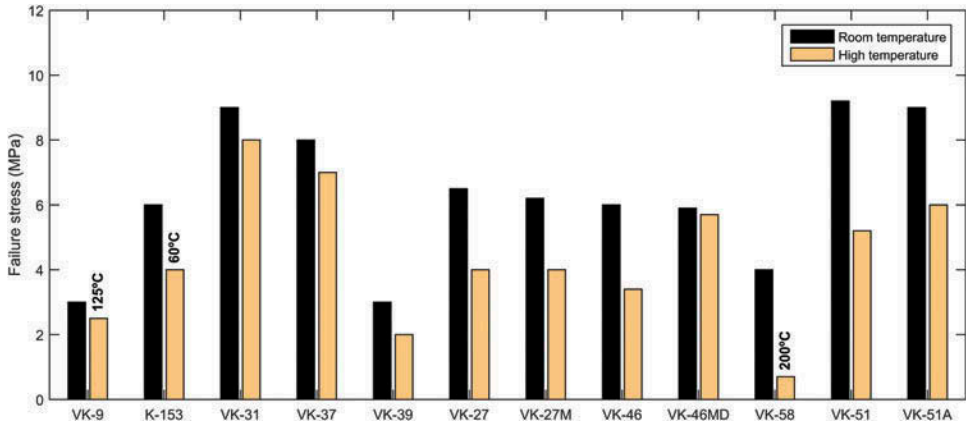### 3.1 *Temperature Influence*

The first case where environmental influence on the fatigue life of adhesive bonded joints was studied dates back to 1966 [41], when Szépe theorized that an increase in temperature leads to a decrease in the initial shear stress, which translates in a $S–N$ curve that is shifted downward. Although Szépe did

a strictly theoretical study, future extensive experimental data would indeed support his claim, such as the work by Harris and Fay [24] in 1992 which studied the fatigue behaviour of adhesives XW1012 (T_g above room temperature) and M51 (T_g below ambient temperature) at −30°C, 20°C and 90°C bonded to mild steel substrates with no surface preparation. As Szépe theorized, the initial resistance decreased as the temperature grew higher, with 90°C proving the worst case by far. For XW1012 adhesive, when the temperature increased from −30°C to 20°C, there was a slight decrease of 13% in the load range for both 0.2 mm and 2 mm adhesive layer thicknesses, while with the increase in temperature from 20°C to 90°C the load range decreased by more than four times. Such a decrease was also visible for M51 adhesive when the temperature increased from 20°C to 90°C, evidencing that for higher temperatures the degradation is more accentuated. Such conclusions are also applicable to composite adherends, which Ashcroft el al. studied in 2001 [26] together with an adhesive with a T_g above the testing temperatures, which were −50°C, room temperature, and 90°C. They observed that at 90°C the maximum load decreased drastically, while the difference from −50°C to room temperature was practically non-existent for the unidirectional substrates and small for the multidirectional substrates. Petrova and Lukina [42] later studied the effect of temperature on the fatigue resistance of 17 different epoxy adhesives bonded to duralumin and 1 bonded to steel, but using a different fatigue perspective. Instead of defining a fixed stress and analysing the influence of temperature on the number of cycles, they analysed the stress decrease with temperature so that the number of cycles until failure was similar, effectively designing a joint for a specific number of cycles and providing a picture of the decrease in the joint strength. In 2014 [43], the same authors published the updated results of the study with the same adhesives, and Fig. 3 presents the results of both works, where all room temperature tests were done at 20°C and most high temperature tests were done at 80°C, except three adhesives that were tested at different high temperatures, which are overlaid in the corresponding bar. All conditions correspond to 10^7 cycles at failure, with the exception of K-153 that failed at 5×10^6 cycles at room temperature.

All the presented works [24,26,41–43] focus on the influence of temperature on the fatigue performance of adhesive joints and all present the same trend: with an increase in temperature, the fatigue life decreases by a specific amount.

3.2 *Moisture Influence*

Underhill and DuQuesnay [44] studied the effect of moisture on *S–N* curves, and found that water has a negligible effect on the fatigue performance at lower cycles, but starts to become noticeable at very long lives (considered as about

Figure 3. Temperature influence on the maximum fatigue stress of different adhesives withstanding 107 cycles (exception of K-153 which failed at 5×106 cycles) [42,43].

5 million cycles), where the dry joints appear to approach a fatigue limit while the wet joints show a stress of about 80% that of the dry joints and no indication of a fatigue limit being reached. Sugiman et al. [45] reached different conclusions when joints aged for 1 year had their fatigue life decrease approximately by a factor of 10 compared with the unaged joints for the same load level. Joints aged for 2 years were also tested, which showed a marginal decrease in strength when compared with those aged for 1 year. Both studies tested SLJs with the same adherend material (aluminium 2024-T3), surface preparations that guaranteed cohesive failure in the adhesive layer, and similar adhesives (FM 73 vs. FM 73M), but with the major difference of studying distinct overlap lengths, where Underhill and DuQuesnay [44] tested joints with 12.5 mm overlap and Sugiman et al. [45] tested an overlap of 30 mm, effectively showing that a joint with a smaller overlap does not have its fatigue life influenced as much as a joint with a bigger overlap length.

3.3 *Hygrothermal Effects*

The individual effects of both temperature and moisture have been presented, and it is important to understand how each environmental factor differently influences the fatigue performance of the joint, but their combination may also bring additional clarifications. In 1987, Chen et al. studied [46] how joints bonded with Araldite AW106 reacted to both temperature (45°C and 55°C) and moisture (30% RH and 90% RH), and found that the fatigue life was independent of moisture but dependent on temperature. This is interesting considering that temperature was varied by only 10°C, but moisture was varied in a wider range (from 30% RH to near saturation), and even under these conditions temperature has a considerable influence while moisture does not. In 1992, Su et al. [47] performed an extensive study and tested five epoxy

adhesives with distinct mechanical properties in six different environments where the specimens were aged for 8 years. They concluded that, as expected, some adhesives would withstand the environmental effects better than others, and that in some specific situations environment degradation actually improved the average fatigue life. The focus of this study was to measure the number of cycles until failure as a function of different environmental factors. To make sense of the data, Fig. 4 (top) shows the mechanical properties of all adhesives, where the general trend is that mechanical properties are highest for adhesive 1 and then decrease gradually until adhesive 5, which presents the
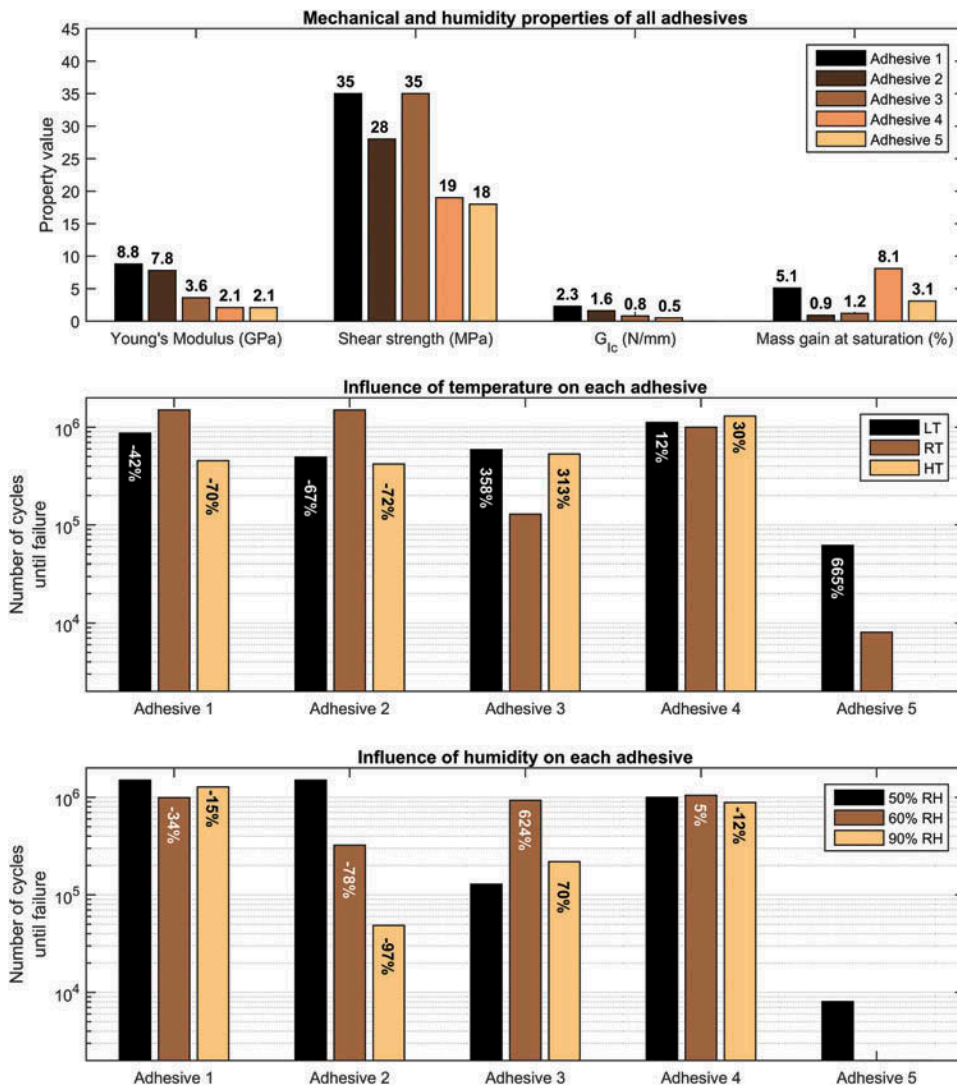
Figure 4. Mechanical properties of all adhesives (top), average number of cycles each adhesive could withstand for different temperatures (middle), and different relative humidity (RH) levels (bottom). Adapted from [47].

lowest values. An exception to this rule is adhesive 3, which presents a high shear strength (the same as adhesive 1). Also, it should be noted that the authors did not give a value for the fracture toughness of adhesive 5, and the mass at saturation is included because it may help understand the results, as shown in Fig. 4 (middle) and (bottom). The first remark is that there is not a clear trend for all adhesives, neither for temperature of moisture influence, with some adhesives having their performance maintained or increased with an increase in temperature and moisture. One thing that may be relevant is the mass gain at saturation, because a higher value of mass gain is visible in adhesives that appear to withstand both temperature and moisture fluctuations (specifically adhesives 1 and 4). A correlation between mechanical properties does not seem possible because both adhesives 1 and 4 have very distinct properties and yet present similar cycles at failure and resistance for both the environmental factors.

These effects were later studied in 2002 for composite single lap joints [48], where the influence of water content was analysed, amongst other factors such as overlap length. The studied adhesive was Bostik 7452-Super Glue 4, which has a Young's modulus of 956 MPa and a tensile strength of 4.3 MPa [49], which was subjected to water at 20°C, 40°C, and 70°C. At 20°C and 40°C, the analysis showed that the shear strength of the joint decreased from the initial value (approximately 13 MPa) until a point where it is stabilized: at 20°C, the shear strength reached a stable value of around 9.5 MPa after 45 days, while at 40°C the shear strength roughly declined to 9 MPa after 15 days. A higher temperature, therefore, translates in a faster decrease of mechanical properties that reach a stabilized value smaller than the value of a lower temperature, a notion even more evident due to an enormous loss of fatigue strength observed at 70°C after only 8 days of ageing. As for the effect of water at different temperatures in the number of cycles until failure, the result is visible in Fig. 5 (left), where the dashed line represents the number of cycles before water emersion. It is visible that, for 30 days, at 20°C the joint strength is maintained, while at 40°C it decreases by 87%. After 60 days, at 20°C there is a slight reduction of 12%, while at 40°C the reduction is much higher, at 80%. These results allow us to conclude that, for a temperature similar to room temperature, water content has minimal impact on both static and dynamic conditions of this adhesive, while an increase in temperature leads to much higher losses in strength.

In 2004 [50], single lap joints with aluminium substrates with a diglycidyl ether of bisphenol A (DGEBA) based epoxy resin (mechanical properties in listed Table 1) were studied, where besides testing the joints at different moisture levels, the influence of a pretreatment was also analysed. Some results are shown in Fig. 5 (right), where an evident decrease in number of cycles until failure for the situation where the adhesive was almost fully saturated (96% RH) can be seen, when compared to an RH around 50%. The untreated joint experienced a decrease of 83% in resistance, while the
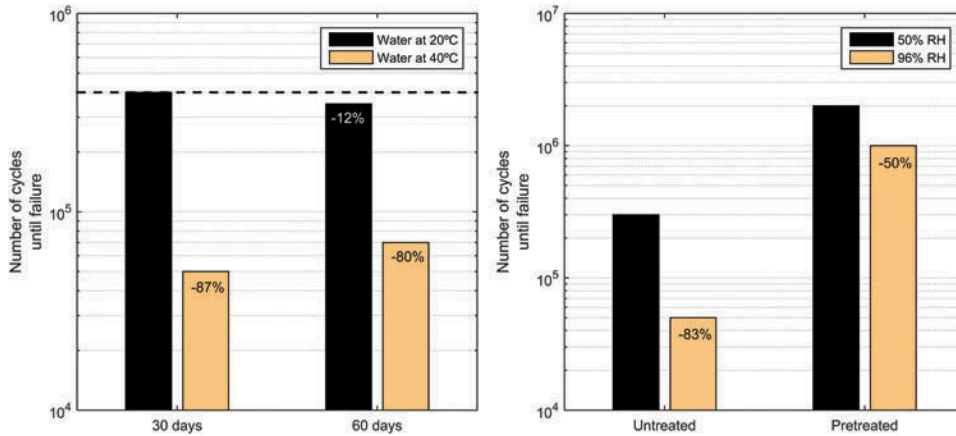
Figure 5. Effect of water at different temperatures after 30 days and 60 days submersion [48] (left), influence of pre-treatment in the fatigue endurance at 50% relative humidity and near full saturation (96% RH) [50] (right).

**Table 1.** Mechanical properties of the DGEBA-based epoxy resin.

Young's modulus (GPa)	Tensile strength (MPa)	Fracture toughness (N/mm)
1.91–2.71 [51, 52]	72–79 [51, 52]	0.5 [52]

pre-treated joint saw the strength decrease by 50% RH. It should be noted that, even for 96% RH, the pre-treated condition exhibited much higher fatigue resistance than even the 50% RH untreated specimens, proving again that a surface treatment is mandatory for aluminium-bonded joints subjected to fatigue.

It was shown through the previously presented works [46,48,50] that although moisture and temperature decrease the joint strength, temperature has a higher toll on the resistance of adhesive joints than moisture. An exception to this rule seems to be shown by Su et al. [47], where there is not a clear decrease in resistance for all adhesives with hygrothermal ageing, but there seems to be a relationship between mass gain at saturation and environmental resistance.

4. Fatigue Crack Growth Curves

While S–N curves study the impact on the number of cycles of a specific phenomenon as a function of applied stress, fatigue crack growth tests measure the crack propagation behaviour through parameters such as crack velocity (variation of the crack length between a specific number of cycles) and fracture toughness threshold (the fracture toughness value before which there is no crack propagation). The Paris Law (Fig. 6), introduced in 1963 by Paris and Erdogan [53], is extensively used to characterize the fatigue crack
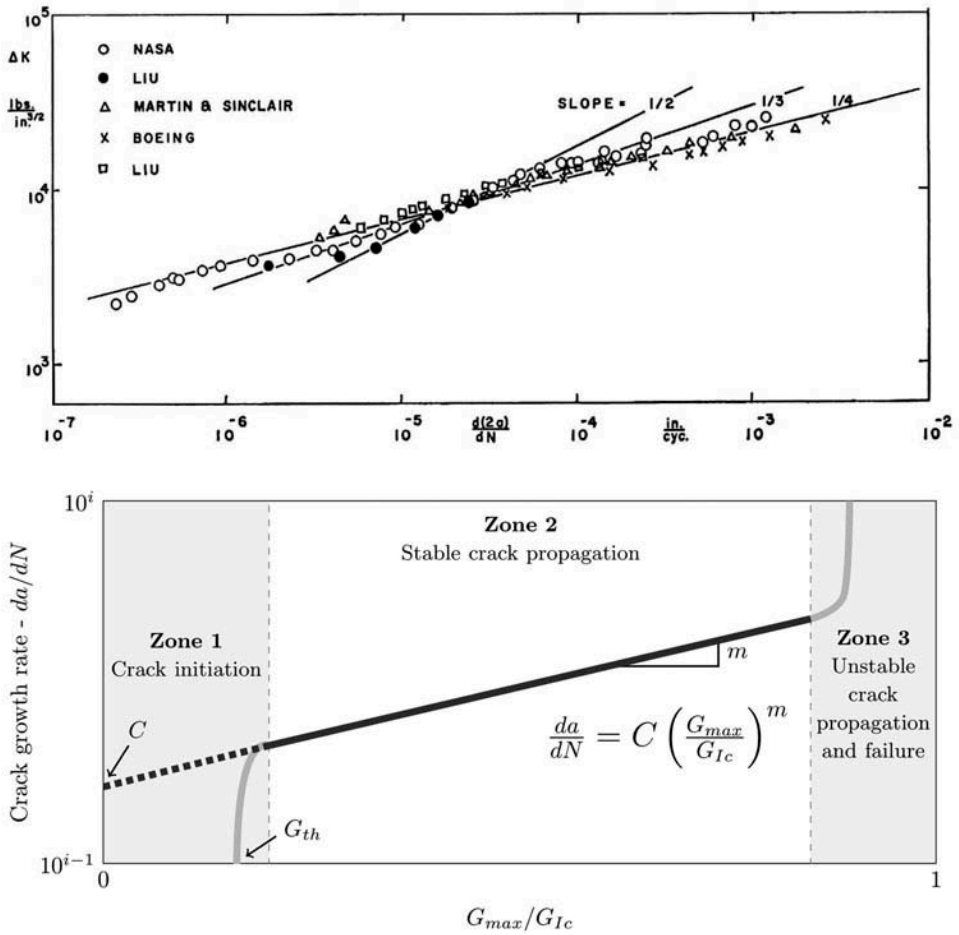
Figure 6. Paris Law: (top) Paris Law for 2024-T3 aluminium alloy (adapted from [53]), (bottom) representation of the key areas and variables obtainable from the Paris Law adapted for adhesive joints.

growth behaviour of various materials, including adhesive joints. Paris Law can be defined as $da/dN = C \cdot \Delta K^m$, where da/dN is the crack length variation (velocity of propagation), C and m are material constants, and ΔK the stress intensity factor. The use of ΔK is especially useful for metals, but when studying adhesive joints it is often substituted by G_{max}/G_c (ratio of the maximum energy release rate and critical energy required for abrupt failure), which is particularly useful to compare between different loading modes. The effect that moisture and temperature have on these parameters are presented in the following section.

4.1 *Temperature Influence*

Williams and Marshall presented in 1975 [54] a study on the effect that temperature has on the crack propagation of different polymers such as

PMMA and polyethylene. They found that the threshold stress intensity factor (K_{th}) decreased with an increase in temperature (ranging from −40°C to +80°C), meaning that the crack started to propagate sooner with a rise in temperature. This is expected because increasing the temperature decreases the properties of the material, therefore it can withstand a lower stress before cracking. Although a decrease in K_{th} was evident, the slope of the crack propagation remained unaffected, meaning that the crack propagation velocity was found unaffected by temperature. Ashcroft and Shaw [55] reached similar conclusions when studying epoxy bonded carbon fibre reinforced polymer joints who found that an increase in temperature produced an abrupt decrease in the threshold value, lowering 25% from −50°C to 22°C and 62.5% from 22°C to 90°C. As for the slope, it remained unaffected in the 22°C and 90°C cases, but for the −50°C it increased by more than 2.5 times, suggesting that the brittle state at which the joints were tested at the low temperature led to a much faster crack propagation.

Both these works paint the same picture for the effect that temperature has on the crack initiation parameters: higher temperatures translate to cracks initiating sooner. Crack velocity (slope of the Paris Law) does not present such a clear trend, but, in general, it seems unaffected by temperature changes.

4.2 Moisture Influence

Mostovoy and Ripling [56] studied the effect that water has on two different combinations of an epoxy resin (DER 332) mixed with hardener (TEPA) and cured at different temperatures, concluding that an increase in RH decreased the toughness threshold value and the slope of the Paris Law remained largely unaffected. Jethwa and Kinloch [57] reached the same conclusions concerning the slope and threshold value, effectively verifying that a higher moisture content translates to a crack that starts propagating sooner in its service life, while the crack growth rate is shown to be independent of water content, although they found that the fracture toughness value remained constant and independent of RH.

Two studies [58,59] investigated the influence of varying RH (15% and 80%) in three epoxy systems: Devcon DGEBA, Shell EPON 828 hardened with V-40, and Desoto 950-008. They reached three major conclusions: RH has no influence on the slope of the curve, a higher RH translates in a lower threshold value, and a decrease in fracture toughness was also evident with an increase in water content.

If we focus our analysis on the threshold variation with moisture, most works [16,18,20,56–60] agree that there is a decrease in G_{th} with higher moisture content, but some exceptions exist. In 1983, Mizutani and Iwatsu [61] looked at the effect that different external environments have on the Paris Law of an epoxy resin— Shell Epikote 828. While not strictly a study of moisture influence, it does compare

between no-water and water immersion, as well as immersion in various liquids such as acetone, ethanol, methanol, and others. They found that the slope was largely unaffected by the different liquids, but the threshold value exhibited some odd behaviour: instead of decreasing with water, it increased. Furthermore, testing without any liquid was found to be the worst case, while immersion in any of the other environments improved the performance of the joint. A similar trend for the increase in the threshold value with an increase in moisture was also found in two other studies [62, 63], where an increase in G_{th} was evident when the RH was increased from <20% to >95% in a bonded epoxy/glass, as well as when comparing joints without ageing to aged joints for 34 hr in water.

Different conclusions were found by other authors [17,19,64] with regard to the slope of the Paris Law curve, which was in this case found to be dependent of RH, effectively decreasing with an increase in RH. With regard to the threshold value, their conclusions agree with previous works, where the value of G_{th} decreased with an increase in moisture. Two of those works [17,19] also studied the effect of the surface treatment, with the results visible in Fig. 1.

All the works presented until now focus on mode I crack growth, which may be argued to be the most important, but information for other scenarios should also be available. Such different scenarios are studied by Meziere et al. [65], who analysed the slope of the Paris Law in three situations: pure mode I, pure mode II, and 50% of mode I. Ageing produced a 21% decrease in the slope for pure mode I, a decrease of 27% for 50% mode I, and an increase of 13% for pure mode II.

Figure 7 presents an overview based on various references of the moisture's effect on both G_{th} and slope of the Paris Law.
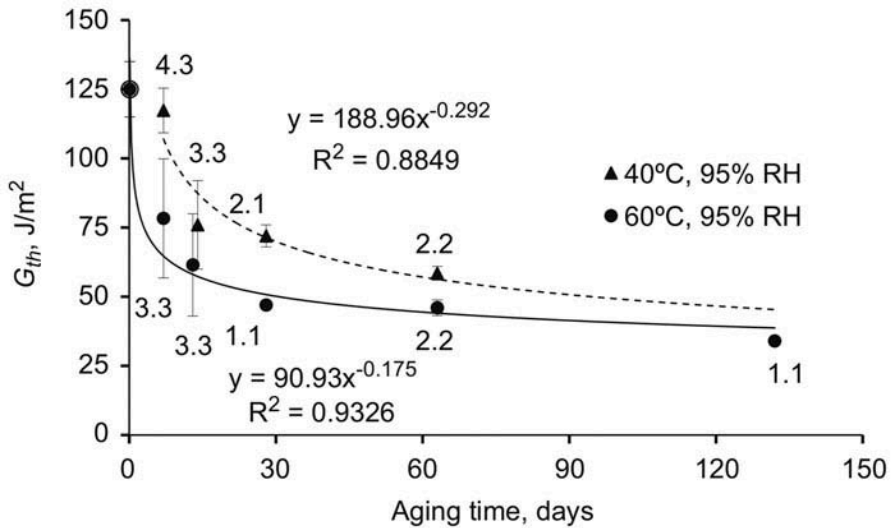

4.3 Hygrothermal Effects

Gurumurthy et al. [66,67] studied the hygrothermal influence on the interface of an epoxy and a polyimide, reaching conclusions similar to the previously presented studies: an increase in RH leads to a decrease in the threshold and the slope of the Paris Law, while an increase in temperature had the same effect. They also made an additional study regarding the influence of the rate at which temperature was changed, and found out that varying the temperature at a lower rate (0.3°C/min) degraded the interface at a higher rate (3°C/min). This result can be used to infer that, if the joint is degraded by temperature, we can expect a higher degradation if the change in temperature throughout time is lower.

Datla et al. published several studies [68–71] in the combined effect of water and temperature, which provide extensive evidence on the effects of these factors in adhesive joints. They studied a proprietary DGEBA-based, heat-cured, rubber-toughened structural epoxy adhesive bonded to aluminium adherends, and one of the conclusions of their study was that higher
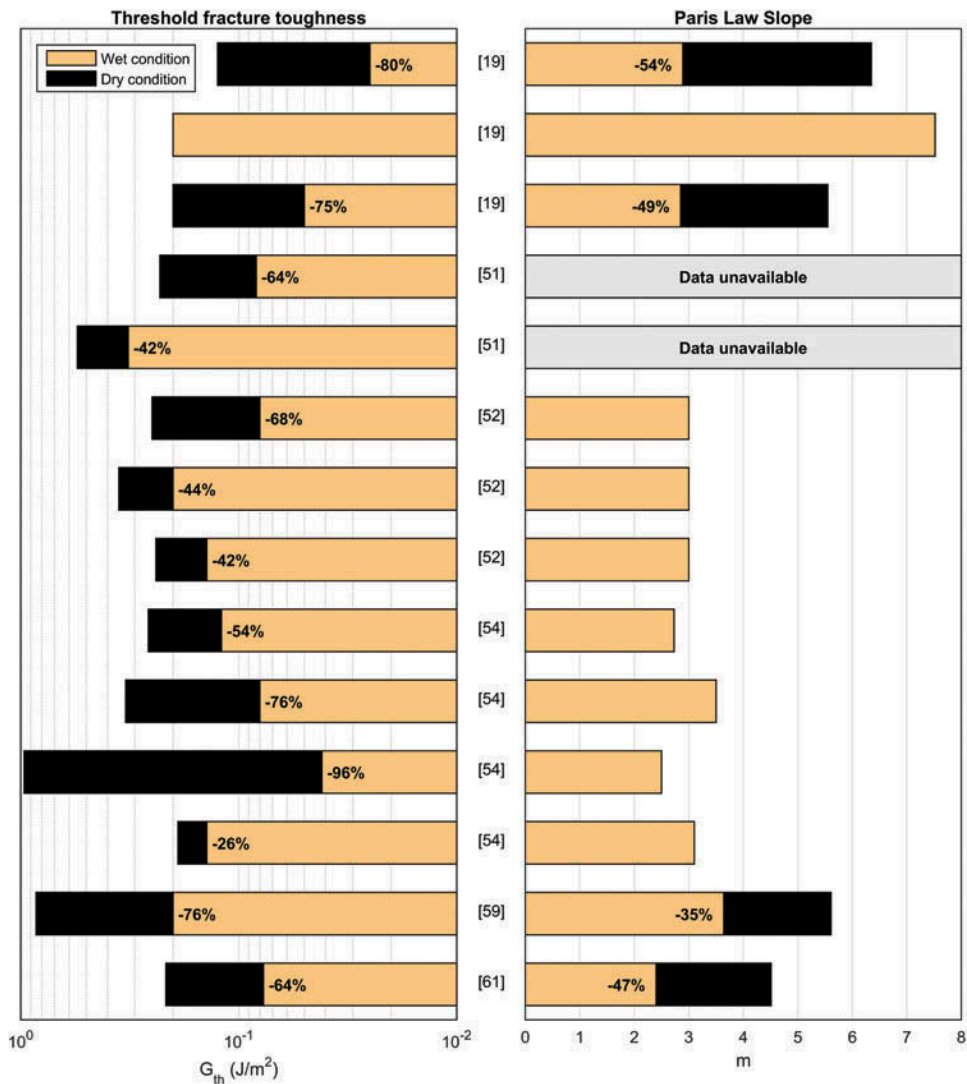
Figure 7. Effect of humidity on the Paris Law parameters. Each line corresponds to a situation described in the cited paper (evidenced in the respective line), and the percentage of reduction due to water content is overlaid on each affected property. Different lines for the same reference mean that various adhesives were studied.

moisture translated to a decrease in the threshold value, and the decrease in G_{th} was even more accentuated if the temperature was higher, a trend that was found to be satisfactorily modelled by an inverse power relationship showing a much steeper decrease in G_{th} after only 7 days of ageing for 60°C when compared with 40°C, although both tend to be roughly similar values after more than 120 days (Fig. 8) .

Figure 8. Example of the hygrothermal effect on the threshold fracture toughness of an adhesive joint, adapted from [71].

5. Conclusion

From the previously presented works, two major conclusions may be drawn: the tendencies do not consistently follow the same trend, and not many studies exist in the field of temperature and moisture influence on the fatigue behaviour of adhesive joints. One may be inherently linked to the other, as more studies would certainly paint a clearer picture and provide more uniform effects. For example, most studies exhibit a decrease in the threshold fracture toughness with increasing moisture, but various exceptions occur. The same can be said for the slope of the Paris Law, the number of cycles until failure, and virtually any of the parameters. This is most certainly related to the mechanical properties and behaviour of the specific adhesives, but many of the works presented do not analyse these parameters, although an effort was made to find them elsewhere. Although the oldest analysed work is from 1966 [41], the concern with the effect of the environment on the long-term behaviour of adhesive joints is still not fully studied, something that will certainly change in the short-term future as adoption of adhesives as substitutes for conventional joining methods is seen in more industries and products.

Funding

ORCID

Lucas da Silva ⓘ http://orcid.org/0000-0003-3272-4591

References

[1] Pizzi, A., and Mittal, K. L., *Handbook of Adhesive Technology, Revised and Expanded*, (Taylor & Francis, New York, USA, 2003).

[2] Hart-Smith, L. J., *Handbook of Adhesion Technology*, (Springer, Berlin, Heidelberg, 2011), Ch. 44, pp. 1101–1147.

[3] Désagulier, C., *Handbook of Adhesion Technology*, (Springer, Berlin, Heidelberg, 2011), Ch. 45, pp. 1149–1184.

[4] Davies, P., *Handbook of Adhesion Technology*, (Springer, Berlin, Heidelberg, 2011), Ch. 48, pp. 1237–1262.

[5] Astm, D1183 - Practices for Resistance of Adhesives to Cyclic Laboratory Aging Conditions, ed: ASTM International, 2011.

[6] Astm, D3166 - Test Method for Fatigue Properties of Adhesives in Shear by Tension Loading (Metal/Metal), ed: ASTM International, 2012.

[7] Hartung, I., and Boehm, S., *Handbook of Adhesion Technology*, (Springer, Berlin, Heidelberg, 2011), Ch. 49, pp. 1263–1288.

[8] Suzuki, Y., *Handbook of Adhesion Technology*, (Springer, Berlin, Heidelberg, 2011). Ch. 47, 1213–1236.

[9] De Bruyne, N., "Fundamentals of adhesion," presented at the Bonded aircraft structures, Cambridge, England, (1957).

[10] Schliekelmann, R., *Prog. Sci. Eng. Compos.* **1**, 63–78 (1983).

[11] Astm, D3762 - Test Method for Adhesive-Bonded Surface Durability of Aluminum (Wedge Test), ed: ASTM International, 2010.

[12] Kinloch, A., Welch, L., and Bishop, H., *J. Adhes.* **16**, 165–177 (1984).

[13] Briskham, P., and Smith, G., *Int. J. Adhes. Adhes.* **20**, 33–38 (2000).

[14] Lefebvre, D., Ahn, B., Dillard, D., and Dillard, J., *Int J Fracture* **114**, 191–202 (2002).

[15] De Barros, S., Kenedi, P., Ferreira, S., Budhe, S., Bernardino, A., and Souza, L., *J. Adhes.* **just accepted**, DOI: 10.1080/00218464.2015.1122531 (2015).

[16] Fernando, M., Harjoprayitno, W., and Kinloch, A., *Int. J. Adhes. Adhes.* **16**, 113–119 (1996).

[17] Kinloch, A., Little, M., and Watts, J., *Acta Mater.* **48**, 4543–4553 (2000).

[18] Kinloch, A., Korenberg, C., Tan, K., and Watts, J., *J. Mater. Sci.* **42**, 6353–6370 (2007).

[19] Hadavinia, H., Kinloch, A., Little, M., and Taylor, A., *Int J Adhes. Adhes.* **23**, 449–461 (2003).

[20] Abel, M.-L., Adams, A., Kinloch, A., Shaw, S., and Watts, J., *Int. J. Adhes. Adhes.* **26**, 50–61 (2006).

[21] Pethrick, R. A., Proceedings of the Institution of Mechanical Engineers, Part L: Journal of Materials Design and Applications, 1464420714522981 (2014).

[22] Pachauri, R. K., Allen, M., Barros, V., Broome, J., Cramer, W., Christ, R., et al., *Climate Change 2014: Synthesis Report*, (IPCC, Geneva, Switzerland, 2014).

[23] Marques, E., Da Silva, L. F., Banea, M., and Carbas, R., *J. Adhes.* **91**, 556–585 (2015).

[24] Harris, J., and Fay, P., *Int. J. Adhes. Adhes.* **12**, 9–18 (1992).

[25] Pirondi, A., and Nicoletto, G., *Eng. Fract. Mech.*, **71**, 859–871 (2004).

[26] Ashcroft, I., Hughes, D., Shaw, S., Wahab, M. A., and Crocombe, A., *J. Adhes.* **75**, 61–88 (2001).

[27] Reis, P., Monteiro, J., Pereira, A., Ferreira, J., and Costa, J., *Int. J Adhes. Adhes.* **63**, 66–73 (2015).

[28] Bowditch, M., *Int. J. Adhes. Adhes* **16**, 73–79 (1996).

[29] Da Silva, L. F. M., and Sato, C., *Design of Adhesive Joints Under Humid Conditions*, (Springer, Berlin Heidelberg, 2013).

[30] Robeson, L., and Crisafulli, S., J. *Appl. Polym. Sci.* **28**, 2925–2936 (1983).

[31] Wright, W., *Composites* **12**, 201–205 (1981).

[32] Hu, Y., Li, X., Lang, A. W., Zhang, Y., and Nutt, S. R., *Polym. Degrad. Stab.* **124**, 35–42 (2016).

[33] Kropka, J. M., Adolf, D. B., Spangler, S., Austin, K., and Chambers, R. S., Int. *J. Adhes. Adhes.* **63**, 14–25 (2015).

[34] Zhou, J., and Lucas, J. P., *Polymer* **40**, 5513–5522 (1999).

[35] Ellis, T. S., and Karasz, F. E., *Polymer* **25**, 664–669 (1984).

[36] Zhang, Y., Adams, R., and Da Silva, L. F., *Int. J. Adhes. Adhes.*, **50**, 85–92 (2014).

[37] Barbosa, A., Da Silva, L., and Öchsner, A., *J. Adhes. Sci. Technol.*, **29**, 1714–1732 (2015).

[38] Tao, G., and Xia, Z., *Polym. Test.* **26**, 451–460 (2007).

[39] Shen, X., Xia, Z., and Ellyin, F., *Polym. Eng. Sci.* **44**, 2240 (2004).

[40] Zhang, D., Gao, H., Gao, L., and Ma, J., *Polym. Test.* **32**, 1545–1550 (2013).

[41] Szépe, F., *Exp. Mech.* **6**, 280–286 (1966).

[42] Petrova, A., and Lukina, N., *Polym. Sci. Ser. C*, **49**, 99–105 (2007).

[43] Petrova, A., Lukina, N., and Sharova, I., *Polym. Sci. Ser. D*, **7**, 228–232 (2014).

[44] Underhill, P., and Duquesnay, D., *Int. J. Adhes. Adhes.* **26**, 62–66 (2006).

[45] Sugiman, S., Crocombe, A., and Aschroft, I., *Int. J. Adhes. Adhes.* **41**, 80–91 (2013).

[46] Chen, N., Niem, P., and Lee, R., *J. Adhes.* **21**, 115–128 (1987).

[47] Su, N., Mackie, R., and Harvey, W., *Int. J. Adhes. Adhes.* **12**, 85–93 (1992).

[48] Ferreira, J., Reis, P., Costa, J., and Richardson, M., *Compos. Sci. Technol.* **62**, 1373–1379 (2002).

[49] Ferreira, J., Silva, H., Costa, J., and Richardson, M., *Compos. Part B* **36**, 1–7 (2005).

[50] Rushforth, M., Bowen, P., Mcalpine, E., Zhou, X., and Thompson, G., J Mater. Process. Technol. **153**, 359–365 (2004).

[51] Qi, B., Zhang, Q., Bannister, M., and Mai, Y.-W., *Compos. Struct.* **75**, 514–519 (2006).

[52] Thomas, R., Yumei, D., Yuelong, H., Le, Y., Moldenaers, P., Weimin, Y., et al., *Polymer* **49**, 278–294 (2008).

[53] Paris, P., and Erdogan, F., *J. Fluids Eng.*, **85**, 528–533 (1963).

[54] Williams, J., and Marshall, G., Environmental crack and craze growth phenomena in polymers, in *Proceedings of the Royal Society of London A: Mathematical, Physical and Engineering Sciences*, 1975, pp. 55–77.

[55] Ashcroft, I., and Shaw, S., *Int. J. Adhes. Adhes.*, **22**, 151–167 (2002).

[56] Mostovoy, S., and Ripling, E., *J. Appl. Polym. Sci.* **13**, 1083–1111 (1969).

[57] Jethwa, J., and Kinloch, A., *J. Adhes.* **61**, 71–95 (1997).

[58] Conley, K., Ritter, J., and Lardner, T., *J. Mater. Res.*, **7**, 2621–2629 (1992).

[59] Ritter, J., and Conley, K., *Int. J. Adhes. Adhes.* **12**, 245–250 (1992).

[60] Wang, M., Liu, A., Liu, Z., and Wang, P.-C., *Int. J. Adhes. Adhes.* **40**, 1–10 (2013).

[61] Mizutani, K., and Iwatsu, T., Polym. Eng. Sci. **23**, 183–185 (1983).

[62] Ritter, J., Learned, J., Jacome, G., Russell, T., and Lardner, T., *J. Adhes.* **76**, 335–351 (2001).

[63] Ritter, J. E. and Huseinovic, A., *J. Electr. Packaging*, **123**, 401–404 (2001).

[64] Curley, A., Hadavinia, H., Kinloch, A., and Taylor, A., *Int. J. Fract.* **103**, 41–69 (2000).

[65] Meziere, Y., Michel, L., and Carronnier, D., *Eur. Struct. Integr. Soc.* **27**, 97–110 (2000).

[66] Gurumurthy, C. K., Kramer, E., and Hui, C.-Y., *Acta mater.* **49**, 3309–3320 (2001).

[67] Gurumurthy, C. K., Kramer, E. J., and Hui, C.-Y. *Int. J. Fract.* **109**, 1–28 (2001).

[68] Datla, N., Ameli, A., Azari, S., Papini, M., and Spelt, J., *Eng. Fract. Mech.* **79**, 61–77 (2012).

[69] Datla, N., Papini, M., Schroeder, J., and Spelt, J., *Int. J Adhes. Adhes.* **30**, 439–447 (2010).

[70] Datla, N., Papini, M., Ulicny, J., Carlson, B., and Spelt, J., *Eng. Fract. Mech.* **78**, 1125–1139 (2011).

[71] Datla, N., Ulicny, J., Carlson, B., Papini, M., and Spelt, J., *Int. J Adhes. Adhes.* **31**, 88–96 (2011).

Paper B

Effect of the size reduction on the bulk tensile and double cantilever beam specimens used in cohesive zone models

M Costa[1], G Viana[1], C Canto, LFM da Silva[2], MD Banea[2], F Chaves[1], RDSG Campilho[3] and AA Fernandes[2]

Abstract
Cohesive zone elements used in finite element analysis are a reliable way to design and predict the behaviour of the joint. The characterisation of the traction separation law used in these models is done using tensile and fracture tests, and the parameters of such laws depend on humidity and temperature. Water diffusion tests are therefore necessary, which are dependent on specimen geometry, meaning a bigger specimen takes longer to fully saturate. To solve this problem and increase the efficiency of the ageing process, smaller tensile bulk and double cantilever beam (DCB) specimens are necessary. Another advantage of smaller DCB specimens is that they can be tested in smaller high-temperature chambers, where normal DCB specimens do not fit. Smaller geometries of the bulk tensile and DCB tests are analysed, and a proposed geometry for each test is shown to produce very satisfactory results, validating the use of these specimens.

Introduction

Cohesive zone elements have been developed to simulate static damage, damage due to fatigue and, more recently, damage due to the environment. In a cohesive damage analysis no initial crack is needed, and its propagation is the result of a simulated degradation of the material. A finite element analysis (FEA) that uses a cohesive damage model uses both continuum mechanics and fracture mechanics, considering both strength and energy to characterise the debonding process.[1] By combining these parameters, the cohesive zone models (CZM) allow whichever factor is predominant to control the fracture process of the crack in the numerical analysis.[2]

The cohesive zone parameters are characterised experimentally using bulk tensile tests, thick adherend shear test (TAST), double cantilever beam (DCB) and end-notched flexure (ENF) tests, where data from those test results are incorporated in a numerical analysis. This methodology has given very satisfactory results and it is possible to predict with accuracy the behaviour of adhesive joints.[3] Different laws for the cohesive zone have been put forward: triangular law, trapezoidal law, exponential law and others. Although being more suited for modelling brittle adhesives, the triangular law provides good results for most of the real world situations.[4] For ductile materials, both the exponential law[5] and trapezoidal law[6] can also be of interest.

The triangular traction separation law available in state of the art FEA programs, such as Simulia Abaqus® (Providence, Rhode Island, USA), initially assumes a linear elastic behaviour followed by a linear evolution of damage. The determination of the tensile and shear strength of the adhesive enables the characterisation of the linear elastic behaviour, while the area under the curve is equal to the respective fracture energy. Additional parameters, such as the initial cohesive stiffness K, are not measured experimentally and are usually assumed or found by trial and error, as there are yet no well-established universal rules for determining those CZM parameter values.[7]

[1]INEGI Polo FEUP, Rua Dr. Roberto Frias, Oporto, Portugal
[2]Departamento de Engenharia Mecânica, Faculdade de Engenharia da Universidade do Porto (FEUP), Rua Dr. Roberto Frias, Oporto, Portugal
[3]Departamento de Engenharia Mecânica, Instituto Superior de Engenharia do Porto (ISEP), Instituto Politécnico do Porto, Rua Dr. António Bernardino de Almeida 431, Oporto, Portugal

Corresponding author:
LFM da Silva, Departamento de Engenharia Mecânica, Faculdade de Engenharia da Universidade do Porto (FEUP), Rua Dr. Roberto Frias, 4200-465 Oporto, Portugal.
Email: lucas@fe.up.pt

Bulk tensile tests, similar to those for plastic materials, are commonly used to determine the tensile strength of the adhesive, under a uniform and uniaxial state of stress. Other properties such as tensile modulus, yield strength, failure strength and elongation at break can be obtained, although not relevant for inclusion in the CZM. Although axially loaded butt joints can be used as an alternative to bulk tensile tests, the stress–strain curve is not representative of the intrinsic adhesive behaviour, and despite the use of precise apparatus the reproducibility of this test is low.[8]

The measurement of the fracture toughness is more complex and can be done using several geometries. The two most common bulk specimens are compact tension (CT) and single-edge notched bending (SENB), and in both cases the toughness results are intrinsic to the adhesive and do not directly relate to the joint properties. Although these techniques are of interest, the most accurate tests to characterise the fracture energy in adhesive bonds are DCB test and tapered double cantilever beam (TDCB) test. Since the machining of the DCB specimens is much simpler this is the most used test.[9]

To conduct the DCB test, two different standards exist, ASTM D3433 and ISO 25217. The first determines the fracture toughness through several loadings of the specimen. This is done in order to induce crack propagation and measure the peak load required, while the load for crack arrest is also recorded and the final crack length measured. Both load values are used to measure the fracture toughness. In standard ISO 25217, the specimen is loaded with a constant crosshead displacement up to crack propagation starts. Usually the crack increases slightly, 2–5 mm, and at this point the machine is reset. This pre-crack is not part of the test but a prerequisite. Subsequently, the specimen is reloaded again and the resistance to crack initiation and steady-state propagation are calculated.[9]

Some work has been done on the study of how specific geometric parameters influence the resulting fracture toughness (G_{IC}). An increasing trend of G_{IC} with adherend thickness was found,[10] which is relevant to our study on DCB size reduction. This behaviour was considered to be due to an increasing degree of adherend restraining for bigger thickness values, as a larger region is loaded ahead of the crack tip. Besides the adherend thickness, an increase in the thickness of the adhesive also increases the fracture toughness.[11,12]

The mechanical properties of the adhesive are also influenced by environmental factors, which therefore also influence the CZM parameters. Temperature and humidity have been found to degrade the joint,[13] which translates to a decrease in tensile strength and fracture energy. Because the CZM parameters are therefore dependent on temperature and humidity, water diffusion tests are necessary to fully characterise the traction separation law for degraded situations. The duration of humidity tests is also an important aspect that should be related with specimen geometry, because smaller specimens are useful to decrease the duration of water uptake tests.[14] Durability tests are currently being performed as part of a study on the combined effect of temperature, humidity, fatigue and environmental degradation of joints, and specimens with smaller geometries will prove very useful to shorten the study duration.

This paper is structured in two main sections: one to study the effect of size on bulk tensile specimens and the other for DCB specimens. In order to validate the proposed geometries of the dogbone and DCB specimens, two epoxy adhesives were used: one that shows ductile failure, and the other with brittle behaviour. Each section presents experimental results for standard specimens, followed by a numerical study of the geometry and finally a validation of said geometry by experimental tests. In the end small specimens are suggested which present the best results when compared with those obtained with standard specimens.

Adhesives

Two epoxy adhesives are used for this study. The first, XNR 6852-1, supplied by NAGASE CHEMTEX® (Osaka, Japan), is a one-part system that cures at 150°C for 3 h. It has a linear structure, which allows greater freedom of movement to the chains, unlike the cross-linked structure of a conventional epoxy adhesive. As a consequence, this polymer has some features of thermoplastic polymers due to the resulting linear structure.[15]

The second adhesive was SikaPower 4720, supplied by SIKA® (Portugal, Vila Nova de Gaia). This adhesive is a two-part system that cures at room temperature for 24 h. Both these adhesives will be characterised in the following section.

Bulk tensile test

Characterisation of the tensile strength

Experimental procedure. The bulk tensile specimens were produced by curing the adhesive between steel plates in a mould with a silicone rubber frame, according to the French standard NF T 76-142.[16] A silicone rubber frame was used to avoid the adhesive from flowing, and the thickness of the silicone is also used to guarantee specimen thickness. Both adhesives were cured under 2 MPa hydrostatic pressure in a hot-plates press according to the manufacturer's specification, and the dimensions of the adhesive plate after cure were defined from the internal dimensions of the silicone rubber frame. After that, dogbone specimens (Figure 1) were machined from the bulk sheet plates.

The bulk tensile tests were performed in an INSTRON® model 3367 universal test machine (Norwood, MA, USA) with a capacity of 30 kN, at room temperature and constant displacement rate of 1 mm/min. Two methods were used to measure the
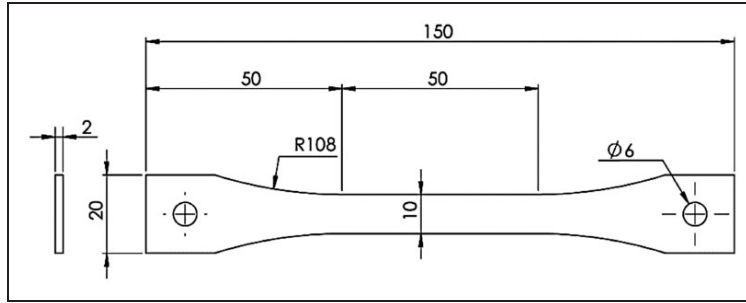
Figure 1. Dimensions of the bulk tensile specimens used in accordance with standard BS 2782 (dimensions in mm).
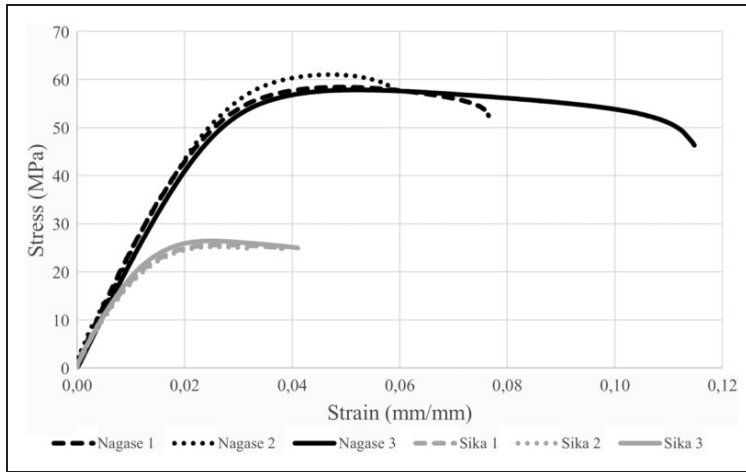
Figure 2. Stress–strain curves of standard dogbone specimens for Nagase XNR 6852-1 and SikaPower 4720.

displacement: an optical method, and an extensometer with 25 mm grip length. The optical method consisted of markings being placed on the specimens at the extremities of the allowable deformation zone (50 mm apart), and photos were taken every 5 s during the test. The photos were then post-processed in a custom MATLAB program developed in-house. There are two reasons both methods were used: first, because Nagase XNR 6852-1 exhibits necking after fracturing, and even if fracture occurred between the extensometer arms, the deformed part could extend beyond them, which would cause a strain value lower than the actual test. The second reason was the validation of the optical method, which will be needed in future studies where an extensometer cannot be used, such as high and low temperature tests. Three specimens of each adhesive were tested.

Experimental results and discussion. Figure 2 shows three stress–strain curves for each tested adhesive. Reproducibility is important to define the basis for

Table 1. Results of bulk tensile tests.

	Tensile strength (MPa)	Tensile modulus (MPa)	Strain to failure (%)
XNR 6852-1	59.1 ± 1.39	2276.1 ± 89.27	8.4 ± 2.31
SikaPower 4720	25.8 ± 0.61	2171.1 ± 244.81	3.4 ± 0.27

comparison of properties between standard and future small specimens, and it can also be seen that the adhesives have distinct mechanical properties. Table 1 synthesises the most important data obtainable from the stress–strain curves.

The stress–strain curves of polymeric materials are not linear in tension and have usually low rigidity in the elastic domain. Despite the evident non-linear behaviour, the tensile modulus is commonly used to describe most adhesives, as it is simple to determine. Before fracturing, adhesive XNR 6852-1 deforms in a ductile manner (Figure 3(a)) suffering a reduction of area and acquiring an opaque colour, behaviour
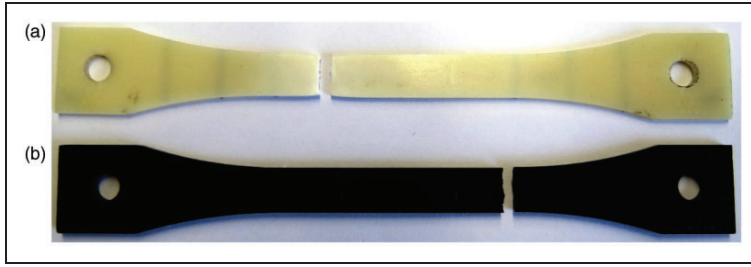
Figure 3. Bulk tensile specimens after testing: (a) XNR 6852-1 and (b) SikaPower 4720.

typical of thermoplastic polymers. This behaviour is an improvement in the properties of epoxy adhesives, also evident in the increased ductility of the material when compared with SikaPower 4720, which has a very brittle behaviour with little deformation (Figure 3(b)).

Effect of variations on the geometry of the bulk tensile test specimen

Numerical modelling. Three reduced specimens were evaluated (Figure 4): a short tensile specimen according to EN ISO 527-2 (test specimen type 5A), a second specimen with a transition radius of 25 mm, and finally a specimen with a 54 mm radius in the transition area. The geometry in Figure 4(b)) is not in accordance with any standard and was developed with the purpose of eliminating, as far as possible, the concentration of stress, by using a higher (double) radius. A further improvement of the previous geometry, with an increased radius and increased cross-sectional area, was also evaluated and is shown in Figure 4(c). In all cases, the specimen thickness was 2 mm. Thinner specimens would mean quicker humidity tests, but in the case of bulk specimens the biggest area exposed to moisture is their surface, and compared to other specimens (such as DCBs) they saturate faster, so it was felt there was no need to reduce the cross section.

Using Abaqus®, a 2D linear elastic analysis was performed on the simplified geometry of each specimen type (Figure 5(a)) shows the assumed simplification), and a plane stress case was chosen. The simulation was run with the tensile modulus of XNR 6852-1 (Table 1), a Poisson's ratio (v) of 0.4, and with the boundary conditions and applied displacement as shown in Figure 5(b).

Numerical results and discussion. Figure 5(c) to (e) shows the relative stress comparison between the small specimens for the same applied displacement. The EN ISO 527-2 specimen (Figure 5 c)) is used as the basis for comparison, because there is a severe change in stress from the holding part of the specimen to the test area, and it exhibits the worst stress concentration of all the considered geometries (due to the smaller radius). The remaining specimens try to reduce the stress concentration by using a radius of higher magnitude, and it can
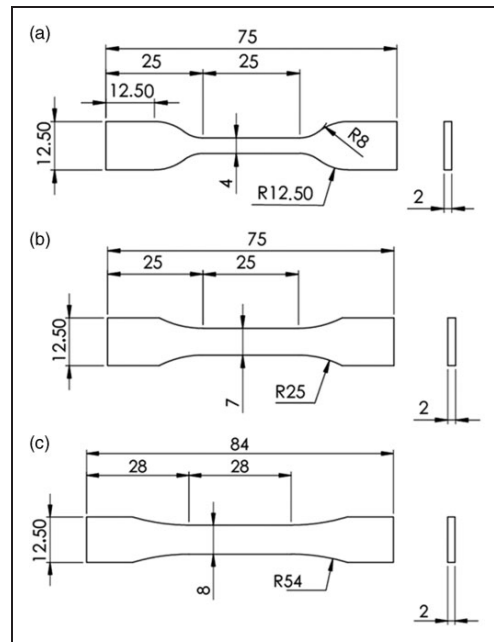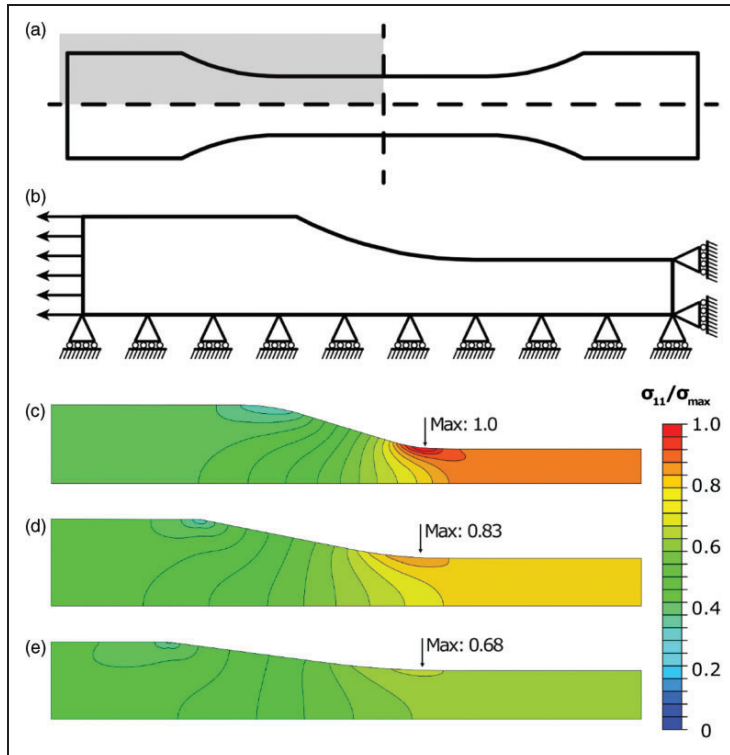

Figure 4. Geometry of the three small specimens studied: (a) short tensile specimen according to EN ISO 527-2, (b) short specimen with transition radius of 25 mm, and (c) short specimen with a 54 mm radius in the transition area (dimensions in mm).

be seen that the maximum stress is reduced through this methodology. The reduction is important because, for example in tensile tests at high temperature and high strain rates, failure is more likely to occur where higher stress concentrations exist.

Experimental results and discussion. The experimental procedure for manufacturing and testing the small specimens follows the same as described before for the long dogbones.

The stress–strain curves for the short specimen A (EN ISO 527-2 standard) are presented in Figure 6. The first thing to note is the considerably higher tensile strength of the short specimens when compared to the long dogbone. This happens for both adhesives,

Figure 5. FEM model and resulting relative stress distribution comparison: (a) full specimen with symmetry lines, where the grey area is the considered geometry for analysis, (b) boundary conditions and applied displacement, (c) results for the short tensile specimen according to EN ISO 527-2, (d) short specimen with transition radius of 25 mm, (e) short specimen with a 54 mm radius in the transition area.

which confirms that it is an effect not related to adhesive properties but to specimen geometry. One reason for this may be that smaller specimens are less prone to microscopic defects such as voids and cracks. The failure strain values further support this theory, as it is visible that, at least for Nagase XNR 6852-1, a ductile adhesive, the maximum strain for each small specimen was higher than the long dogbone.

Figure 7 shows the stress–strain results for short specimen B (25 mm radius). The tensile strength of these specimens has been reduced from the previous geometry, which further validates the idea of refining the standard EN ISO 527-2 specimen. The reason for this reduction is assumed to be the proposed specimen geometry, where both the smaller stress concentrations and the larger cross-sectional area contribute to the apparent approximation of the curves for the small specimens to the long dogbone. This is visible for Nagase XNR 6852-1 and even more prominent for the SikaPower 4720.

The results for the final short specimen, geometry C (54 mm radius) are visible in Figure 8. For Nagase XNR 6852-1, the tensile strength is now even further reduced from the EN ISO 527-2 specimens, which

confirms that the approach of decreasing the stress concentration has positive effects on the resulting tensile strength values for the small geometries. For SikaPower 4720 there was a slight increase in the tensile stress values from the previous 25 mm radius geometry, which may be related to the fact that this adhesive is more brittle, therefore for smaller and more rigid geometries the resulting stress is a bit higher.

The main outcomes of the previously shown stress–strain curves are: first, all the small geometries exhibit higher tensile strength values than the long dogbone results, which has been justified as being due to the smaller probability of microscopic defects in the smaller specimens. This is further supported by the fact that the smaller specimens of Nagase XNR 6852-1, a ductile adhesive, show a higher failure strain, while the ones from SikaPower 4720, a brittle adhesive, show roughly the same failure strain. Finally, there is an evident decrease in the tensile strength values as we further refine the geometry, which validates the geometry chosen as final. Figure 9 shows a concise picture of the average tensile strength results and respective deviation for all geometries and adhesives.
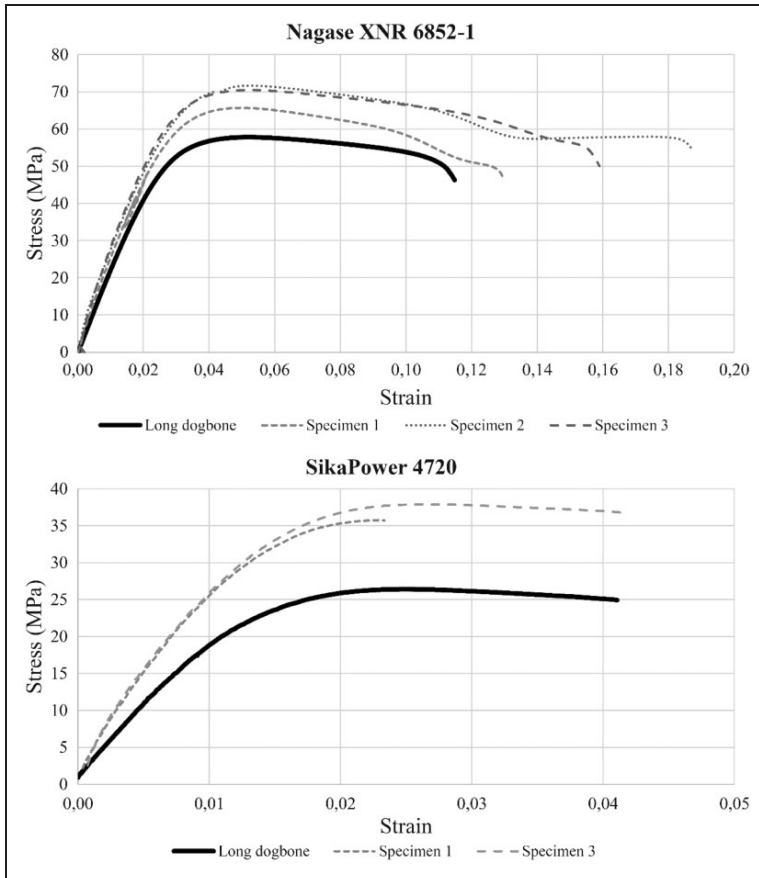
Figure 6. Comparison of stress–strain curves between the EN ISO 527-2 short specimen and long dogbone specimen using both adhesives.

We can conclude that, for our purpose, which is the determination of the tensile strength of the adhesive for inclusion in the respective traction–separation curve of the cohesive zone model, small geometry C presents the best results for both types of adhesives.

Double cantilever beam tests

Characterisation of the fracture toughness

Experimental procedure. The DCB specimens used (based on ASTM D3433) are shown in Figure 10. A high tensile strength steel (DIN 40 CrMnMo 7) was used to avoid plastic deformation of the substrates.

Blades with a thickness of 0.2 mm were used to impose the adhesive thickness as well as the initial crack length of 45 mm. The mould was then put in a hot press, where the adhesives were cured at the temperature and during the time specified by each manufacturer, both at a pressure of 2 MPa. Three DCB specimens were manufactured for each adhesive, and

the tests were conducted in an INSTRON® model 3367 universal test machine (Norwood, MA, USA) with a capacity of 30 kN, at room temperature, with a constant displacement rate of 0.5 mm/min.

Experimental results and discussion. The determination of the fracture energy (G_{IC}) for the DCB specimens was accomplished using the compliance-based beam method (CBBM),[17,18] which only uses the load and displacement curves of a DCB test to determine the G_{IC}. This has two advantages, as it eliminates the uncertainty of an eye measure of the crack length, and also makes it possible to conduct tests where the crack can be obstructed by the machine's structure or loading apparatus, which can happen with smaller specimens.

The resulting *R*-curves are presented in Figure 11.

We can see two distinct behaviours: XNR 6852-1 shows an initial peak followed by stabilisation of the fracture energy, and SikaPower 4720 is always stable at a lower fracture energy. This happened because, for

44
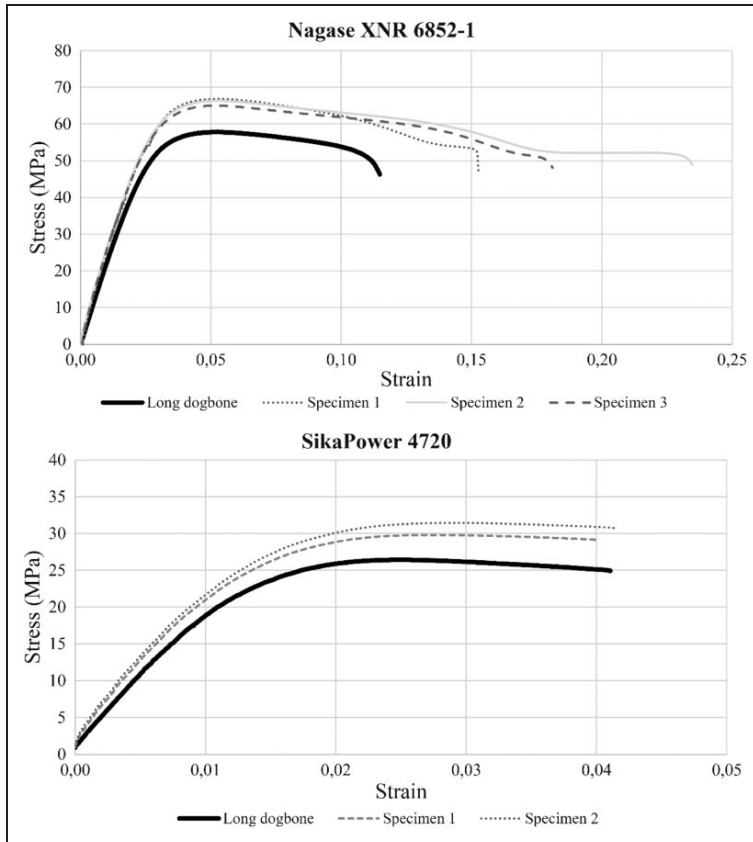
Figure 7. Comparison of stress-strain curves between the short specimen (25 mm radius) and long dogbone specimen using both adhesives.

SikaPower 4720, the DCB test was performed until the crack had propagated slightly. The experiment was then stopped, the new crack length was recorded, and the test was restarted until failure of the specimen. The implications of using this methodology is that we now have a "perfect" crack, which means that when the test is restarted and until failure, the adhesive's fracture toughness always represents the energy of a true crack. Without this methodology, the initial crack is more rounded (in the micro scale), which means that the energy needed to propagate this crack is much higher than the energy needed for a "perfect" crack. This is what happens with the XNR 6852-1 curve, which shows the initial peak (microscopically rounded crack) and then decreases and stabilises to a value representative of the energy needed to propagate a true crack. Previous studies have validated this approach.[19]

These two distinct methods were chosen to illustrate the difference between the standard test (with pre-crack) and the proposed methodology (without pre-crack). Since both methodologies are considered

to be correct (both allows the fracture energy to be determined), and thus doing the test in one-go (without stopping and restarting) was the chosen procedure for the results shown ahead.

Effect of variations on the geometry of the DCB specimens

Numerical modelling. The study on the geometry of the DCB specimens was performed in Abaqus®, where the influence of changes in DCB dimensions on the fracture toughness was studied. A 2D model analysis was performed, and Figure 12 shows the boundary conditions as well as the mesh that was used. A fracture toughness of 2 N/mm was considered for the analysis, where COH2D elements (with a width of 0.2 mm) were used for the adhesive and CPE4R (plane-strain 4-node quadrilateral solid, reduced integration) elements for the adherends.

Numerical results and discussion. The effect of the initial crack length, specimen length, width and thickness are
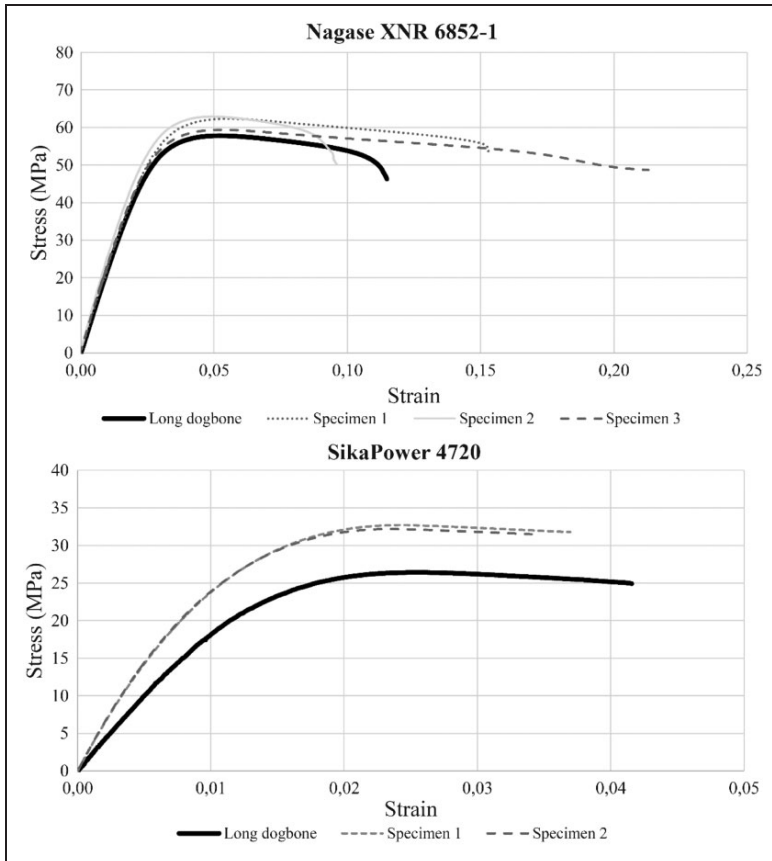
Figure 8. Comparison of stress-strain curves between the short specimen (54 radius) and long dogbone specimen using both adhesives.
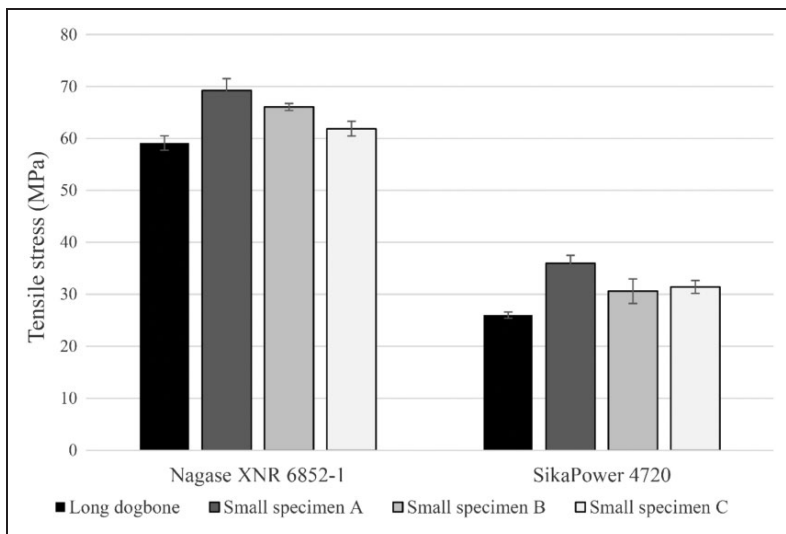
Figure 9. Average and standard deviation of tensile strength results for all the tested dogbone specimens.
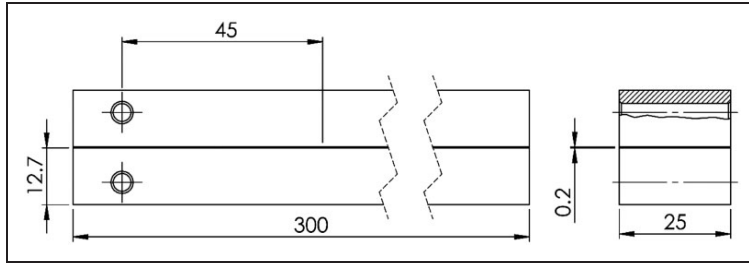
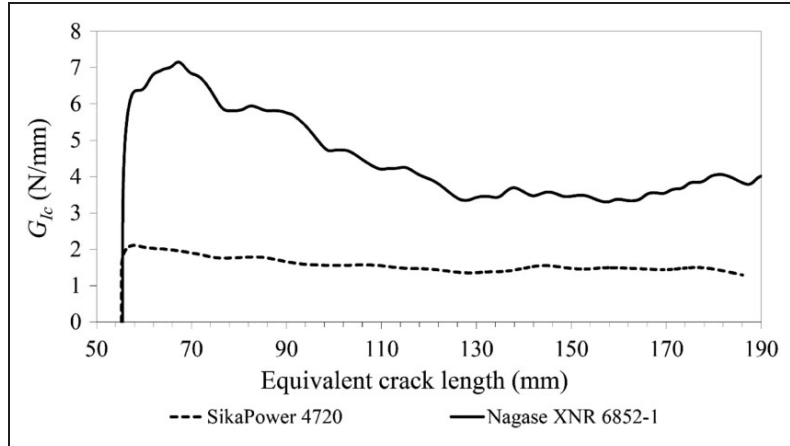**Figure 10.** DCB specimen used, with dimensions in mm, based on ASTM 3433.

Figure 11. Experimental G_{IC} results for both adhesive's normal DCB specimens, using the CBBM method.
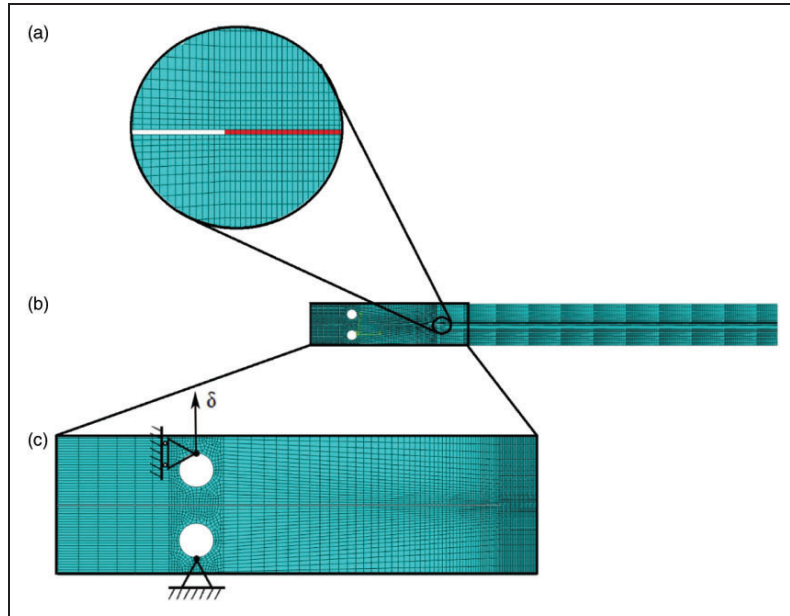

Figure 12. Modelled DCB specimens with finite element mesh: (a) cohesive zone (red), (b) view of the entire specimen, (c) boundary conditions.

analysed in this section. All these geometric parameters may have an effect on the values of fracture toughness, because it has been suggested that G_{IC} is not a material parameter, but a geometry-dependent quantity instead.[10] Furthermore, all these parameters are used in the CBBM data reduction scheme, suggesting they influence the end values.[17]

Initial crack length. Three initial crack lengths were studied to investigate their effect on the fracture toughness: 20 mm, 56 mm and 120 mm. The force–displacement (P–δ) curves presented in Figure 13 show a high rigidity for the specimen with a short crack, a

softer linear loading for the intermediate and a further decrease in compliance for the bigger crack. For longer cracks the maximum load is lower, but the displacement needed to reach the peak load is higher. All the graphs coincide once the displacement is the same.

The R-curves calculated from the numerical data acquired are presented in Figure 14, and the fracture toughness was determined using the plateau region of the R-curve, where it can be seen that the CBBM is affected by the initial crack length.

Specimen length. Another crucial parameter is the length of the specimen because, for certain
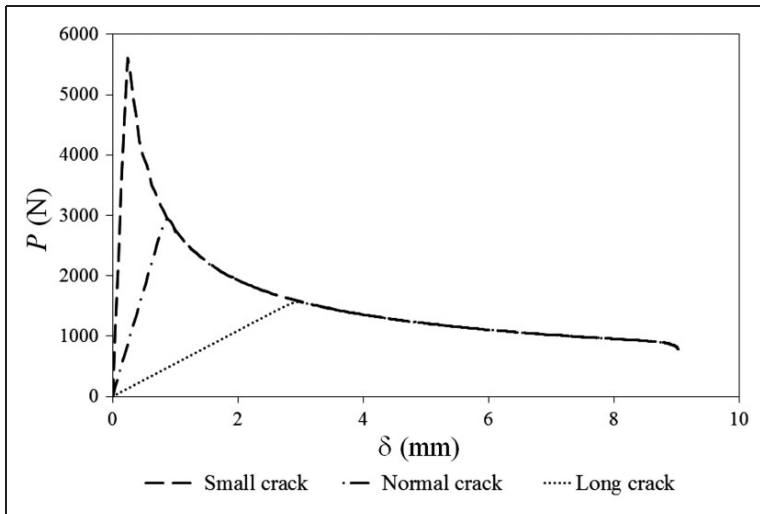
Figure 13. Numerical P–δ curves of three different initial crack lengths. All the dimensions are of the normal DCB specimen, except the initial crack length.
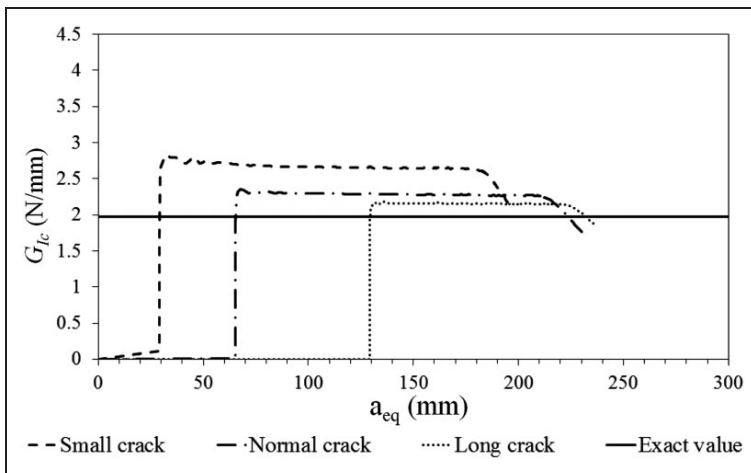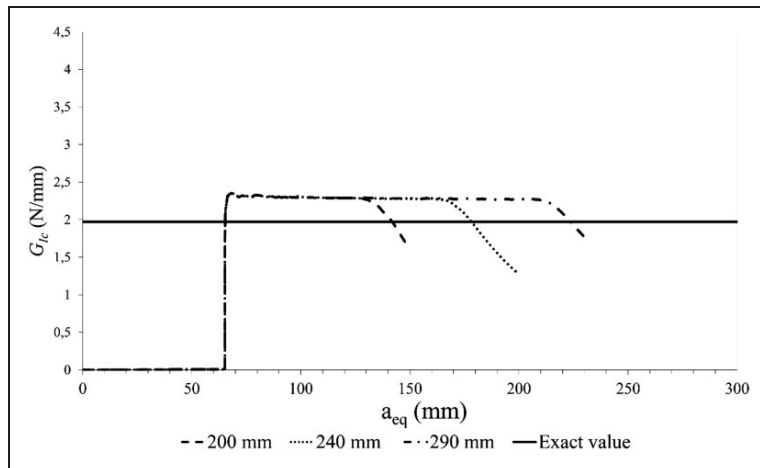

Figure 14. Numerical R-curves of three different initial crack lengths, using the CBBM method. All the dimensions are of the normal DCB specimen, except the initial crack length.

environmental chambers, the test process often requires a specimen with a reduced length. In order to investigate this parameter, three specimen lengths were used: 290 mm, 240 mm and 200 mm. The fracture toughness in the plateau region (Figure 15) is in this case almost constant and it can be assumed that there is no influence of this parameter. This means that if there is enough length for a stable propagation of the crack, the fracture toughness is not influenced by the length of the specimen, which can be reduced even further if need be.

Specimen width. Three different widths were used: 50 mm, 25 mm and 10 mm. The failure load increased proportionally with the width, but the shape of the R-curves was identical, as was the fracture toughness in the plateau region. This shows that the decrease of the width has no influence on the G_{IC}, which is useful because diffusion in the bondline of the DCB specimen is slower for wider specimens, and a reduction of the section can greatly decrease the period of a durability study.

Substrate thickness. Three substrate thicknesses were studied: 15 mm, 12.7 mm and 9 mm. The CBBM method shows a fracture toughness that is the same in all cases (Figure 16). The equivalent crack length (a_{eq}) presents a different initial value in

Figure 15. Numerical R-curves of the three different specimen lengths, using the CBBM method. All the dimensions are of the normal DCB specimen, except the length.
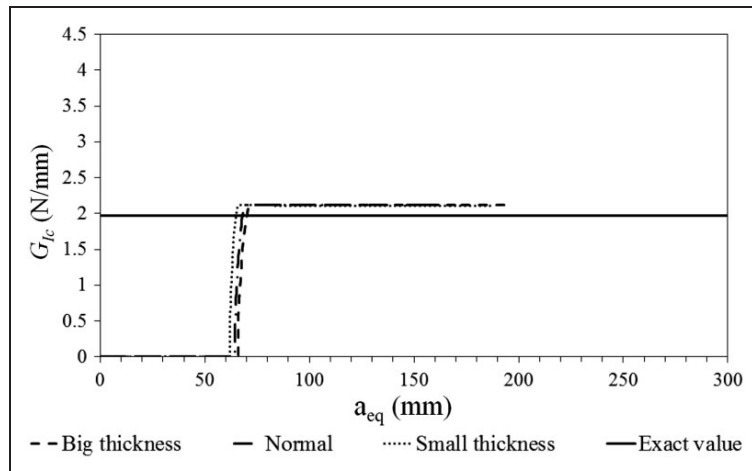
Figure 16. Numerical R-curves of the three different substrate thicknesses, using the CBBM method. All the dimensions are of the normal DCB specimen, except the substrate thickness.
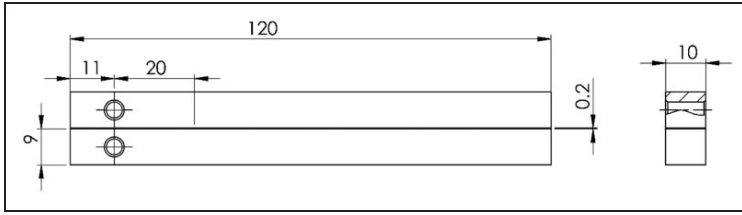
Figure 17. Geometry of the small DCB specimen (dimensions in mm).
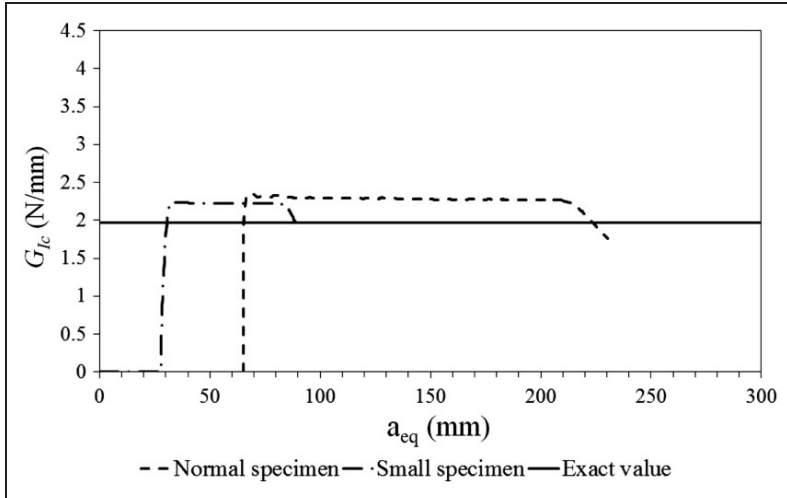

Figure 18. Numerical *R*-curves for the normal and small DCB specimen, using the CBBM method.
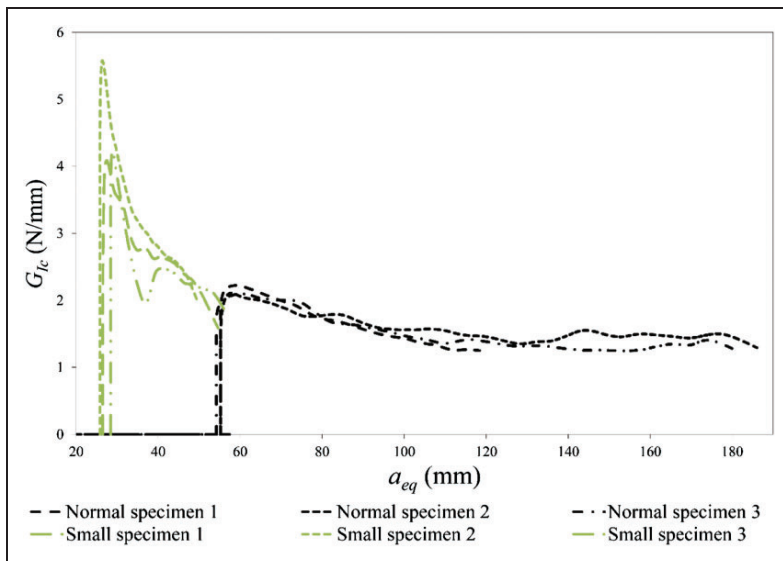

Figure 19. *R*-curves of experimental small and normal DCB specimen tested with SikaPower 4720 using the CBBM method.

all tests because it accounts for the fracture process zone (FPZ), which depends on the substrate thickness: a wider substrate means a bigger FPZ.[17]

Small specimen. After the evaluation of the different parameters presented above, a small specimen was designed with the geometry presented in Figure 17. It takes advantage of the lack of influence on the fracture toughness of both specimen length and width, while keeping the fracture toughness results similar to the normal specimen (Figure 18). The reason for the width being defined to 120 mm was to fit in the environmental chamber we have available, which would only allow a maximum width of 125 mm. The stresses in the specimen were also studied, and those present on the proposed small specimen are in the same order of magnitude as the ones in normal DCB specimen, meaning that same steel can be used.

Experimental validation of the smaller specimens

To manufacture the smaller specimens, the same techniques used for the normal specimens were employed.
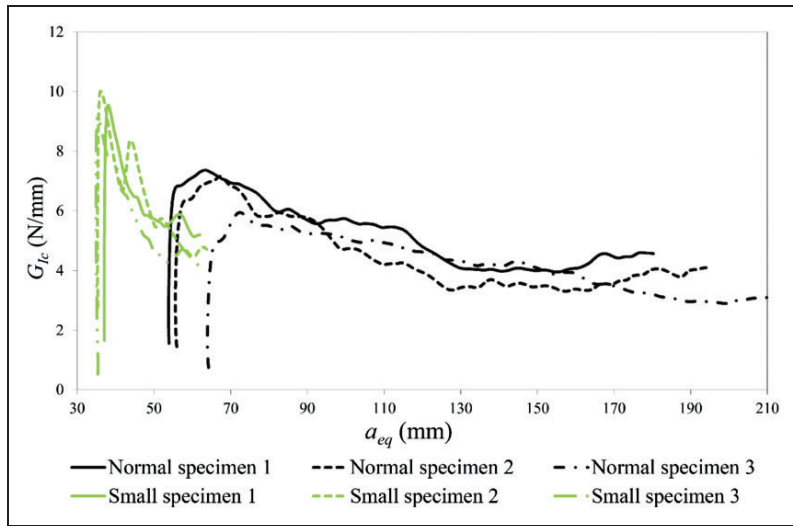
Figure 20. R-curves of experimental small and normal DCB specimen tested with XNR 6852-1 using the CBBM method.
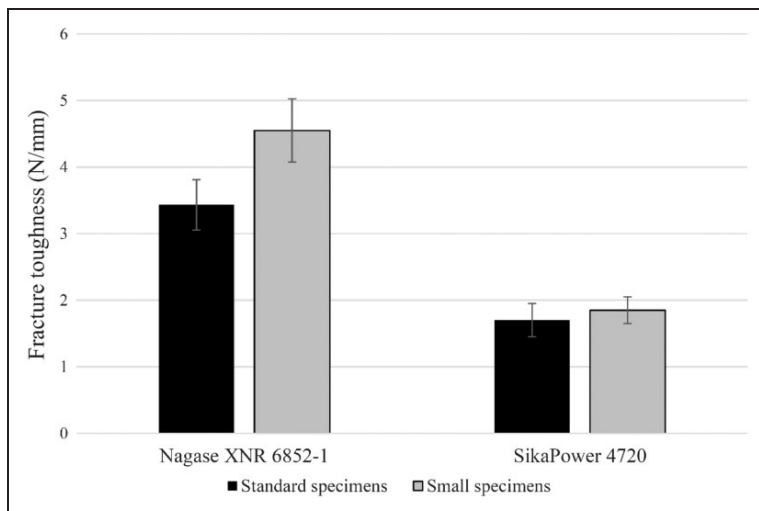
Figure 21. Average and standard deviation of fracture toughness results for all the tested DCB specimens.

51

The initial rigidity (Figure 19, the difference in the peak fracture toughness for small and normal specimens) is not the same for all the specimens, part of the reason being the variation of the initial crack length for the normal and short DCB specimens. Throughout the work done with the normal and small specimens it is clearly much easier to control the manufacturing process for the small specimens, e.g. bondline thickness and the initial crack length. The disadvantage is that because of the reduced dimensions of the small specimens, the initial crack propagation was obstructed by the machine's holding mechanism, but by using the CBBM method we could overcome this problem.

The initial fracture toughness is higher for the small specimen (Figures 19 and 20). This is because a smaller initial crack produces higher fracture toughness (see Figure 14), which then stabilises to a value representative of the true fracture toughness through the stable propagation of the crack which happened in all specimens.

Figure 21 shows that the difference for the obtained fracture toughness between small and normal DCB specimens is small, and therefore can be used to determine the fracture toughness of the adhesives with accuracy. The rupture was cohesive in all tests, guaranteeing that the adhesive toughness was being measured.

Conclusion

The proposed final geometries were able to produce acceptable results similar to those obtainable using standard specimens. Refined bulk specimens showed that by decreasing the stress concentration in the specimen, the values for tensile strength were increasingly closer to those obtainable by standard dogbone specimens. The chosen specimen geometry (Figure 4(c) with a 54 mm radius) produces better results for the tensile strength mechanical property than both the EN ISO 527-2 specimen and 25 mm radius specimen, which validates the use of said geometry for future studies. Average values for the tensile strength in the proposed small bulk specimen of 61.9 MPa and 34.1 MPa for the Nagase XNR 6852-1 and SikaPower 4720, respectively, are similar to the average values of 59.1 MPa and 25.8 MPa for the standard dogbones. Furthermore, the increase of the cross section in the small specimen is useful to prevent unexpected failure during tests, which can be further aggravated through degradation tests.

Regarding DCBs, the reduced geometry has proven that values similar to the standard defined by ASTM 3433 can be obtained, at the expense of obstructed view of the initial crack propagation, which is a problem solved by using the CBBM method. Average values of the fracture toughness for the small DCB where 4.55 N/mm and 1.84 N/mm for the Nagase XNR 6852-1 and SikaPower 4720,

respectively, which were also similar to the standard DCB results of 3.44 N/mm and 1.63 N/mm.

Due to both these refined specimens the full characterisation of cohesive zone model properties (through the tensile strength and fracture toughness) is possible, using smaller and easier to manufacture specimens, without compromising the accuracy of the measured properties. It also eases the process of ageing and testing, because smaller specimens translate to quicker water saturation on the adhesive.

References

1. da Silva LFM and Öchsner A. *Modeling of adhesively bonded joints*. Berlin: Springer, 2008, p.x.
2. Thouless MD. Cohesive-zone modeling of adhesive joints. In: Denier JP and Finn MD (eds) *Mechanics down under*. Netherlands: Springer, 2013, pp.249–255.
3. Banea MD and da Silva LFM. Adhesively bonded joints in composite materials: An overview. *Proc IMechE, Part L: J Materials: Design and Applications* 2009; 223: 1–18.
4. Liljedahl CDM, Crocombe AD, Wahab MA, et al. Damage modelling of adhesively bonded joints. *Int J Fract* 2006; 141: 147–161.
5. Liu J, Li J and Liu L. Finite element analysis for brittle and ductile fracture using a unified cohesive zone model. *Adv Mech Eng* 2013; 2013.
6. Campilho RDSG, Banea MD, Neto JABP, et al. Modelling adhesive joints with cohesive zone models: Effect of the cohesive law shape of the adhesive layer. *Int J Adhes Adhes* 2013; 44: 48–56.
7. Chen X, Deng X, Sutton MA, et al. An inverse analysis of cohesive zone model parameter values for ductile crack growth simulations. *Int J Mech Sci* 2014; 79: 206–215.
8. da Silva LFM, Öchsner A and Adams R. *Handbook of adhesion technology*. Springer reference. Berlin; London: Springer, 2011.
9. da Silva LFM. *Testing adhesive joints best practices*. Weinheim: Wiley VCH, 2012.
10. Campilho RDSG, Moura DC, Banea MD, et al. Adherend thickness effect on the tensile fracture

toughness of a structural adhesive using an optical data acquisition method. *Int J Adhes Adhes* 2014; 53: 15–22.

11. Carlberger T and Stigh U. Influence of layer thickness on cohesive properties of an epoxy-based adhesive—An experimental study. *J Adhes* 2010; 86: 816–835.

12. Mostovoy S and Ripling E. Effect of joint geometry on the toughness of epoxy adhesives. *J Appl Polym Sci* 1971; 15: 661–673.

13. Crocombe AD and Ashcroft IA. Prediction of joint strength under humid conditions with cyclic loading. In: *Design of adhesive joints under humid conditions*. Berlin-Heidelberg: Springer, 2013, pp.147–182.

14. Sugiman S, Crocombe AD and Aschroft IA. Experimental and numerical investigation of the static response of environmentally aged adhesively bonded joints. *Int J Adhes Adhes* 2013; 40: 224–237.

15. Tsujimura TY. High toughness composites based on insitu polymerizable thermoplastic epoxy-resin. In: *9th international conference and forum - SAMPE Europe SEICO 12*, 2012.

16. da Silva LFM, Adams RD and Gibbs M. Manufacture of adhesive joints and bulk specimens with high-temperature adhesives. *Int J Adhes Adhes* 2004; 24: 69–83.

17. de Moura MFSF, Campilho RDSG and Goncalves JPM. Crack equivalent concept applied to the fracture characterization of bonded joints under pure mode I loading. *Compos Sci Technol* 2008; 68: 2224–2230.

18. de Moura MFSF, Goncalves JPM, Chousal JAG, et al. Cohesive and continuum mixed-mode damage models applied to the simulation of the mechanical behaviour of bonded joints. *Int J Adhes Adhes* 2008; 28: 419–426.

19. da Silva LFM, Esteves VHC and Chaves FJP. Fracture toughness of a structural adhesive under mixed mode loadings. *Mater Werks* 2011; 42: 460–470.

Paper C

Effect of humidity on the mechanical properties of adhesively bonded aluminium joints

M Costa[1], G Viana[1], LFM da Silva[2] and RDSG Campilho[3]

Abstract

The presented work focuses on the effects of water degradation on the long-term behaviour of adhesive joints. The objective of this study is to measure the evolution of various mechanical properties such as tensile stress and fracture toughness as a function of humidity for two distinct adhesives, using bulk adhesive and double cantilever beam specimens in unaged and aged conditions in order to understand the influence of humidity on the adhesive properties. A mathematical equation that allows the prediction of each property degradation as a function of water is proposed and validated, which takes into account various parameters such as the diffusion coefficient, resulting in a general equation for mechanical property degradation prediction of potentially any adhesive. It was also found that the distinct adhesive properties such as strength, stiffness and fracture toughness all decreased due to water degradation with the exception of the strain that increased, concluding that water reduces the joint strength and lifespan of the studied adhesives, although in different ways.

Introduction

Adhesion technology is increasingly more studied and implemented in various industries, such as the automotive and aeronautical, in order to solve some problems related to the traditional methods of joining (bolting, riveting, welding, and others). Regarding the automotive industry, adhesion technology is increasingly more used both in the assembly of supplementary elements (windows, windscreens, rubber joints and inside cladding) as in structural applications.[1] Aeronautical joints were the pioneers of adhesive bonding, where both structural and sealing capacities are desired, each with distinct stiffness and mechanical requirements, resulting in incredible structural efficiency and durability present in some aircrafts that could not have been achieved with conventional riveted structures.[2] Both these industries, and others, are not only concerned with adhesion effectiveness but also with weight efficient structures, which are essential for optimising fuel consumption. As such, aluminium and composites components are often employed and bonded with adhesives, therefore achieving maximum weight reduction. The growing availability of a variety of new materials and significant advances in bonding technology have allowed engineers to trust adhesive

joints as a viable alternative to other joining techniques. Because of this, the study and understanding of adhesives has never been more pertinent.

Adhesive joints are, in many situations, exposed to severe environment conditions during their lifetime that will weaken the adhesive properties as well as the bond strength, thus losing the ability to maintain a good adhesion.[3] For both aeronautical and automotive applications, the majority of adhesive-bonded components are exposed to moist air, with varying humidity[4] and temperature[5] throughout the year and location. When the relative humidity is high over a period of time, the strength and fatigue performance of the joint will gradually decline.[6] Temperature is also known to influence the fracture toughness of an adhesive joint.[7] Furthermore,

[1]INEGI Polo FEUP, Oporto, Portugal
[2]Departamento de Engenharia Mecânica, Faculdade de Engenharia da Universidade do Porto (FEUP), Oporto, Portugal
[3]Departamento de Engenharia Mecânica, Instituto Superior de Engenharia do Porto (ISEP), Instituto Politécnico do Porto, Oporto, Portugal

Corresponding author:
Marcelo Costa, INEGI – FEUP Rua Dr. Roberto Frias, 400 Porto, 4200-465 Portugal.
Email: marcelo.costa@fe.up.pt

environmental conditions may have an indirect impact on an adhesive joint, for example if they influence the adherend (by thermal expansion of a metal adherend or humidity infiltration in a composite adherent) or the interface between adherend and adhesive.

Focusing on humidity, water diffusion on to an adhesive joint can be through the adhesive, the adhesive–adherend interface and by cracks or flaws in the adhesive. There are some phenomena responsible for the water degradation of a joint which are: plasticisation, swelling, hydrolysis or cracking of the adhesive, degradation or change of the interface resulting in loss of adhesion, and corrosion of the substrate. Even though water can negatively affect the adhesive properties, the main factor in the weakening of joints is the water attack on the interface, which causes the most damage and leads to degradation and loss of adhesion between the adhesive and the adherends. As mentioned before, aluminium structures are very interesting for structural applications, but the interface between aluminium–adhesive is severely weakened when subjected to moisture. To counteract this effect, surface treatments such as acid etching and phosphoric acid anodising are mandatory for structural joints that rely on aluminium components. Interestingly, the pioneering industries in the use of adhesively bonded weight efficient structures using aluminium joints were the ones that developed surface treatments, notably Boeing who patented the phosphoric acid anodising treatment in 1978.[8] The characterisation of humidity's influence on an adhesive is made using Fick's law, which represents the mass gain of a specimen as a function of submersion time, and as a result two parameters can be defined: the diffusion coefficient (related to the speed of water penetration) and the mass at equilibrium (the final mass of the specimen when total water saturation is achieved). Adhesives can exhibit two distinct Fickian behaviours: single Fick and dual Fick. Single Fick is represented by a linear initial behaviour (whose slope is the diffusion coefficient) that eventually stabilizes when saturation is achieved, unlike dual Fick adhesives which have two consecutive and distinct linear stages (therefore they have two diffusion coefficients) and only after the second stage is saturation achieved. In theory, specimen thickness should not influence the behaviour of water or the parameters of Fick's law, a notion postulated by Fujita[9] who suggested that sorption with different film thicknesses superimpose on a plot of M_t/M_∞ against $\sqrt{h}/e$ (where M_t/M_∞ is the mass gain, $\sqrt{h}$ is the square root of submersion time and e is the film thickness), but recent studies have found that adhesives which exhibit dual Fick behaviour shift to single Fick with an increase in specimen thickness.[10]

The mechanical properties are key parameters to characterise and differentiate adhesives, and as such the study of humidity on their influence is mandatory to correctly characterise their degradation due to the environment. Various studies have been made in this regard, from analysis of the stress distribution changes due to humidity on single lap joints,[11] the joint strength decrease with water exposure time,[12] and the effect humidity has on the stress–strain curves and the fracture toughness of an adhesive.[13] In any case, further studies are needed in this regard because humidity influence is very important for adhesive performance and various different types of adhesives behave differently when in contact with water.

In the present work, humidity's influence on two adhesives is experimentally investigated, including the mass gain due to water, the effect on the stress–strain curves and corresponding mechanical properties, how the fracture toughness varies with humidity, and also how the degraded properties can be predicted using a proposed mathematical model.

Geometric study

When studying humidity, one must equate the time it takes for water to penetrate the adhesive and degrade the adhesive fully throughout the joint. In the case of bulk specimens, this is not as relevant because all the specimen surfaces are in contact with humidity and therefore the time it will take for the specimen to saturate is only related to the thickness. But when dealing with adhesive joints, studied using specimens such as single lap joints (SLJ) and double cantilever beams (DCB), the saturation time is directly related to the length water must travel to fully saturate the joint, which in most cases means the width of said specimens.

In the case of SLJs, previous works[14] have studied and defined optimised geometries for aluminium joints exposed to water, reducing the width of 25.4 mm recommended by the standard[15] to 5 mm, obtaining excellent agreement of experimental and predicted results. For DCB specimens, a previous work was performed[16] to reduce the standard defined width of 25.4 mm[17] to 10 mm. A geometry study was performed to define aluminium adherends with 5 mm width (equivalent to that of Sugiman et al.[14]). It is mandatory that the adherends do not reach the elastic limit and results are comparable with those resulting of standard specimens.

The considered aluminium alloy was 6082-T6, which is commonly used in the railway and automotive industries. Experimental characterisation of the alloy was made using three specimens as shown in Figure 2(c), and the resulting properties are presented in Table 1.

The geometry of the aluminium adherends was set to 120 mm length (due to dimensional restrains imposed by the climatic chamber were these adherends may be used), a width of 5 mm (to match the thickness used in other works[14] and accelerate the

diffusion of water), and an initial crack length of 10 mm (this is the critical case, as the crack length cannot be inferior due to manufacturing difficulties and problems applying the load). What remains to be defined is the thickness of the adherends, where no yielding can occur, and thus the maximum stress may not be higher than the yield strength (Table 1). Two different fracture toughness values were considered, 2 N/mm and 4 N/mm, with the objective of visualising the effect of G_{Ic} on the maximum stress and also to have adherends that are able to withstand very high values of fracture toughness (4 N/mm is unusually high, thus serving as a safety factor). Simulia ABAQUS® (Providence, RI) was used to calculate the stresses in a DCB joint using the previously mentioned geometry and properties with a bondline thickness of 0.2 mm, and the results are presented in Figure 1. COH2D elements (with a size of 0.2 mm) were used for the adhesive layer and CPE4R (plane-strain 4-node quadrilateral solid, reduced integration) elements for the adherends.

It can be seen in Figure 1 that, for a G_{Ic} of 2 N/mm, even a 5 mm thick adherend will be able to perform without yielding, making it a cost effective solution

when testing adhesives with a fracture toughness equal or below that value. For a G_{Ic} of 4 N/mm the stresses present in the adherend are naturally higher, and thicknesses inferior to 8 mm cannot be used. Selecting a thickness of 10 mm marginally increases the used material cost and provides an extra safety factor, thus justifying the use of such thickness for DCB specimens studying adhesives with a fracture toughness up to 4 N/mm.

## Experimental details

Adhesive characterisation

Two adhesives with distinct properties were studied with the objective of determining a degradation law that encompasses as many situations as possible. Studying both a brittle and a ductile adhesive that have very different behaviour when in contact with water allows for a more generalized trend to be found. The first epoxy adhesive, XNR 6852-1, supplied by NAGASE CHEMTEX® (Osaka, Japan), is a one-part system that cures at 150 °C for 3 h. It has a linear structure, which allows greater freedom of movement to the chains, unlike the cross-linked structure of a conventional epoxy adhesive. As a consequence, this polymer has some features of thermoplastic polymers due to the resulting linear structure. The second adhesive is SikaPower 4720, supplied by SIKA® (Vila Nova de Gaia, Portugal). This adhesive is a two-part system that cures at room temperature for 24 h. Both these adhesives are characterised in the following section.

Table 1. Experimental properties obtained for the 6082-T6 alloy.

Yield strength (MPa)	Ultimate strength (MPa)	Strain at failure (%)
284.1 ± 6.8	322.1 ± 4.8	15.5 ± 0.7
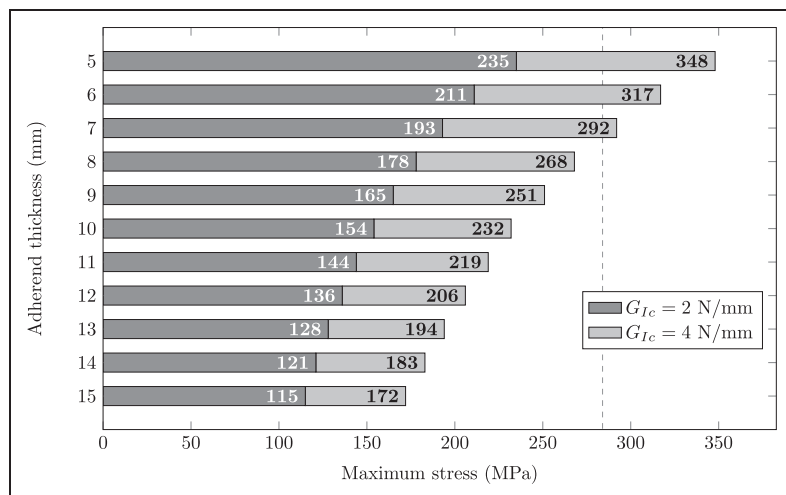
Figure 1. Maximum stress value measured in the adherend for varying thicknesses and two fracture toughness values, with a dashed line corresponding to the yield strength of the aluminium alloy.
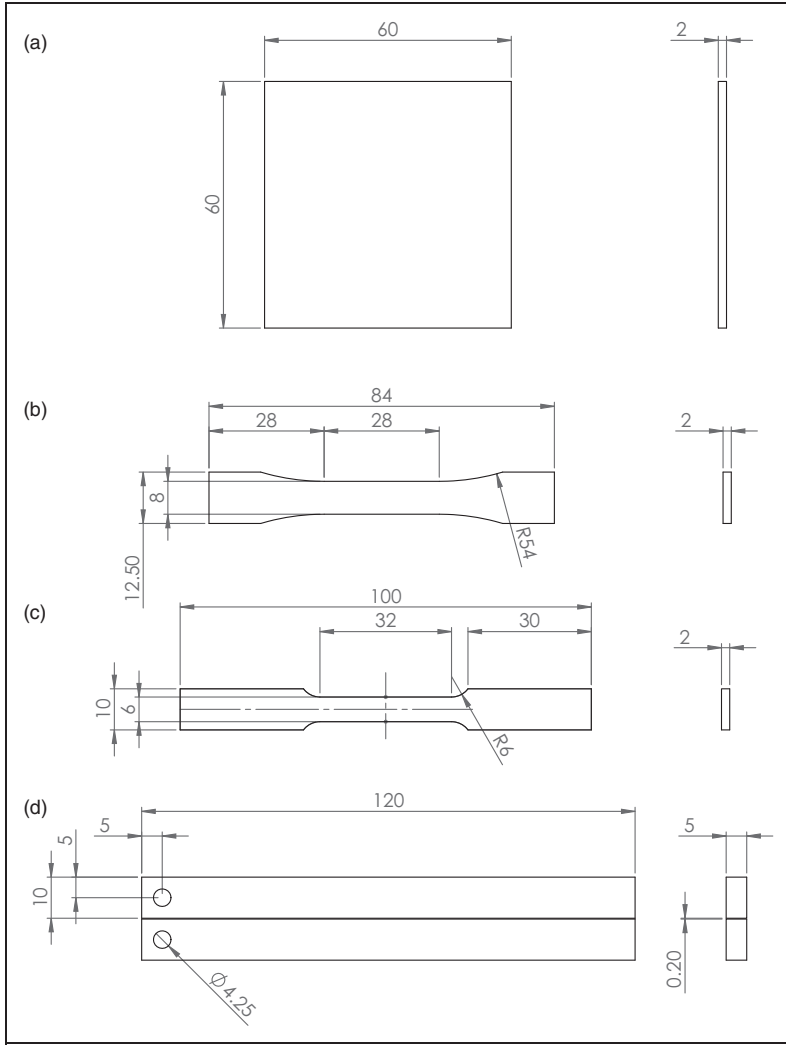
Figure 2. Specimen used in this work and respective geometries: a) diffusion square plates,[18] b) adhesive bulk specimens,[16] c) aluminium bulk specimens[19] and d) DCB specimens (dimensions in mm).

Specimen geometry

To characterise the effects of humidity on adhesively bonded aluminium joints several types of specimens are needed. First, the diffusion of water must be measured, using bulk adhesive square plates of 60 mm sides and 2 mm thickness as defined by ASTM D955,[18] shown in Figure 2(a). The adhesive bulk specimen geometry is in accordance with a previous study[16] and is shown in Figure 2(b). The characterisation of the aluminium alloy was according to ASTM E8[19] subsize specimen, as shown in Figure 2(c). Finally, the geometry of the DCB specimens, which was determined in 'Geometric study' section, is shown in Figure 2(d).

Humidity characterisation

The water diffusion on to adhesives and adhesive joints can be modelled using Fick's law which can then be used to easily predict the mass of water absorbed or desorbed as a function of time. Fick's first law states that the flux in x-direction (F_x) is proportional to the concentration gradient (dC/dx), and the proportionality is defined by a constant D called the diffusion coefficient.[11] Fick's second law defines the non-steady state of diffusion where diffusion will occur onto all axis, and is commonly arranged as a function of the critical direction, such that:

$$\frac{dC}{dt} = D\frac{\partial^2 C}{\partial x^2} \tag{1}$$

If we assume a film of adhesive of thickness h that is submerged in an infinite bath (water is always available to penetrate the adhesive), equation (1) has the following solution:

$$\frac{M_t}{M_\infty} = 1 - \frac{8}{\pi^2} \sum_{n=1}^{\infty} \left(\frac{1}{(2n-1)^2} \right) \exp\left(-\frac{(2n-1)^2 D\pi^2}{h^2} t \right)$$

(2)

Where M_t is the mass at time t and M_∞ is the mass at equilibrium. Using equation (2) one can model the mass increase due to water of an adhesive for any instant t, with the pre-requisite of performing experimental tests to determine both M_∞ and D parameters.

When an adhesive is subjected to water, the mass gain is linear up until the point of $M_t/M_\infty \sim 0.6$,[9] and before this point the following relationship is valid:

$$\frac{M_t}{M_\infty} = \frac{4\sqrt{Dt}}{\sqrt{\pi}h}$$

(3)

Equation (3) can then be used to determine D as a function of the experimental details such as the total mass at saturation M_∞, the time t needed to reach $M_t/M_\infty = 0.6$ and the specimen thickness h.

Testing conditions

To obtain the adhesive properties (in both dry and wet stages) and the aluminium properties, the specimens shown in Figure 2(b) and (c) were tested in an INSTRON® model 3367 universal test machine (Norwood, MA) with a capacity of 30 kN, at room temperature and constant displacement rate of 1 mm/min. The stress is obtained directly from the load cell read force divided by the test area, but the strain required the use of an optical method, as an extensometer could not be used due to the grip length of 50 mm while the specimen has only 28 mm of test area. Also, in the case of adhesive bulk specimens, the extensometer inflicts some stress concentrations when it grips the adhesive, which can cause severe problems especially for aged specimens which have reduced mechanical properties.

The DCB specimens presented in Figure 2(d) were tested in an MTS® servo hydraulic machine (Eden Prairie, MN), using a constant displacement rate of 0.5 mm/min. Both the applied load and displacement were measured, which were then post-processed using the Compliance-based beam method (CBBM)[20] to obtain the fracture toughness. The advantage of the CBBM is that it makes it possible to deduce an equivalent crack length through the application of Timoshenko's beam theory, eliminating the need to constantly measure the crack visually and the inevitable visual errors.

Experimental results

Diffusion tests

Three specimens according to Figure 2(a) were manufactured for each adhesive and dried in an oven. They were weighed and afterwards submerged in a recipient filled with distilled water, in a controlled temperature environment of 32 °C. The weight of all specimens was measured periodically, and the resulting Fick's Law is shown in Figure 3, along with the respective parameters in Table 2.

The x-axis of Figure 3 is represented as the square root of time divided by the thickness of the specimen.
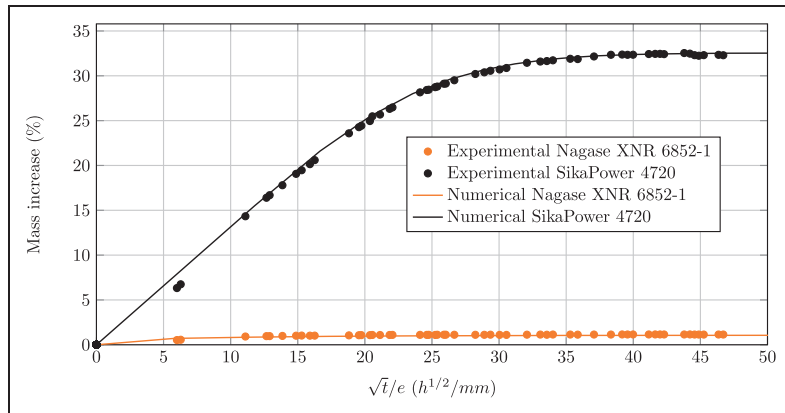

Figure 3. Experimentally measured weight increases overlaid on equation (2) results for both adhesives.

This happens for two reasons: first, the square root of time makes it easier to calculate the slope of the initial linear part, which is the coefficient of diffusion; secondly, the division by the thickness of the specimen is to make sure the diffusion coefficient is independent of specimen thickness (because in the manufacturing of the water submerged bulk specimens slight differences in the thickness occur, and also different types of specimens may have different thicknesses when submerged in water). Both adhesives have very different total mass uptake, with SikaPower 4720 gaining 32.5% of mass due to distilled water, while Nagase shows an increase of 1.3%. This is a clue to the

different behaviour of each adhesive when subjected to water, which will translate to noticeable changes in the mechanical properties. Although SikaPower 4720 absorbs much more water than Nagase XNR 6852-1, the velocity of absorption (the diffusion coefficient) is approximately five times lower than Nagase XNR 6852-1, meaning that it takes five times more time than Nagase XNR 6852-1 to absorb the same amount of water.

Mechanical properties as a function of humidity

Bulk tensile tests were performed with the specimens shown in Figure 2(b), for both adhesives in the dry state and in various aged stages, with the objective of determining the variation of mechanical properties as a function of water content. Figure 4 presents the resulting stress–strain curves for three aged stages and the unaged state.

Figure 4 presents some interesting results. First, the very different unaged properties of both adhesives can be visualised, particularly the different tensile stress and strain at failure. SikaPower 4720 is brittle while Nagase XNR 6852-1 is ductile, and the tensile strength of SikaPower is roughly half of Nagase's. The ageing of each adhesive is also very

Table 2. Key properties for both adhesive's diffusion behaviour.

| Property | Adhesive | | Units |
	Nagase XNR 6852-1	SikaPower 4720	
Diffusion coefficient (D)	5.02×10^{-13}	0.89×10^{-13}	(m²/s)
Mass at equilibrium (M_{∞})	1.3	32.5	(%)
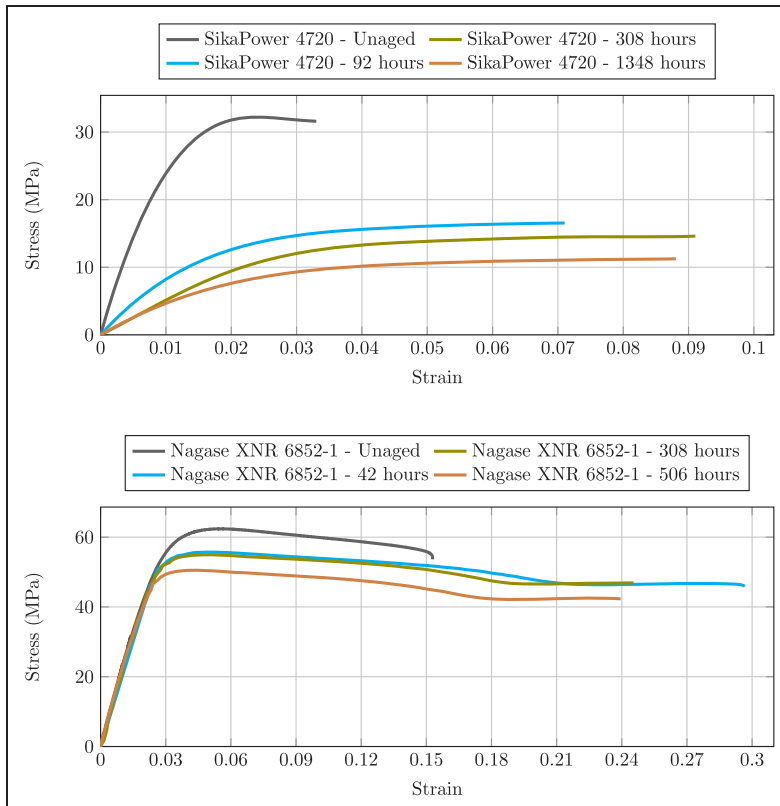
Figure 4. Stress–strain curves for both adhesives in the unaged and three aged stages.

different: SikaPower 4720 shows a clear decrease of tensile strength and Young's modulus with water, while Nagase XNR 6852-1 presents a less pronounced decrease of tensile strength and maintains the Young's modulus. The strain is also increased for both adhesives with water, as expected.

Prediction of properties degradation due to water

Now that various water content data is gathered, it is possible to model a mathematical formulation to fit the existing experimental data and make it possible to deduce the reduction of mechanical properties for each adhesive. Equation (4) presents the proposed solution.

$$y(x) = (y_0 - y_f) * e^{-x/C} + y_f \qquad (4)$$

Where y is the property being predicted, y_0 is the property value in the unaged stage, y_f the value in the fully saturated stage, x is the amount of relative humidity present in the joint, and C is an empirical constant that in theory would be related to each adhesive. Eureqa® (Somerville, MA) was used to find an approximation of C as a function of each adhesive properties, which was further refined to reach the following definition:

$$C = \frac{10^{13}}{2} \cdot D \cdot M_\infty \qquad (5)$$

Figure 5 shows the result of combining Equation (4) and (5) and applying them to the mechanical properties previously shown.

The results presented in Figure 5 show a very good correlation between experimental values and predicted values from the equations. Furthermore, the equation constant C changes for each adhesive but is not dependent on the mechanical property being predicted. In other words, the same C for Nagase XNR 6852-1 can be used to predict the degradation of Young's modulus, tensile strength and also strain at failure for that adhesive.

## Fracture toughness as a function of water

Another important mechanical property of adhesive joints is the energy they are able to absorb before failure, usually measured through the fracture toughness.[21] It is expected that the fracture toughness decreases with an increase in the water content, a trend often seen in the literature.[22,23] For these tests the specimens shown in Figure 2(d) were used, and Figure 6 shows the effect of humidity on the fracture toughness of the studied adhesives. Due to the amount of time needed to fully saturate each DCB specimen the relative humidity was studied up to 60%, which already presents a very clear trend in degradation of the fracture toughness.

A moderate decrease in the fracture toughness, corresponding to SikaPower 4720, can be seen in Figure 6 (top) with the increase in water content on the joint. Because, with humidity, the maximum load that the joint can withstand decreases, but the displacement increases, the area beneath the curve (which is directly related to the fracture toughness) may change in either way (increase, decrease or stay constant). In this case, it appears to decrease slightly. A different trend, visible in Figure 6 (bottom), is exhibited by Nagase XNR 6852-1, where an increase in fracture toughness is evident from the unaged stage (6 N/mm) to 25% relative humidity (10 N/mm). Because Nagase XNR 6852-1 experiences very little water absorption (see Table 2), the maximum load that the aged joint can withstand is similar to the unaged joint. But because the ductility of the aged joint increases, this leads to an area beneath the load–displacement that is higher, and thus a higher fracture toughness is observed. This can be compared with the results of the bulk specimens (Figure 5), where a decrease in tensile strength is much less evident for the 25% RH Nagase XNR 6852-1 specimens. Increasing the relative humidity of Nagase XNR 6852-1 past 25% leads to a decrease in the fracture toughness similar to the one exhibited by SikaPower 4720.

Humidity also influences the glass transition temperature (T_g) by decreasing it,[24,25] and a decrease in T_g leads to a decrease in the tensile stress the adhesive can withstand and also an increase in ductility. In a study on the effect of humidity on both studied adhesives,[26] it was found that the T_g of Nagase XNR 6852-1 decreases by approximately 20 °C (from 120 °C to 100 °C) from the dry state to full saturation, which is a small difference and likely to have little effect on the results. On the other hand, SikaPower 4720 exhibits a much higher decrease in T_g from the dry to wet stage (from approximately 100 °C to below room temperature). This means that the fracture toughness of SikaPower 4720 will be reduced even further due to the drastic change in T_g, while for Nagase XNR 6852-1 only the effect of ductility should be noticeable, because small changes in T_g and tensile stress due to low water absorption will not affect the maximum load as much as SikaPower 4720. The failure surface was cohesive in all cases.

The results presented in Figure 6 can be visualized in such a way that a trend may be inferred, as shown in Figure 7.

The presented equation is a polynomial formula, and the relevant constants were determined using the same methodology and software as described in 'Prediction of properties degradation due to water' section. The constants all depend on each adhesive's mechanical properties in the dry state (for example, the fracture toughness, tensile strength, etc.) and on Fick's law parameters (see Table 2), but due to their complexity are not presented here. The maximum deviation between the experimental value and the
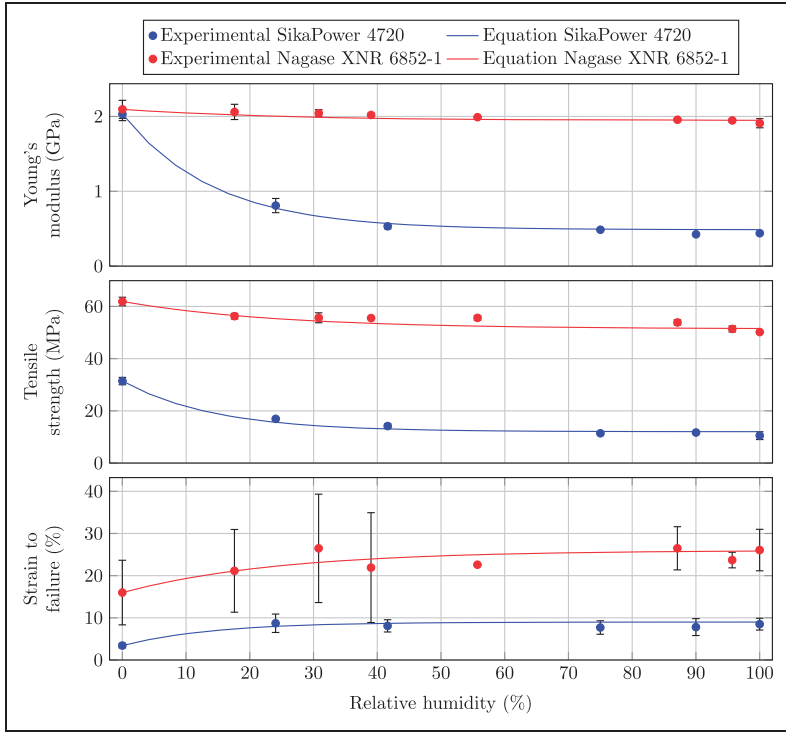
Figure 5. Prediction of mechanical properties using the proposed mathematical equation.

value predicted by the formula is 0.09 N/mm (for SikaPower 4720 at 60% RH, which still falls within the standard deviation), which is considered in excellent agreement with the experimental data.

The difference between the formulas presented in Figure 5 and Figure 7 may be explained by the different mechanisms of water ingress in the distinct specimens: in bulk specimens water penetrates much quicker because all specimen sides are exposed, while for DCB specimens only a small fraction of the adhesive is exposed to water, which has an effect on the velocity of water penetration, thus degrading the properties in a different manner.

Conclusions

The degrading influence of different humidity levels on the various properties of adhesive joints was determined. Mass uptake experimental tests were performed and two very distinct adhesive behaviours were found: Nagase XNR 6852-1 absorbs a very little amount of water when submerged compared with SikaPower 4720 (1.3% and 32.5% respectively), which is a desirable property in an adhesive, because less water content translates to smaller decreases in the mechanical properties of an adhesive. But although Nagase XNR 6852-1 is preferable in terms of total mass increase, SikaPower 4720 absorbs water roughly five times more slowly than Nagase XNR

6852-1 (the diffusion coefficients are 0.89×10^{-13} m^2/s and 5.02×10^{-13} m^2/s respectively), which can be considered a safety factor because there is more time to detect and fix issues in a structural joint that uses an adhesive with slower water absorption velocity. Regarding the mechanical properties, the decrease in both Young's modulus and tensile strength of Nagase XNR 6852-1 was much less evident than the decrease of SikaPower 4720, as seen in Figure 5, which is related to the fact that Nagase absorbs much less water. Evident in Figure 5 is a new proposed mathematical equation that presents a very good correlation between experimental data of degraded properties and the predicted values. Furthermore, the equation was written in terms of adhesive properties and water uptake coefficients, signalling that it should be capable of predicting not only the properties of the studied adhesives but others as well. In terms of fracture toughness degradation due to water, SikaPower 4720 shows a decrease in G_{Ic} with an increase of humidity, while Nagase XNR 6852-1 exhibits an increase of G_{Ic} initially when water is present in the adhesive, but then decreases as well with increasing humidity. This is in accordance to what is expected: humidity is known to reduce the maximum load the joint can withstand, but that effect is compensated with the increase in displacement before failure, and thus the area beneath the curve (which is related to the fracture toughness) can vary in a way
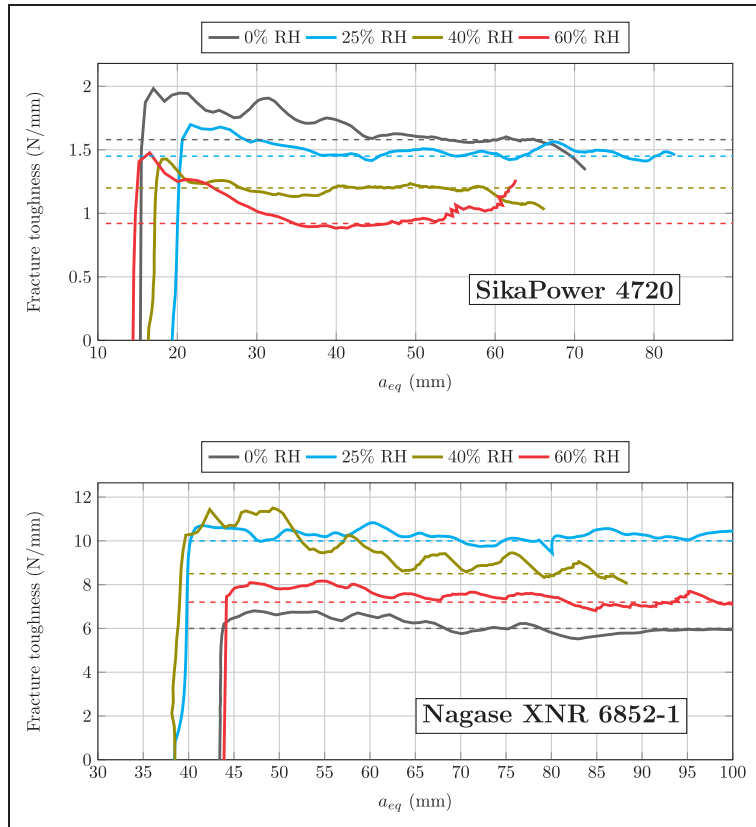
Figure 6. *R*-curves for SikaPower 4720 (top) and Nagase XNR 6852-1 (bottom) in the unaged and aged stages, with the plateau corresponding to each curve shown as a dotted line.
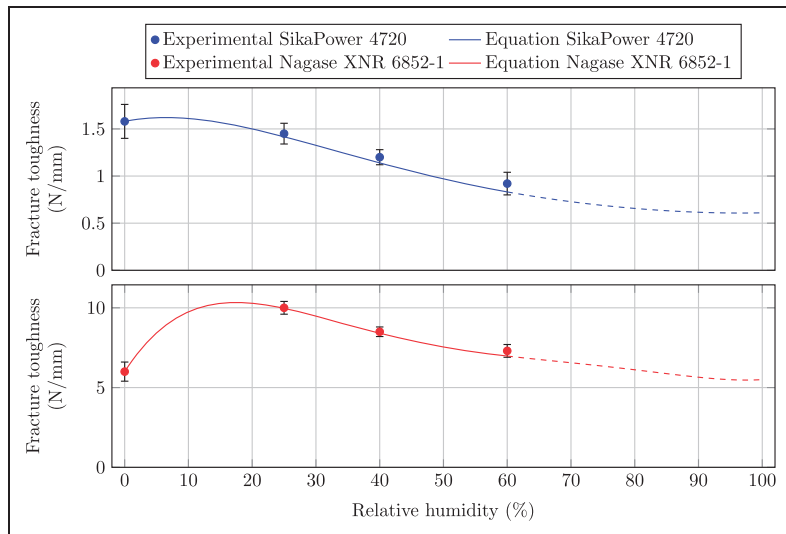
Figure 7. Fracture toughness values for both the studied adhesives as a function of humidity content, overlaid with a proposed formula for prediction of said properties.

specific to each adhesive. The presented results will be very useful to understand further investigations made into humidity effects on adhesive joints, such as the fatigue behaviour.

Declaration of conflicting interests

The author(s) declared no potential conflicts of interest with respect to the research, authorship, and/or publication of this article.

References

1. Pizzi A and Mittal KL. *Handbook of adhesive technology, revised and expanded.* New York, USA: Taylor & Francis, 2003.
2. Hart-Smith LJ. Adhesively bonded joints in aircraft structures. In: da Silva LM, Öchsner A and Adams R (eds) *Handbook of adhesion technology*. Berlin, Germany: Springer Berlin Heidelberg, 2011, pp.1101–1147.
3. Katnam K, Sargent J, Crocombe A, et al. Characterisation of moisture-dependent cohesive zone properties for adhesively bonded joints. *Eng Fract Mech* 2010; 77: 3105–3119.
4. Pethrick RA. Design and ageing of adhesives for structural adhesive bonding – A review. *Proceedings of the Institution of Mechanical Engineers, Part L: Journal of Materials Design and Applications* 2015; 229: 349–379.
5. Marques E, da Silva LF, Banea M, et al. Adhesive joints for low-and high-temperature use: an overview. *J Adhes* 2015; 91: 556–585.
6. Wang M, Liu A, Liu Z, et al. Effect of hot humid environmental exposure on fatigue crack growth of adhesive-bonded aluminum A356 joints. *Int J Adhes Adhes* 2013; 40: 1–10.
7. Banea M, Da Silva L and Campilho R. Mode I fracture toughness of adhesively bonded joints as a function of temperature: experimental and numerical study. *Int J Adhes Adhes* 2011; 31: 273–279.
8. Marceau JA, Firminhac RH and Moji Y. *Method for providing environmentally stable aluminum surfaces for adhesive bonding and product produced.* USA: The Boeing Company, 1978.
9. Fujita H. Free-volume model of diffusion in polymer solutions. *Adv Polym Sci* 1961; 3: 1–47.
10. Loh W, Crocombe A, Wahab MA, et al. Modelling anomalous moisture uptake, swelling and thermal characteristics of a rubber toughened epoxy adhesive. *Int J Adhes Adhes* 2005; 25: 1–12.
11. Ashcroft I and Crocombe A. Prediction of joint strength under humid conditions: damage mechanics approach. In: da Silva LFM and Sato C (eds) *Design*

of adhesive joints under humid conditions*. Berlin, Germany: Springer Berlin Heidelberg, 2013, pp.123–146.
12. Brewis D, Comyn J and Shalash R. The effect of moisture and temperature on the properties of an epoxide-polyamide adhesive in relation to its performance in single lap joints. *Int J Adhes Adhes* 1982; 2: 215–222.
13. Crocombe A and Ashcroft I. Prediction of joint strength under humid conditions with cyclic loading. In: da Silva LFM and Sato C (eds) *Design of adhesive joints under humid conditions*. Berlin, Germany: Springer Berlin Heidelberg, 2013, pp.147–182.
14. Sugiman S, Crocombe AD and Aschroft IA. Experimental and numerical investigation of the static response of environmentally aged adhesively bonded joints. *Int J Adhes Adhes* 2013; 40: 224–237.
15. International A. D1002 – Standard Test Method for apparent shear strength of single-lap-joint adhesively bonded metal specimens by tension loading (metal-to-metal). ASTM international, 2010.
16. Costa M, Viana G, Canto C, et al. Effect of the size reduction on the bulk tensile and double cantilever beam specimens used in cohesive zone models. *Proc IMechE, Part L: J Materials Design and Applications.* Epub ahead of print 7 October 2015. doi: 10.1177/1464420715610248.
17. International A. D3433 – Test method for fracture strength in cleavage of adhesives in bonded metal joints. ASTM International, 1999.
18. International A. D955 – Standard test method of measuring shrinkage from mold dimensions of thermoplastics. ASTM International, 2000.
19. International A. E8 – Standard test methods for tension testing of metallic materials. ASTM International, 2000.
20. de Moura MFSF, Campilho RDSG and Goncalves JPM. Crack equivalent concept applied to the fracture characterization of bonded joints under pure mode I loading. *Compos Sci Technol* 2008; 68: 2224–2230.
21. Chaves FJ, da Silva L, de Moura M, et al. Fracture mechanics tests in adhesively bonded joints: a literature review. *J Adhes* 2014; 90: 955–992.
22. Armstrong G, Banks W, Pethrick R, et al. Dielectric and mechanical studies of the durability of adhesively bonded aluminium structures subjected to temperature cycling. Part 2: examination of the failure process and effects of drying. *Proc IMechE, Part L: J Materials Design and Applications* 2004; 218: 183–192.
23. Pethrick R, Armstrong G, Banks W, et al. Dielectric and mechanical studies of the durability of adhesively bonded aluminium structures subjected to temperature cycling. Part 1: examination of moisture absorption. *Proc IMechE, Part L: J Materials Design and Applications* 2004; 218: 169–182.
24. Zhang Y, Adams R and da Silva LF. Absorption and glass transition temperature of adhesives exposed to water and toluene. *Int J Adhes Adhes* 2014; 50: 85–92.
25. Barbosa A, da Silva L and Öchsner A. Hygrothermal aging of an adhesive reinforced with microparticles of cork. *J Adhes Sci Technol* 2015; 29: 1714–1732.
26. Viana G, Costa M, Banea M, et al. Behaviour of environmentally degraded epoxy adhesives as a function of temperature. *J Adhes* 2016. Submitted for publication.

Paper D
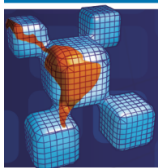
Effect of Humidity on The Fatigue Behaviour of Adhesively Bonded Aluminium Joints

Abstract

The present work focuses on the effects of water degradation on the fatigue behaviour of adhesive joints bonded with aluminium adherends. The objective of this study is to measure the influence that humidity has on the fatigue crack growth velocity of two distinct adhesives characterized using the Paris Law, using double cantilever beam (DCB) specimens in unaged and various aged conditions loaded in mode I in order to understand the influence that water content has on the Paris Law constants. It was found that the slope of the Paris Law curve is not heavily changed with the presence of water, but a shift in the curves does occur, generally resulting in a crack initiating at a lower threshold than in the unaged adhesive. Based on this behaviour, it can be concluded that an increase in water content reduces the fatigue joint strength and lifespan of adhesive joints bonded with the studied adhesives.

Keywords

fatigue, environment, humidity, Paris Law.

M. Costa [a*]

G. Viana [a]

L. F. M. da Silva [b]

R. D. S. G. Campilho [c]

[a] INEGI, Rua Dr. Roberto Frias 400, 4200-465 Oporto, Portugal

[b] DEM, FEUP, Rua Dr. Roberto Frias s/n, 4200-465 Oporto, Portugal

[c] DEM, ISEP-IPP, Rua Dr. António Bernardino de Almeida 431, 4200-072 Oporto, Portugal

* Author e-mail: marcelo.costa@fe.up.pt

1 INTRODUCTION

Adhesion technology is increasingly more studied and implemented in various industries, such as the automotive and aeronautical, in order to solve some problems related to the traditional methods of bonding (bolting, riveting, welding, and others). For the automotive industry, adhesives are increasingly more applied both in the assembly of supplementary elements (inside cladding, rubber joints, windows and windscreens) as in structural applications (Pizzi and Mittal 2003). These adhesives are then subjected to humidity due to the various places vehicles may exist in, and are also subjected to fatigue solicitations (driving through holes, hills, even driving in a simple road will cyclically load the structure of a car). Aeronautical joints were the pioneers of adhesive bonding, where both structural and sealing capacities are desired, each with distinct stiffness and mechanical requirements, resulting

in incredible structural efficiency and durability present in some aircrafts that could not have been achieved with conventional riveted structures (Hart-Smith 2011). Airplanes experience environments with distinct humidity conditions, and are also subjected to cyclic loads (with higher intensity at take-off and landing, but also during flight). Both these industries, and others, are not only concerned with adhesion effectiveness but also with weight efficient structures, which are essential for optimising fuel consumption. As such, aluminium and composites components are often employed and bonded with adhesive, therefore achieving maximum weight reduction. The growing availability of a variety of new materials and significant advances in bonding technology have allowed engineers to trust adhesive joints as a viable alternative to other joining techniques. Because of this, the study and understanding of adhesives has never been more pertinent.

Expanding on the humidity and fatigue remarks made before, adhesive joints are, in many situations and industries, exposed to severe environment conditions during their lifetime that will weaken the adhesive properties as well as the bond strength, thus losing the ability to maintain a good adhesion (Katnam et al. 2010). For both aeronautical and automotive applications, the majority of adhesive-bonded components are exposed to moist air, with varying humidity and temperature throughout the year and location. When the relative humidity (RH) is high over a period of time, the strength and fatigue performance of the joint will gradually decline (Wang et al. 2013). Furthermore, environmental conditions may have an indirect impact on an adhesive joint, for example if they influence the adherend (by thermal expansion of a metal adherend or humidity infiltration in a composite adherend) or the interface between adherend and adhesive.

If we focus on humidity, water diffusion on to an adhesive joint can happen through the adhesive, the adhesive-adherend interface and by cracks or flaws in the adhesive. There are some phenomena responsible for the water degradation of a joint, which are: plasticisation, swelling, hydrolysis or cracking of the adhesive, degradation or change of the interface resulting in loss of adhesion, and corrosion of the substrate. Even though water can negatively affect the adhesive properties, the main factor in the weakening of joints is the water attack on the interface, which causes the most damage and leads to degradation and loss of adhesion between the adhesive and the adherends. The characterisation of humidity's influence on an adhesive is made using Fick's law, which represents the mass gain of a specimen as a function of submersion time, and as a result two parameters can be defined: the diffusion coefficient (related to the speed of water penetration) and the mass at equilibrium (the final mass of the specimen when total water saturation is achieved). Adhesives can exhibit two distinct Fickian behaviours: single Fick and dual Fick. Single Fick is represented by a linear initial behaviour (whose slope is the diffusion coefficient) that eventually stabilizes when saturation is achieved, unlike dual Fick adhesives which have two consecutive and distinct linear stages (therefore they have two diffusion coefficients) and only after the second stage is saturation achieved. In theory, specimen thickness should not influence the behaviour of water or the parameters of Fick's law, a notion postulated by Fujita (1961) who suggested that sorption with different film thicknesses superimpose on a plot of M_t/M_∞ against $\sqrt{h}/e$ (where M_t/M_∞ is the mass gain, $\sqrt{h}$ is the square root of submersion time and e is the film thickness), but recent studies have found that adhesives which exhibit dual Fick behaviour shift to single Fick with an increase in specimen thickness (Loh et al. 2005). Temperature is also known to affect the Fickian behaviour of an adhesive, as an increase in temperature leads to an higher coefficient of diffusion, although the mass at equilibrium remaining the same (Rodrigues

et al. 2016. Submitted). This is useful to reach saturation faster in experimental tests, although care must be taken so the test temperature is well below the glass transition temperature (T_g) of the adhesive.

As mentioned before, aluminium structures are very interesting for structural applications, but the interface between aluminium-adhesive is severely weakened when subjected to moisture. To counteract this effect, surface treatments such as acid etching and phosphoric acid anodising are mandatory for structural joints that rely on aluminium components. Interestingly, the pioneering industries in the use of adhesively bonded weight efficient structures using aluminium joints were the ones that developed surface treatments, notably Boeing who patented the phosphoric acid anodising (PAA) treatment in 1978 (Marceau et al. 1978). The issue of bonding adhesives to aluminium adherends gave rise to various types of surface treatments being investigated and developed, such as chromic acid anodizing (CAA), chromic acid etching (CAE), sulphuric acid anodization (SAA), the aforementioned PAA, and others. Under static conditions the effect of the surface treatment is not extremely felt, for example in the case of a lap shear strength test performed by Briskham and Smith (2000) were the PAA treated joint exhibited a 25 MPa strength compared to 21 MPa by the simply abraded joint. The true benefit has been shown in various works (Briskham and Smith 2000, Lefebvre et al. 2002, Fernando et al. 1996, Kinloch et al. 2000, Abel et al. 2006) to happen under fatigue conditions where PAA joints have proved to be the superior surface treatment for the various conditions studied by the authors. As a result, PAA is the optimal treatment to apply in adhesive bonds subjected to environment, especially those that are subjected to fatigue (Costa et al. 2016. Submitted).

When studying fatigue, two approaches may be taken: establishing S-N curves, where joints are tested under varying stresses and/or environments until failure and plotted in a diagram to determine the expected fatigue life, or Paris Law curves, which measure the crack growth velocity of an adhesive under different environments. Both are useful and have consequently been studied by various authors, although not as much as would be expected (Costa et al. 2016. Submitted). As a result, results exist but do not always paint a clear picture on what happens to an aged joint (Costa et al. 2016. Submitted).

Paris Law, which is the fatigue approach studied in this work, consists on the cyclical solicitation of a joint, which is then subjected to periodic measurements of crack length. Simply put, this leads to information on the various crack dimensions at specific cycles, which is then used to obtain the variation of the crack length through the entire test. How that variation is obtained depends on the method selected, and ASTM E647 (2000)defines two: the secant method and the polynomial method. With this information the Paris Law may be obtained, as is shown in Figure 1.

Paris Law consists of three regions: the first (Zone 1) where crack initiation occurs, the second (Zone 2) where stable crack propagation happens, and lastly Zone 3 where failure of the joint takes place. Zone 2 is the key area, where a line (after logarithmic axis are applied) can be obtained and two constants obtained: m, the slope, and C, the intersection of the line with the y-axis. A bigger value for m (maintaining C) would translate in a crack that propagates more quickly, while a higher C (maintaining m) means that the crack propagates by a larger length each time, although at the same speed.

Although studying fatigue, the static mechanical properties are also important. They need to be obtained to define the fatigue loading (for example, maximum fatigue load is 60% of maximum static

load), and also are needed to help justify the fatigue differences between aged stages (for example, if the ductility increases a lot from 40% to 60% RH, we may expect that the crack propagation speed decreases for those same stages) and between different adhesives.

In the present work, humidity's influence on the fatigue properties of two adhesives is experimentally investigated, including the mass gain due to water and the effect on the Paris Law curves and corresponding constants.
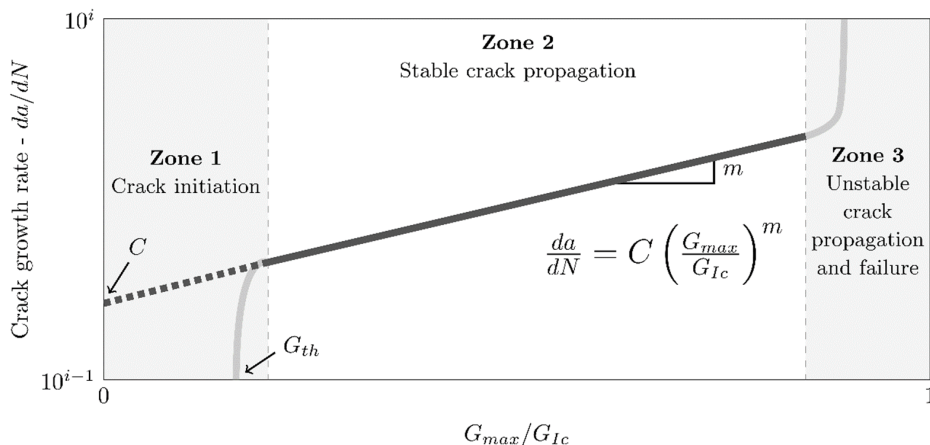

Figure 1: Representation of the Paris Law for adhesive joints.

2 EXPERIMENTAL DETAILS

2.1 Adhesive Characterization

Two adhesives with distinct properties were studied with the objective of determining the fatigue behaviour degradation due to humidity for distinct conditions. The first epoxy adhesive, XNR 6852-1, supplied by NAGASE CHEMTEX® (Osaka, Japan), is a one-part system that cures at 150 °C for 3 hours. It has a linear structure, which allows greater freedom of movement to the chains, unlike the cross-linked structure of a conventional epoxy adhesive. As a consequence, this polymer has some features of thermoplastic polymers due to the resulting linear structure. The second adhesive is SikaPower 4720, supplied by SIKA® (Vila Nova de Gaia, Portugal). The tensile properties of each adhesive and the fracture toughness (G_{IC} have been determined in a previous work (Costa et al. 2016) and are reproduced in Table 1.

Adhesive	Young's Modulus (MPa)	Tensile Strength (MPa)	Strain at failure (%)	G_{IC} (N/mm)
NagaseXNR 6852-1	2095 ± 120.8	61.88 ± 1.64	15.99 ± 7.66	5.89 ± 0.62
SikaPower 4750	2030.9 ± 86.7	31.41 ± 1.41	3.45 ± 0.55	1.58 ± 0.18

Table 1: -Mechanical properties of each adhesive for the unaged state (Costa et al. 2016).

Moisture absorption tests have also been performed to determine the behaviour of each adhesive when submerged in water (Costa et al. 2016), which was modelled using Fick's law. The diffusion coefficient (D) and mass at equilibrium (M_∞) for each adhesive are reproduced in Table 2.

Adhesive	Diffusion coefficient (m^2/s)	Mass at equilibrium (%)
Nagase XNR 6852-1	5.02×10^{-13}	1.3
SikaPower 4750	0.89×10^{-13}	32.5

Table 2: Fick's law coefficients for both studied adhesives (Costa et al. 2016).

The remaining needed adhesive information is how they degrade when in contact with water. The fatigue behaviour will be studied and presented in this paper, but the static behaviour will also be necessary to aid in the discussion of results. The degradation of each mechanical property presented in Table 1 has been determined (Costa et al. 2016), and a handy formula was established to find the value of the property as a function of the relative humidity content. The formula for Young's modulus, tensile strength and strain is the following:

$$y(RH) = \left(y_0 - y_f\right) * \exp\left(-\frac{RH}{(10^{13}/2) \cdot D \cdot M_\infty}\right) + y_f \tag{1}$$

Where y is the mechanical property being predicted, y_0 is the property value in the unaged stage, y_f the value in the fully saturated stage, RH is the percentage value of relative humidity present in the joint ($0 \leq RH \leq 100$), and both D and M_∞ are the Fick's law coefficients already presented in Table 2 for each adhesive. The formula for the fracture toughness is not so simple and as such is not presented here. Nonetheless, the values themselves are available in (Costa et al. 2016) for examination if desired.

2.2 Specimen Geometry

To characterise the effects of humidity on the fatigue response of adhesively bonded aluminium joints reduced double cantilever beam (DCB) specimens were used as shown in Figure 2. Themainpurpose of suchspecimenisthereduction of thewidth of theadhesivelayer (5 mm in the case of Figure 2 and 25.4 mm for the standard DCB specimens (ASTM 1999)) due to the fact that humidity takes a long time to ingress into the adhesive layer, and thus the level of joint saturation (relative humidity) progresses much slower the thicker the width, as illustrated in Figure 3. Reduction of the length of the specimen (120 mm) is also desirable so that the specimens can be fully immersed in the available flasks and furthermore fit inside the environmental test chamber (so that in future studies temperature may also be studied). Care must be taken so that the reduction of dimensions results in results comparable to those of the standard DCB, and to that effect previous studies have been published (Costa et al. 2015).
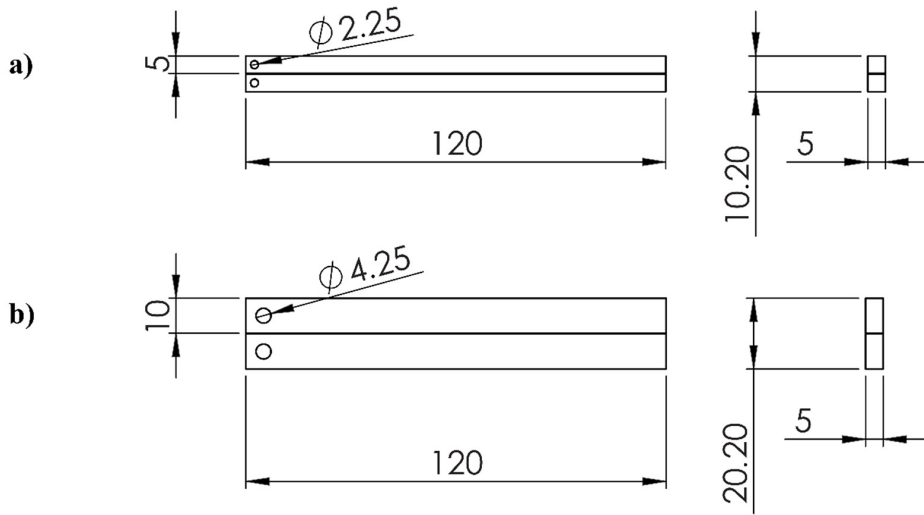
Figure 2: Reduced DCB specimen dimensions used for mode I tests: a) specimen used with the SikaPower 4720 adhesive, b) specimen used with the Nagase XNR 6852-1 adhesive (dimensions in mm).

Figure 2 shows two identical types of reduced DCB specimens, the only difference between them being substrate thickness (in one case 5 mm, and in the other 10 mm). This is the case because a preliminary optimised specimen (Figure 2 a)) was defined under the assumption of $G_{Ic} \cong 2$ N/mm, which was based on the fact that both SikaPower 4720 and Nagase XNR 6852 (the previous version of the adhesive studied in this work – note the absence of "-1" in the designation) had a G_{Ic} inferior or around 2 N/mm (as published in (Saldanha et al. 2013) for Nagase XNR 6852). After specimen manufacturing, immersion and testing it was noticed that while the SikaPower 4720 specimens behaved as expected, Nagase XNR 6852-1 specimens experienced adherend deformation. The fracture toughness tests were performed after this happened, which showed that Nagase XNR 6852-1 had a higher G_{Ic} as shown in Table 1. Because of this a new geometry was defined to avoid plastic deformation of the aluminium adherends, as seen in Figure 2 b). All the Nagase XNR 6852-1 specimens were manufactured according to this geometry, and the 5 mm thickness geometry was maintained for the SikaPower 4720 adhesive (both because of the much longer time needed to saturate the adhesive, as seen in Figure 3, and the fact that several specimens were already submerged and replacing them all would delay the results for SikaPower 4720 for several months).

2.3 Manufacture and Testing Procedures

To obtain the final testable specimen, the following stages had to be followed: application of surface treatment to the aluminum adherends, DCB specimen manufacturing, specimen ageing and finally experimental testing.

The applied surface treatment was phosphoric acid anodizing (PAA), which is the standard surface preparation for aluminum bonds. PAA has positive results under static conditions and excellent results under fatigue conditions (more details can be found in (Costa et al. 2016. Submitted) which reviews various surface treatments for aluminum joints under different conditions). PAA is defined

by ASTM D3933 (ASTM 2010), and as such the procedure detailed in the standard was followed. After application of the surface treatment, the adherends were kept in a contamination-free environment and used for specimen manufacturing between 8 to 24 hours after PAA application. DCB specimen manufacturing was conducted in a custom aluminum mold (to account for the thermal expansion of the aluminum if curing at high temperature and avoid the creation of residual stresses in the joints) and conducted at the temperature and during the time required by each adhesive in a INTOCO® (Staverton, United Kingdom) hot-plates press under 2 MPa hydrostatic pressure. After manufacturing the excess adhesive was removed. Specimen ageing was performed under full immersion in distilled water at 32 °C in a MMM® (Munich, Germany) Friocell environmental chamber. Experimental testing was performed in a MTS® (Minnesota, USA) servo-hydraulic machine under constant load control.
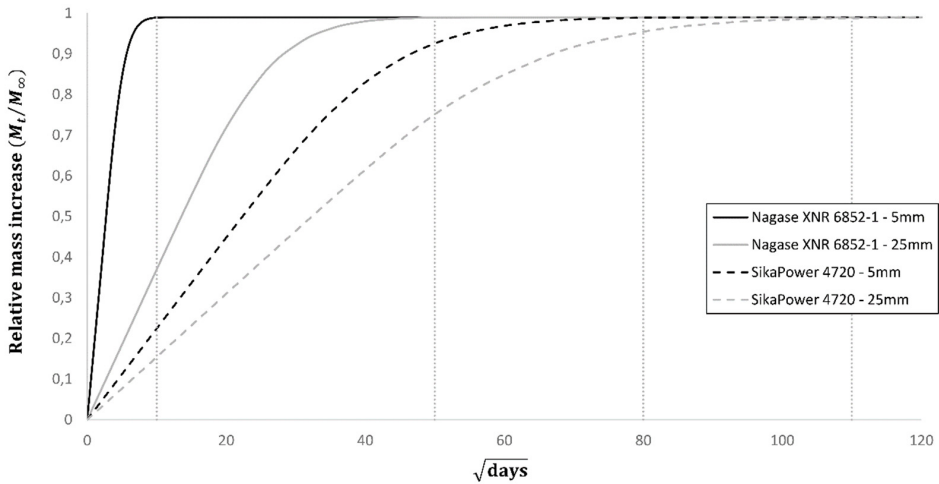
Figure 3: Comparison between saturation times for 5mm and 25mm thicknesses using both adhesives.

Three specimens were first tested under static conditions to obtain the fracture toughness of the adhesive (results published in (Costa et al. 2016)). A side result of such tests was the static failure load (for each adhesive and aged state), which was then used to determine the fatigue parameters. The maximum fatigue load was set to 60% of the static failure load, the frequency was 1 Hz and a ratio of 0.1 was imposed. At least 5 specimens were then tested under fatigue, with the objective of confirming the behavior beyond doubt (fatigue results have a certain associated uncertainty, which could be worsened with) and guaranteeing no further tests are needed (which would require new specimen manufacturing and as such a long time to obtain new results). In each test the applied load and measured displacement were recorded for each cycle. The crack length was obtained using the Compliance-based beam method (CBBM) (de Moura et al. 2008, Fernández et al. 2011), which uses the specimen compliance (determined using the recorded load and displacement) and has the advantage of making it possible to deduce an equivalent crack length through the application of Timoshenko's beam theory, eliminating the need to constantly measure the crack visually and the inevitable visual errors.

Figure 4 shows the raw result of a fatigue test, in this case under a constant load of 120 N, and respective data treatment. Regarding the load-displacement plot, there are three regions: the first part, between 0 and approximately 100 cycles, where the load has not yet, the second section where the load is maintained at the target value and the displacement can be seen to steadily progress in a controlled manner, and finally a third region where unsteady crack growth happens and as such the load can no longer be maintained and the displacement increases abruptly until specimen failure. Through the CBBM method the raw load-displacement data can be used to obtain the equivalent crack length, as pictured in Figure 4 (bottom left), and the maximum strain energy release rate (G_{max}), therefore resulting in all the necessary data to calculate the Paris Law (Figure 4 bottom right). ASTM E647 (ASTM 2000) defines two methods for obtaining the Paris Law: secant method and incremental polynomial method. The latter is more useful for visual measures of the crack length during testing, which will naturally have some errors and as such the method smooths out such errors. The secant method is simpler and, because CBBM already calculates an equivalent crack length, such smoothing is inherent to CBBM and as such the secant method was used in this work.
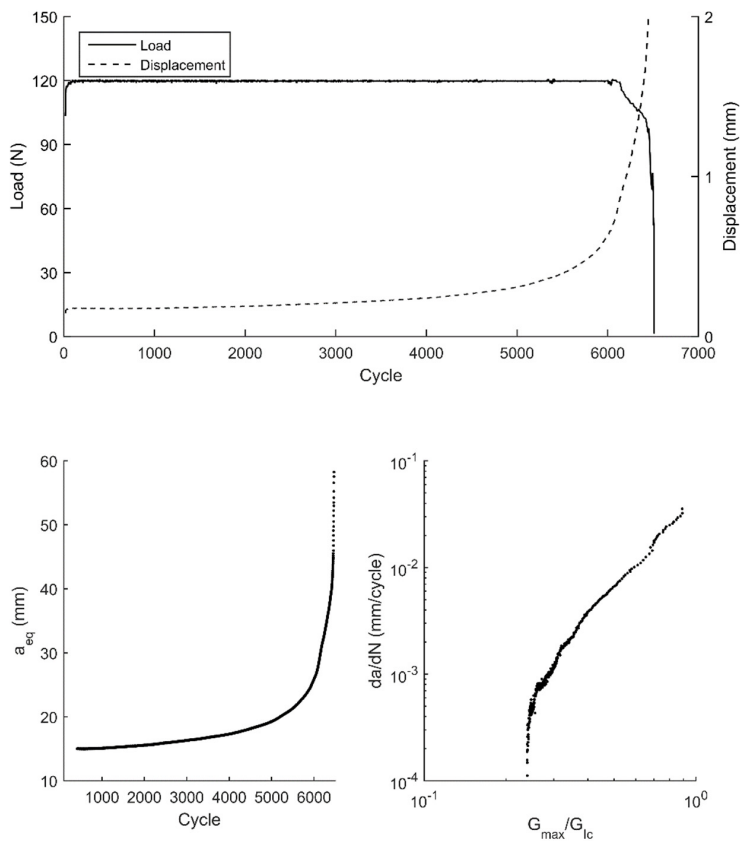

Figure 4: Example of experimental fatigue test: raw load-displacement data direct from machine (top), equivalent crack length as a function of cycles (bottom left), and respective Paris Law representation (bottom right).

3 EXPERIMENTAL RESULTS AND DISCUSSION

3.1 Crack Growth Velocity

Based on the previously presented adhesive moisture absorption data, DCB specimens were taken out of water at specific instances chosen such that the average relative humidity through the joint represented specific values of saturation such as 25% RH, 40%, etc. The results of the unaged state compared with three aged states for both adhesives are presented in Figure 5.
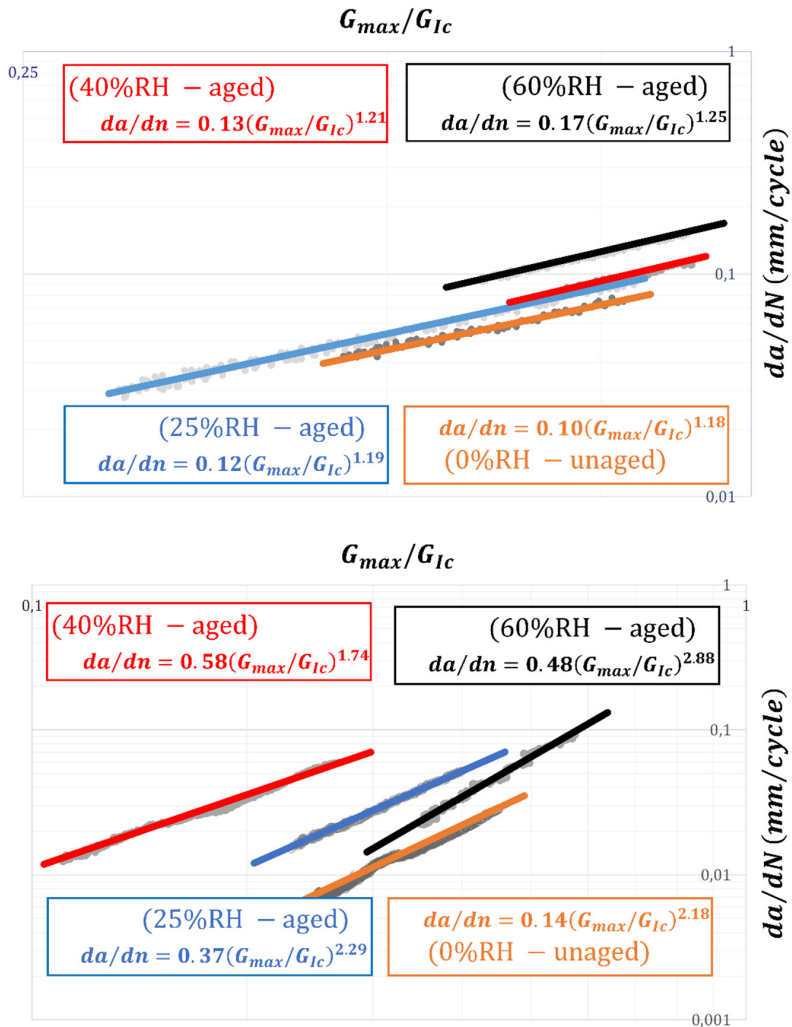
Figure 5: Crack growth velocity as a function of relative humidity:
Nagase XNR 6852-1 (top), SikaPower 4720 (bottom).

For the Nagase XNR 6852-1 adhesive, the results are within what was expected as it is the behaviour usually reported in the literature: an increase of relative humidity translates to a shift in the upper direction of the stable crack propagation part of the Paris Law, which implies that the crack propagates at the same velocity (slope of the line, m, is more or less constant) but starts propagating sooner (G_{th} appears to decrease with an increase of RH, meaning the crack initiates propagation sooner). Specifically regarding the slope, it can be seen that although visually it appears constant, in reality the values in the equation increase with an increase of RH, although very slightly. This makes sense if we consider that the diffusion behaviour of Nagase XNR 6852-1 consists on low mass gain due to water absorption (fully saturates at 1.3%), and thus such a small variation of the slope is not taken into account.

Regarding SikaPower 4720 the situation is not as clear. Although up to 40% RH the behaviour is consistent with the previously exposed notion that an increase in relative humidity shifts the Paris Law upward, for 60% RH the line shifted to the right and the slope increased, effectively signifying that the propagation occurs at a higher velocity (expected), and that the crack starts to propagate at a later G_{th} (which would mean a 60% RH is good to delay crack initiation). This last detail is contradictory with all the previous results, but may be explained due to the huge mass gain experienced by SikaPower 4720 when in contact with water (a 32.5% increase in mass when fully saturated). SikaPower 4720 experiences, when fully saturated, prominent swelling when compared with Nagase XNR 6852-1, as visible in Figure 6, and also attains a rubbery behaviour when handled manually unlike in the unaged state.
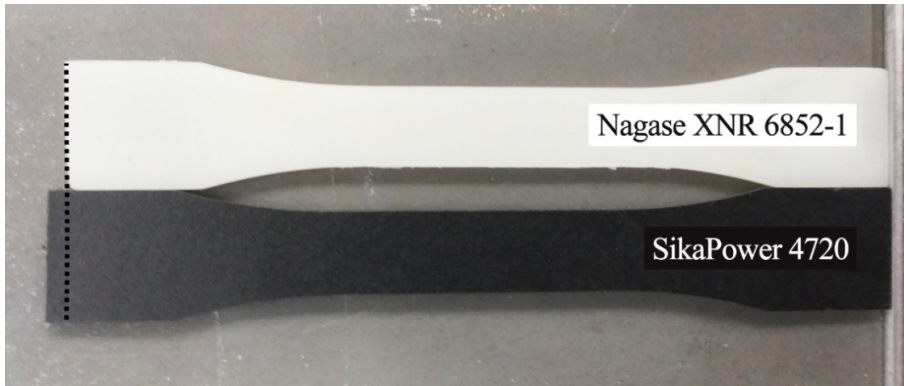
Figure 6: Swelling comparison of both adhesives in the saturated stage.

Such swelling and changes in physical behaviour (rubbery state) may imply hydrolysis and chemical degradation of the adhesive, which explains why the crack propagation velocity is higher. Regarding a later G_{th} than expected, the swelling and increase in ductility (when compared to the unaged and early aged stages) may contribute to extra microscopic obstruction to crack initiation, such as wider voids and water particles absorbing energy, therefore delaying crack initiation. Finally, the glass transition temperature (T_g) of the adhesives in the saturated stage (Viana et al. 2016. Submitted) may offer the final explanation: while in the unaged stage Nagase XNR 6852-1 and SikaPower 4720

have a T_g of 120 °C and 100 °C respectively, in the saturated stage Nagase XNR 6852-1 drops to 100 °C and SikaPower 4720 drops to below room temperature. This has two major consequences: first that there is major degradation of the adhesive due to water, and secondly that the drop from 100 °C at 0% RH to below room temperature at 100% implies that at some stage in-between 0% and 100% RH we begin testing the adhesive at a temperature above its T_g. It is estimated that at around 40% RH the T_g of SikaPower 4720 reaches the ageing temperature and therefore will have its physical properties changed completely, which would certainly explain the change in fatigue behaviour of SikaPower 4720 after that relative humidity value.

Comparing between both adhesives further interesting aspects arise: we see that Nagase XNR 6852-1 has a much slower crack propagation velocity (an m value of around 1.2 when compared to SikaPower which is roughly double), and combining that with the evidence that it absorbs much less water (Table 2), has its mechanical properties barely degraded when in contact with water (Costa et al. 2016), and its fatigue behaviour is more predictable and consistent (Figure 5) makes Nagase XNR 6852-1 an appealing adhesive for long-term applications.

3.2 Prediction of Paris Law Constants

To further compare the fatigue behaviour between both adhesives and in an effort to develop prediction tools for such behaviour, the slope (m) and y-axis intersection (C) values of the Paris Law for all the presented situations was analysed. The behaviour of each variable appears to grow in a quadratic manner with an increase in relative humidity, and as such the following prediction equation was postulated:

$$var(RH) = K \cdot RH^2 + var_0 \tag{2}$$

The idea of Equation 2 is that it is valid for both Paris Law variables and also for both adhesives, and as such the constant K must be determined as dependent on both adhesive properties. Following the same notion as presented in Equation (1) and used in other works (Costa et al. 2016), we postulated that the Fick's Law parameters should be essential to the prediction, and have arrived at the following formulation for K:

$$K = \frac{2}{3} \cdot 10^8 \cdot D \cdot M_\infty \tag{3}$$

By combining Equation 3 with 2 and applying it to both Paris Law parameters results in the behaviour shown in Figure 7 (top and middle), where the experimental points are also overlaid to aid the comparison with the predicted values. The T_g of both adhesives as a function of relative humidity is also presented in Figure 7 (bottom), with further details about the method and results published elsewhere (Viana et al. 2016. Submitted). Two critical areas are shown in the T_g results, which are confined by the temperatures 20 ºC and 32.5 ºC, representing room temperature and ageing temperature, respectively, because when the T_g decreases below such temperatures a drastic change in properties and response may be expected.
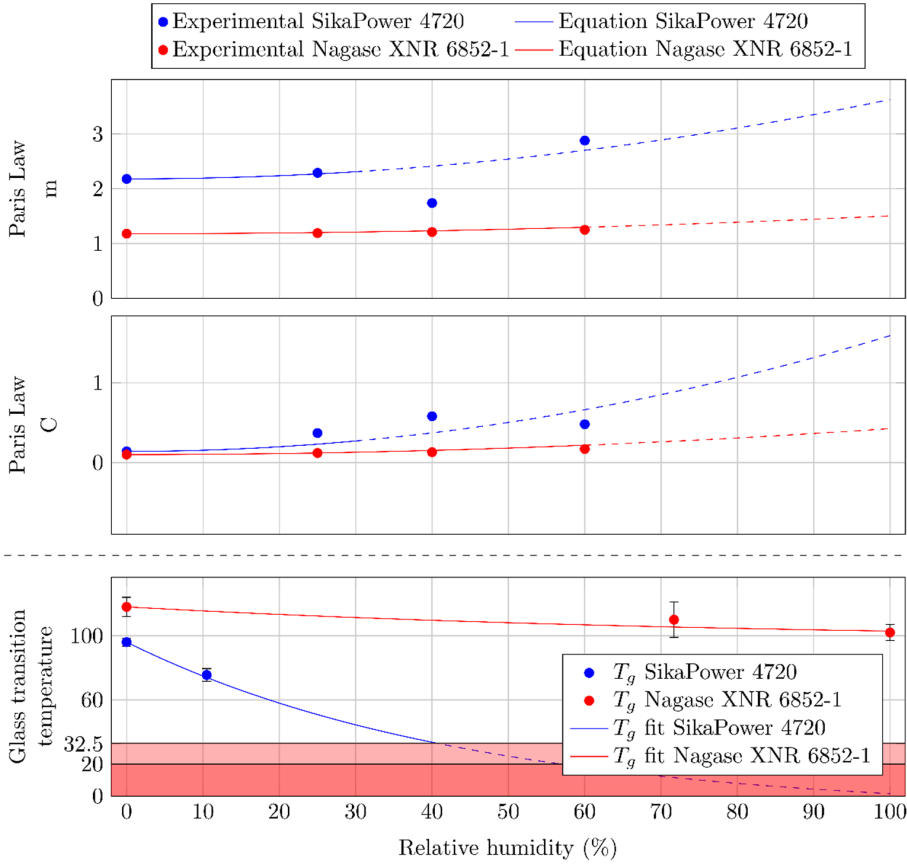
Figure 7: Experimental Paris Law values for both adhesives as a function of relative humidity overlaid on the predicted values obtained using Equation 2 and 3 (top and middle), T_g of both adhesives as a function of relative humidity (Viana et al. 2016. Submitted) (bottom).

Various interesting effects are now easier to visualize: there is a clear shift away from the expected values for SikaPower 4720 after 40% RH, a behaviour consistent with the fact that its T_g fall below ageing temperature at that point, while Nagase XNR 6852-1 behaves precisely as expected due to its T_g being comfortably above the ageing and testing temperature. Another remark is that the exact same equation accurately predicts the behaviour of both Paris Law parameters for both adhesives (while operating below T_g) through the determination of a universal constant (Equation 3) that is dependent on the Fick's Law parameters of each adhesive. Finally, we can infer the future Paris Law values at a higher relative humidity content due to the good correlation between experimental and predicted values. In future works this will be confirmed, especially for SikaPower 4720 where it will be interesting to see how the behaviour evolves due to it being tested above its T_g, and also see how this prediction equation applies to other adhesives.

80

4 CONCLUSIONS

Two epoxy adhesives had their fatigue response studied due to varying degrees of water content, which resulted in crack growth curves that evolve in a predictable manner when the relative humidity content changes. Nagase XNR 6852-1 was expected to experience small changes in the crack growth curves with increasing humidity due to its very stable behaviour when submerged in water, which was confirmed in the experimental Paris Law curves. SikaPower 4720 was expected to have its fatigue behaviour change in a more accentuated manner due to its much larger water absorption parameters (32.5% mass increase when saturated compared to 1.2% for Nagase XNR 6852-1, an increase of over 27 times), which also happened, but the behaviour was not as predictable as Nagase XNR 6852-1 due to the fact that the T_g of SikaPower 4720 decreases drastically with an increase of relative humidity. Based on the experimental data, an equation is proposed which fits the behaviour of both adhesives (while they are away from T_g) and produces results very close to the experimental values. In the future the authors hope to apply this prediction to other adhesives.

The study of changes in the fatigue response on adhesively bonded joints due to varying degrees of relative humidity is an important step in understanding how joints will behave in the long-term, and although there is already some data on the subject it is not enough to draw clear conclusions (Costa et al. 2016. Submitted), which the authors believe this work tries to help in.

References

Abel, M.-L., Adams, A., Kinloch, A., Shaw, S.,Watts, J. (2006). The effects of surface pretreatment on the cyclic-fatigue characteristics of bonded aluminium-alloy joints. International journal of adhesion and adhesives 26:50-61.

ASTM (1999). D3433 - Test Method for Fracture Strength in Cleavage of Adhesives in Bonded Metal Joints

ASTM (2000). E647 - Standard Test Method for Measurement of Fatigue Crack Growth Rates

ASTM (2010). D3933 - Standard Guide for Preparation of Aluminum Surfaces for Structural Adhesives Bonding (Phosphoric Acid Anodizing)

Briskham, P.,Smith, G. (2000). Cyclic stress durability testing of lap shear joints exposed to hot-wet conditions. International journal of adhesion and adhesives 20:33-38.

Costa, M., Viana, G., Canto, C., et al. (2015). Effect of the size reduction on the bulk tensile and double cantilever beam specimens used in cohesive zone models. Proceedings of the Institution of Mechanical Engineers, Part L: Journal of Materials Design and Applications.

Costa, M., Viana, G., da Silva, L. F. M.,Campilho, R. D. S. G. (2016). Effect of humidity on the mechanical properties of adhesively bonded aluminium joints. Part L: Journal of Materials: Design and Applications.

Costa, M., Viana, G., da Silva, L. F. M.,Campilho, R. D. S. G. (2016. Submitted). Environmental effect on the fatigue degradation of adhesive joints: a review. The Journal of Adhesion.

de Moura, M. F. S. F., Campilho, R. D. S. G.,Goncalves, J. P. M. (2008). Crack equivalent concept applied to the fracture characterization of bonded joints under pure mode I loading. Composites Science and Technology 68:2224-2230.

Fernández, M., De Moura, M., Da Silva, L.,Marques, A. (2011). Composite bonded joints under mode I fatigue loading. International Journal of Adhesion and Adhesives 31:280-285.

Fernando, M., Harjoprayitno, W.,Kinloch, A. (1996). A fracture mechanics study of the influence of moisture on the fatigue behaviour of adhesively bonded aluminium-alloy joints. International journal of adhesion and adhesives 16:113-119.

Fujita, H. (1961). Free-volume model of diffusion in polymer solutions. Advances in Polymer Science 3:1-47.

Hart-Smith, L. J. 2011. Adhesively Bonded Joints in Aircraft Structures. In *Handbook of Adhesion Technology*, edited by L. M. da Silva, A. Öchsner, and R. Adams: Springer Berlin Heidelberg.

Katnam, K., Sargent, J., Crocombe, A., Khoramishad, H.,Ashcroft, I. (2010). Characterisation of moisture-dependent cohesive zone properties for adhesively bonded joints. Engineering Fracture Mechanics 77:3105-3119.

Kinloch, A., Little, M.,Watts, J. (2000). The role of the interphase in the environmental failure of adhesive joints. Acta Materialia 48:4543-4553.

Lefebvre, D., Ahn, B., Dillard, D.,Dillard, J. (2002). The effect of surface treatments on interfacial fatigue crack initiation in aluminum/epoxy bonds. International journal of fracture 114:191-202.

Loh, W., Crocombe, A., Wahab, M. A.,Ashcroft, I. (2005). Modelling anomalous moisture uptake, swelling and thermal characteristics of a rubber toughened epoxy adhesive. International journal of adhesion and adhesives 25:1-12.

Marceau, J. A., Firminhac, R. H.,Moji, Y. 1978. Method for providing environmentally stable aluminum surfaces for adhesive bonding and product produced. USA: The Boeing Company.

Pizzi, A.,Mittal, K. L. (2003). Handbook of Adhesive Technology, Revised and Expanded, Taylor & Francis.

Rodrigues, T. A. F., Chaves, F. J. P., da Silva, L. F. M., Costa, M.,Barbosa, A. Q. (2016. Submitted). Determination of the fracture envelope of an adhesive joint as a function moisture. Materialwissenschaft und Werkstofftechnik.

Saldanha, D. F. S., Canto, C., da Silva, L. F. M., et al. (2013). Mechanical characterization of a high elongation and high toughness epoxy adhesive. International Journal of Adhesion and Adhesives 47:91-98.

Viana, G., Costa, M., Banea, M.,da Silva, L. F. M. (2016. Submitted). Behaviour of environmentally degraded epoxy adhesives as a function of temperature. The Journal of Adhesion.

Wang, M., Liu, A., Liu, Z.,Wang, P.-C. (2013). Effect of hot humid environmental exposure on fatigue crack growth of adhesive-bonded aluminum A356 joints. International Journal of Adhesion and Adhesives 40:1-10.

Paper E

A cohesive zone element for mode I modelling of adhesives degraded by humidity and fatigue

M. Costa[a], G. Viana[a], R. Créac'hcadec[b], L. F. M. da Silva[c,*], R. D. S. G. Campilho[a,d]

[a]*INEGI - Rua Dr Roberto Frias 400, 4200-465 Porto, Portugal*
[b]*ENSTA - Bretagne, 2 rue François Verny, 29806 Brest Cedex 9, France*
[c]*FEUP - Rua Dr Roberto Frias s/n, 4200-465 Porto, Portugal*
[d]*ISEP - Rua Dr. António Bernardino de Almeida, 431, 4249-015 Porto, Portugal*

Abstract

A robust finite element is proposed, based on the cohesive zone model approach and implemented as a user element, for the modelling of adhesively bonded joints subjected to degradation by humidity and fatigue using software ABAQUS®. Functionality included in this element that is not available using standard cohesive zone elements includes: (a) various types of traction-separation laws, such as triangular with exponential softening, trapezoidal and exponential, (b) an intuitive and easy to use graphical interface built in MATLAB that helps visualize all traction-separation laws, create the mesh, run the simulation and visualize the results, (c) custom degradation laws for both humidity and fatigue which allow the user to easily model the effects of said degrading parameters. It is shown that the trapezoidal traction-separation law is the most appropriate to model the experimental data in both unaged and aged specimens. The proposed fatigue degradation approach correctly predicts the number of cycles until failure of all unaged and aged conditions, thus proving itself as a very useful tool capable of modelling a vast array of experimental conditions and details that adhesive joints are subjected to in real world applications.

Keywords: Cohesive zone model, traction-separation law, finite element analysis, humidity, fatigue, environmental degradation.

1. Introduction

Adhesive joints are being increasingly used in structures mainly due to their attractive strength to weight ratio, which leads to an overall reduction in weight, costs and, in the case of industries such as the automotive and aeronautical, emissions [1]. Due to the prevalence of adhesive joints in critical structures, precise experimental [2] and numerical methodologies [3] must be developed to characterise and predict joint behaviour for both static and cyclic conditions, while also evaluating the effect that environmental factors may have in a joint. Experimentally, temperature and humidity may be applied to standardized specimens such as bulk and double cantilever beams (DCBs) to obtain both static and cyclic behaviour, but numerical prediction of said phenomena is still not fully understood.

Since the introduction of the cohesive zone model (CZM) concept [4] and its application to finite elements [5], adhesive joints have frequently adopted CZM to model the adhesive layer because of its ability to model delamination. CZM relates the stresses in the material with the relative displacement between adjacent nodes (by using traction-separation laws) and provides an easy to implement methodology that provides accurate results [6]. Some adhesive properties are used to build the traction-separation law (such as the tensile/shear stresses and fracture toughness), which provides limits related to what the specific material can withstand before failing. Various types of traction-separation laws exist: the simplest one being the triangular law, implemented in ABAQUS® and used in most numerical simulations, trapezoidal law, exponential law, and some more complex types of laws [7, 8]. To use these more complex CZM laws in ABAQUS®, one must go through some trouble as they are not directly implemented, thus the information of the damage variable as a function of displacement must first be created [9] (using external routines coded in, for example, MATLAB or python) and only then inserted in ABAQUS®, adding some complexity to the procedure.

The presence of humidity in a joint influences the material parameters, thus to model joints degraded by humidity using CZM the traction-separation law parameters must be adapted accordingly. This is normally done manually for each degradation test, where the CZM parameters are input already affected by the level of humidity (taken from experimental tests) [10, 11], while other approaches consist in using ABAQUS® material degradation subroutines to model moisture degradation [12].

Approaches for fatigue analysis using CZM generally opt for progressively applying damage to the element using a custom formulation to mimic fatigue degradation, which is in itself based on experimental details. The vast majority of fatigue implementations using the CZM approach update the damage variable as a function of several fatigue cycles for each iteration, controlling the number of cycles evaluated by each numerical jump [13, 14, 15, 16], while few opt for a cycle-by-cycle approach [17, 18] which becomes very computationally intensive and not beneficial in terms of results. Generally, all approaches for modelling fatigue follow some kind of complex mathematical model, while works that are based on simple relationships derived from experimental data are scarce.

The objective of this work is to provide a robust and complete finite element based on the CZM approach that corrects various of the previously mentioned problems. By incorporating several types of traction-separation laws such as trapezoidal and exponential, the need for complex workarounds to determine the tabular representation of the CZM is eliminated. Modelling of joints degraded with humidity is also integrated in the element by using a general law for degradation of the properties as a function of the humidity content, thus avoiding manual tweaking of the CZM parameters to fit a specific humidity concentration. Finally, modelling fatigue is also taken into account, by using simple relationships that are obtained using experimental data, thus guaranteeing reproducibility of the results. The proposed finite element is based on the cohesive zone model approach and coded in FORTRAN for use in ABAQUS®, with the final aim of providing robust results by using relatively simple formulations for element degradation. This paper is structured in the following way: section 2 presents everything related to the formulation, from the base finite element code

to the equations implemented in each CZM law and degradation behaviours for humidity and fatigue, while section 3 focuses on the MATLAB developed interface, followed by section 4 which compares experimental data with numerical results while discussing all results, and finally the conclusions are drawn.

2. Formulation

2.1. Finite element method

The finite element method (FEM) summarily consists in studying a domain of arbitrary complexity by discretizing it in several sub-domains called elements, calculating the displacement suffered by each element as a function of the applied loads/boundary conditions, and then combining the information from all elements into the whole model. Mathematically, FEM consists in solving equation:

$$[k] \cdot \{d\} = \{f\} \tag{1}$$

where $[k]$ is the stiffness matrix (constructed as a function of the material parameters), $\{d\}$ is the displacements vector (to be determined by FEM) and $\{f\}$ is the external forces vector (where the applied forces are considered). The cohesive zone model (CZM) approach, used in delamination problems, is based on traction-separation laws, which correlate the stress existing in a specific point of the bond as a function of the displacement that point is subjected to. When using CZM in FEM, $[k]$ and $\{f\}$ from Equation 1 are defined as:

$$[k] = w \cdot [B]^T \cdot [T_d] \cdot [B]$$
$$\{f\} = w \cdot [B]^T \cdot \{T\} \tag{2}$$

where w is the width of the element, $[B]$ is the global displacement–separation relation matrix (defined further ahead), and both $\{T\}$ and $[T_d]$ are a vector and matrix, respectively, in which the traction-separation law considerations are included, such that each traction-separation law type (see Figure 1) will have differing $\{T\}$ and $[T_d]$ formulations.
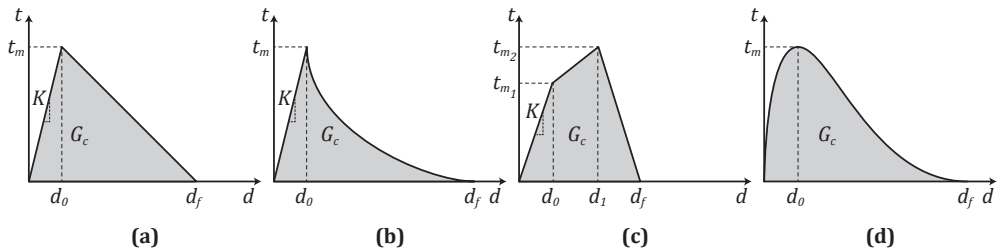

Figure 1: Various traction-separation laws: (a) triangular, (b) triangular with non-linear softening, (c) trapezoidal with non-constant plateau, (d) exponential.

$\{T\}$ and $[T_d]$ may be defined, for mode I loadings in the local coordinate system (see Figure 2), as:

$$\{T\} = \begin{Bmatrix} 0 \\ t(d) \end{Bmatrix} \qquad [T_d] = \begin{bmatrix} 0 & 0 \\ 0 & t'(d) \end{bmatrix} \tag{3}$$

87

where $t(d)$ corresponds to the equation that defines the CZM law under consideration, see Figure 1. Thus defining $\{T\}$ and $[T_d]$ allows for modelling any desired CZM shape. Various types of curves can be considered, as seen in Figure 1, and different types of relationships are usually associated with different situations and selected as a function of either geometry or adhesive properties. For example, the simple triangular shape is often used with brittle adhesives, as the results are usually very satisfactory for these situations, while the trapezoidal shape is recommended when studying ductile adhesives due to the added plateau of the curve which helps modelling the ductile fracture of those types of adhesives.

2.2. Cohesive element

Basic FEM concepts such as number of nodes, shape functions and matrices must be defined for the developed cohesive element. Figure 2 shows a portion of a DCB specimen with the location where the proposed element should be used, together with a representation of the element.
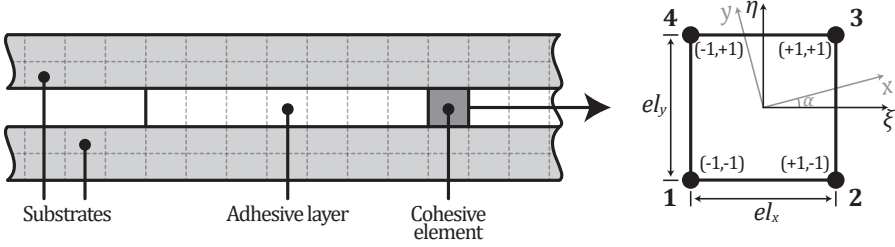

Figure 2: Section of a discretized DCB specimen (exaggerated height of the adhesive layer for easier visualization) and detail of the cohesive zone element in both global (x, y) and local (ξ, η) coordinates.

Figure 2 shows the element in two different coordinate systems: global, which are the original coordinates of each node (related to the rest of the model), and local, which is a coordinate system specifically for the element. An element with 4 nodes was chosen, and in standard 4 noded elements 4 shape functions should be chosen. In reality, in cohesive elements, the height is considered null ($el_y = 0$mm), thus only shape functions for nodes 1/4 and 2/3 are needed, as the same function applies to both nodes at a specific ξ coordinate:

$$N_{1,4} = \frac{1}{2}(1 - \xi) \qquad ; \qquad N_{2,3} = \frac{1}{2}(1 + \xi) \tag{4}$$

It should be noted that 4 nodes were selected as a starting step and the element may be further improved to support additional nodes (such as 6 or 8 nodes), which will help with big models with a high number of total elements (reducing the number of cohesive elements will increase the speed of the simulation and reduce computational time).

Matrix $[N]$ can now be built, which represents the matrix of the shape functions, using the information from Equation 4, such that:

$$[N] = \begin{bmatrix} N_{1,4} & 0 & N_{2,3} & 0 & N_{2,3} & 0 & N_{1,4} & 0 \\ 0 & N_{1,4} & 0 & N_{2,3} & 0 & N_{2,3} & 0 & N_{1,4} \end{bmatrix} \tag{5}$$

88

And matrix $[B]$, which represents the global displacement–separation relation matrix, is defined by:

$$[B] = [R][N] = \begin{bmatrix} cos(\alpha) & sin(\alpha) \\ -sin(\alpha) & cos(\alpha) \end{bmatrix} \begin{bmatrix} N_{1,4} & 0 & N_{2,3} & 0 & N_{2,3} & 0 & N_{1,4} & 0 \\ 0 & N_{1,4} & 0 & N_{2,3} & 0 & N_{2,3} & 0 & N_{1,4} \end{bmatrix} \quad (6)$$

Where $[R]$ represents the transformation matrix from global to local coordinates, and α is the angle between said coordinate systems (see Figure 2). With this matrix defined, all information needed to calculate Equation 2 is obtained as well as a fully working finite element code.

2.3. Traction-separation laws

2.3.1. Pre-defined types of traction-separation laws

As mentioned above, defining $\{T\}$ and $[T_d]$ (Equation 3) is dependent on the formulation of each type of traction-separation law. Table 1 summarizes how $t_i(d)$, $t_i'(d)$ and G_i are defined for each zone i of each CZM, i.e. the number of distinct separations dictated by differing behaviour inside the same curve (for example a change from linear function to exponential), thus both the triangular CZMs have 2 zones ($0 \rightarrow d_0$ and $d_0 \rightarrow d_f$), trapezoidal has 3 zones ($0 \rightarrow d_0$, $d_0 \rightarrow d_1$ and $d_1 \rightarrow d_f$) and finally the exponential CZM has 1 zone ($0 \rightarrow d_f$) because the whole curve is defined by a single equation (Figure 1).

Table 1: Equations needed to define each zone of each implemented traction-separation law.

CZM law	Number of zones	Traction	Derivative	Area
Triangular	2	$t_1(d) = \frac{t_m d}{d_0}$	$t_1'(d) = \frac{t_m}{d_0}$	$G_1 = \frac{t_m d_0}{2}$
		$t_2(d) = t_m \left(1 - \frac{d-d_0}{d_f-d_0}\right)$	$t_2'(d) = \frac{-t_m}{d_f-d_0}$	$G_2 = \frac{t_m(d_f-d_0)}{2}$
Triangular (non-linear softening)	2	$t_1(d) = \frac{t_m d}{d_0}$	$t_1'(d) = \frac{t_m}{d_0}$	$G_1 = \frac{t_m d_0}{2}$
		$t_2(d) = t_m \left(1 - \frac{d-d_0}{d_f-d_0}\right)^C$	$t_2'(d) = t_m C \frac{\left(\frac{-d_f+d}{-d_f+d_0}\right)^C}{-d_f+d}$	$G_2 = \frac{t_m(d_f-d_0)}{K+1}$
Trapezoidal	3	$t_1(d) = \frac{t_{m_1} d}{d_0}$	$t_1'(d) = \frac{t_{m_1}}{d_0}$	$G_1 = \frac{t_m d_0}{2}$
		$t_2(d) = t_{m_1} + (t_{m_2} - t_{m_1})\frac{d-d_0}{d_1-d_0}$	$t_2'(d) = \frac{t_{m_2}-t_{m_1}}{d_1-d_0}$	$G_2 = -\frac{(t_{m_1}+t_{m_2})(d_0-d_1)}{2}$
		$t_3(d) = t_{m_2}\frac{d_f-d}{d_f-d_1}$	$t_3'(d) = \frac{-t_{m_2}}{d_f-d_1}$	$G_3 = \frac{t_{m_2}(d_f-d_1)}{2}$
Exponential	1	$t_1(d) = d\frac{t_m}{d_0}e^{1-\frac{d}{d_0}}$	$t_1'(d) = -\left(\frac{d}{d_0}-1\right)\frac{t_m}{d_0}e^{1-\frac{d}{d_0}}$	$G_1 = d_0 t_m e$

In Table 1, all laws, with the exception of exponential, have an initial stiffness value (K in Figure 1) defined as $K = E/h_a$, where E is the Young's modulus of the adhesive and h_a is the thickness of the adhesive layer. This value is necessary to define d_0 in those curves, otherwise that would not be possible. Furthermore, the adhesive fracture toughness, G_c, is the sum of all the areas of each curve, such that $G_c = \sum G_i$. Also, all traction and fracture values are given at the start of a simulation (based on adhesive properties), thus what remains to be defined are the specific displacements of each curve (i.e. $d_0/d_1/d_f$), which can be obtained by rearranging the equations for the area of the curves. Regarding the triangular law with non-linear softening, C represents the exponent of the softening zone, such that $0 < C < \infty$.

2.3.2. Custom traction-separation law

The previously shown shapes are useful to model a variety of situations, but there may be a need to implement more complex types of traction-separation laws for specific problems. The proposed user element [19] formulation takes this behaviour into account by evaluating fully custom traction-separation laws, which are created by defining the various points and also the behaviour connecting adjacent points, as shown in Figure 3.
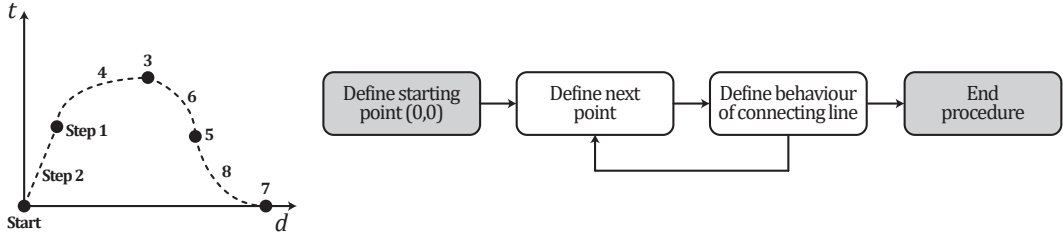

Figure 3: Example of a custom traction-separation law with each step needed for its full definition (left), flowchart of the procedure (right).

It works by defining an equation between each two consecutive points (as a function of their coordinates and line evolution - linear, quadratic, cubic, etc.), such that the equations can then be probed in the finite element code for the specific stress value for the displacement. The advantage of this feature is that there are infinite possibilities for traction-separation curves, allowing the user to adapt the CZM in a way that fully fits its experimental data. Further advantages may include different types of custom CZM curves for each mode that allows to better capture the behaviour of a specific mode, and also the fact that a traction-separation law may be derived from an experimental curve and evaluated in the cohesive zone element directly (by using techniques such as the J-integral [20]).

2.4. Degradation by humidity

The presence of humidity in an adhesive translates into a degradation of its mechanical properties [21, 22, 23], and the way such degradation affects specific adhesives must be understood, specifically for properties that are necessary for the definition of the CZM law (such as Young's modulus, tensile strength and fracture toughness). The traction-separation law parameters are thus adapted in the beginning of the simulation as represented in Figure 4.

Experimental work is therefore needed to characterize how the mechanical properties of the adhesive itself decrease with different humidity levels, and relationships should be found on how each property decreases with an increase in humidity. Previous work has been accomplished with such objective, and the degradation of two distinct epoxy adhesives has been studied [22], which has resulted in equations that allow the CZM code to determine the mechanical properties at any level of humidity content using the following equation:

$$y(x) = (y_0 - y_f) \cdot e^{-x/C} + y_f \qquad \text{with} \qquad C = (10^{13}/2) \cdot D \cdot m_\infty \qquad (7)$$
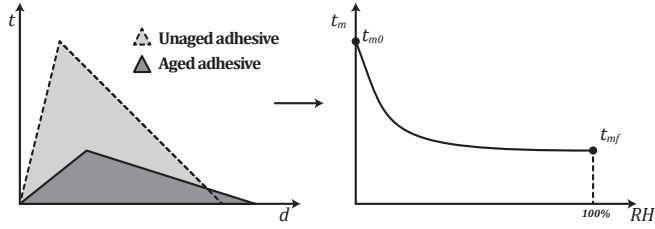
Figure 4: How the CZM is adapted as a function of the degraded adhesive parameters (left), which evolve as a function of relative humidity (right).

where y is the property to be degraded (Young's modulus, tensile stress, etc.), subscripts 0 and f are, respectively, the initial and final values for that property, x is the level of relative humidity present in the joint (such that $0 \leq x \leq 1$), and D and m_∞ are parameters for the Fick's law of each adhesive. Equation 7 is plotted in Figure 4 (right) for the case of tensile stress (other properties follow a similar evolution), and more details on this formulation may be found in the literature [22]. Thus, by simply providing the base mechanical properties, Fick's law parameters and relative humidity content, the cohesive element may estimate the value of each property for the specific humidity concentration and adapt the traction-separation law automatically.

2.5. Degradation by fatigue

Fatigue is characterized by a cyclic accumulation of damage in the adhesive, for loading conditions below those which would result in failure of the joint under study. This translates into a need for the cohesive element to damage the material, in a manner consistent with experimental results, through the use of degradation coefficients for the traction-separation law as a function of the applied fatigue cycles. Thus, the following degradation relationship was implemented:

$$y(N) = y_0 \left(1 - \frac{N}{N_f}\right)^K \tag{8}$$

where y is the property of the cohesive zone law being degraded (such as t_m and G_c, see Figure 1), N is the cycle (or cycle range) being evaluated, y_0 is the undegraded value of that property (for $N = 0$), N_f is the number of cycles at failure, and K is a coefficient which controls the degradation rate. How Equation 8 translates into pratice may be visualized in Figure 5.

The proposed methodology induces degradation such that the crack propagates until failure, but the number of cycles to failure (N_f) must also be defined. To accomplish that, the following relationship is implemented:

$$N_f = \frac{\Delta a}{(da/dN)_{wa}} \tag{9}$$

where Δa is the total length of the bonded area, and $(da/dN)_{wa}$ is a weighted average value deduced from the Paris Law of the adhesive under study.
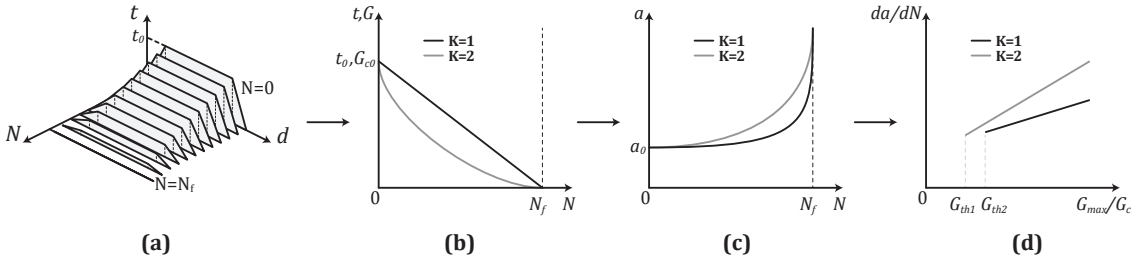
Figure 5: (a) degradation of a trapezoidal traction-separation law as a function of fatigue cycles, (b) CZM parameters change as a function of the number of cycles for two different degradation coefficients, (c) resulting crack length propagation difference, (d) corresponding fatigue crack growth curves.

3. MATLAB interface

Due to the complexity of the development phase (the need to test several geometries with various mesh configurations for various adhesive properties under both static and dynamic conditions), an interactive MATLAB interface was developed with the aim of centralizing all repetitive tasks, from creating all simulation files (.inp and .for) to extracting the simulation results from the .odb file and display them to the user, as seen in Figure 6.
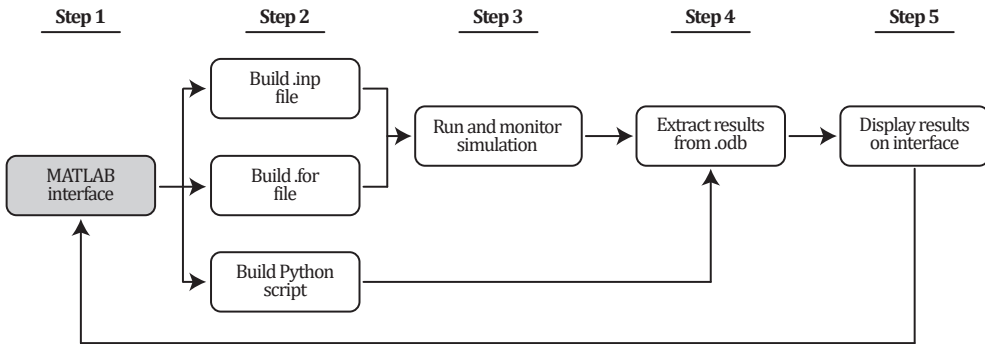

Figure 6: Flowchart of the MATLAB interface.

The advantages of having such an interface are:

- Not having to recreate an ABAQUS[®] model every time there is a change to a geometric/mesh parameter;

- Easily compare results from different simulations (result from each simulation is compared against experimental and previous numerical curves);

- Overlay all traction-separation laws and study the effect that changing each parameter has on the law and on the simulation result;

- Aggregate all functions needed to run the desired ABAQUS[®] simulation without having to open the ABAQUS[®] interface (otherwise needed to both build the model and visualise the results).

92

While the interface was initially built specifically for the development phase (i.e. it would be discarded once the cohesive element was finished), it quickly became apparent that it would also be very useful for the end user to build models and run simulations quickly and easily. The interface is divided in 5 distinct zones, as represented in Figure 7.
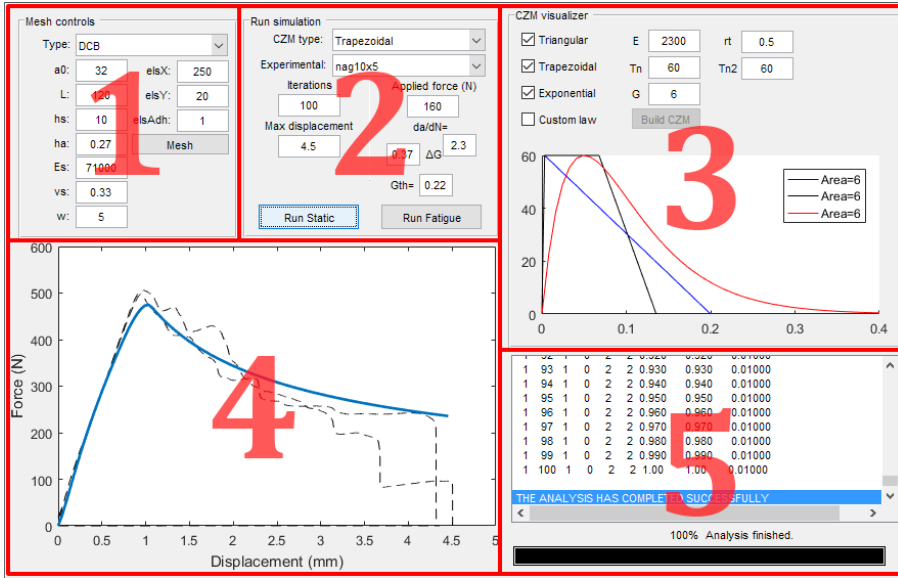

Figure 7: MATLAB interface.

The first zone is related to the geometry of the specimen under study, where the various geometrical parameters are defined and are the same as those presented in Figure 8, such that two types of specimens are currently possible to test, with other types of joints possible to implement if needed.
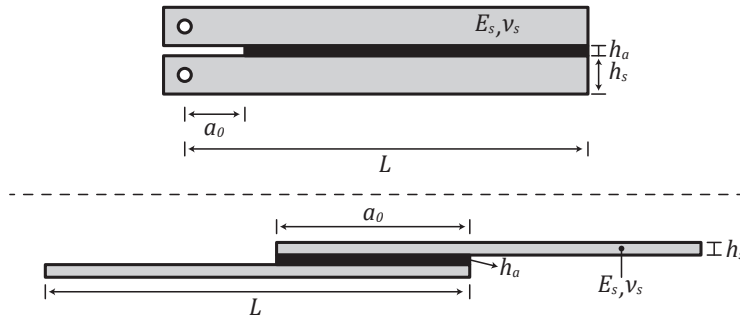

Figure 8: Relationship between physical parameters and interface variables for a Double Cantilever Beam (top), and a Single Lap Joint (bottom)

The second zone is used to start simulations and also define the simulation parameters such as maximum displacement (for static conditions) and applied load and Paris Law parameters (for fatigue conditions). Furthermore it defines the type of traction-separation law that should be evaluated, and can also load

experimental curves which are used to compare against numerical results.

Zone three has two main purposes: defining the material properties (such as Young's modulus E, tensile strength t_m and fracture toughness G), and visualizing the various types of traction-separation laws. Another feature related to this section is the definition of a custom traction-separation law, as described in Section 2.3.2, which is done using the interface shown in Figure 9.
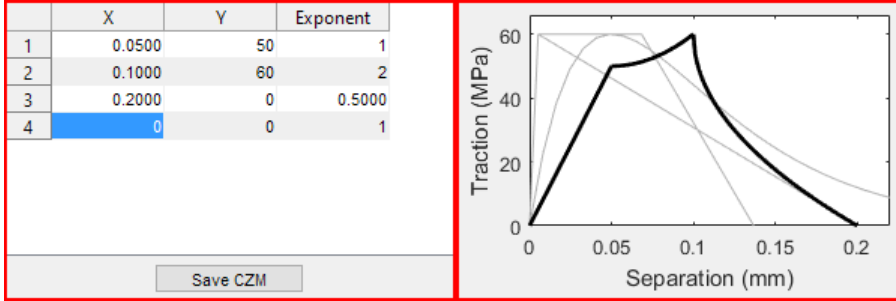

Figure 9: MATLAB interface for defining a custom traction-separation law: defining each point and type of curve connecting adjacent points (left), and resulting CZM (right).

Zone four has two purposes: display the mesh and geometry prior to the start of the simulation for validation purposes, and displaying the results of the simulation after the end (and, in case there is an experimental file selected in zone two, overlay the numerical results on the experimental curves).

Finally, zone five is a debugging area, showing the progress of the simulation in a progress bar while simultaneously showing the output from ABAQUS® during the analysis.

4. Results and discussion

The validation phase of the developed cohesive element was performed based on extensive experimental tests, with the objective of feeding enough data into the model so that the degradation laws could be obtained. Two adhesives were studied, Nagase XNR 6852-1 and SikaPower 4720, both epoxy adhesives with very different mechanical properties, as shown in Table 2.

The diffusion properties were determined by defining Fick's law, the mechanical properties using bulk tensile specimens, and the fatigue crack growth properties by determining the Paris Law for each adhesive in mode I. Further details on all methodology may be found in the literature [22, 24].

4.1. Convergence tests

The size of the mesh is an important parameter in any FEM simulation, where a balance between a coarse mesh (which will lead to faster but more inaccurate results) and a refined mesh (which will take more computational time to solve but yields more accurate results) must be found. To that end, various levels of mesh refinement were tested using the proposed element formulation, and the results may be seen in Figure 10.

Table 2: Various properties of both studied adhesives [22, 24].

	Property	Nagase XNR 6852-1	SikaPower 4720
Diffusion properties	Diffusion coefficient (m^2/s)	$5.02 \cdot 10^{-13}$	$0.89 \cdot 10^{-13}$
	Mass at saturation (%)	1.2	32.5
Mechanical properties	Young's modulus (MPa)	2300	2100
	Tensile strength (MPa)	60	30
	Mode I fracture toughness (N/mm)	6	2
Fatigue crack growth properties	Intersection C	0.10	0.14
	Slope m	1.18	2.18
	Crack initiation threshold G_{th}	0.55	0.22
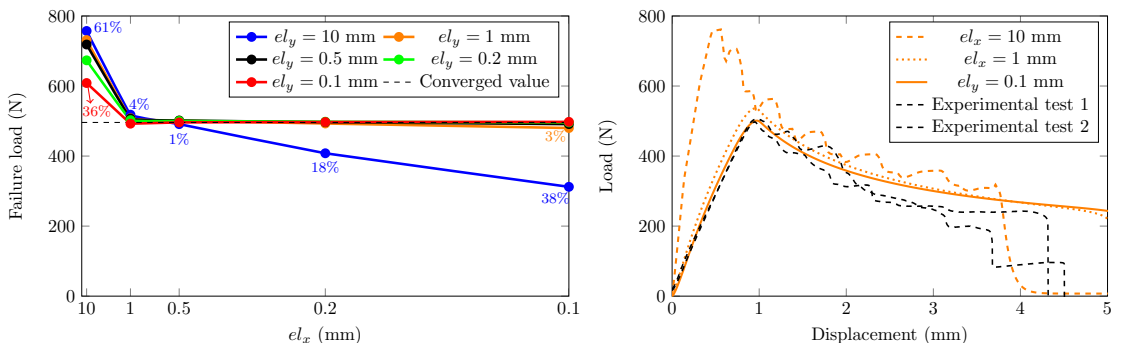
Figure 10: Effect of element size for both x and y direction in the simulated failure load of DCB specimens (left), and effect of element size in the x direction ($el_y = 1$ mm) on the load displacement curve (right).

The test was performed for the case of the Nagase XNR 6852-1 double cantilever beam model, and the results shown were obtained using the trapezoidal law, although the same trend is obtainable for the remaining CZM laws. The dimensions of the element are el_x and el_y for the x and y direction, respectively, and higher mesh refinement levels yields more elements in one direction, thus a smaller dimension. el_x affects the entire model (both substrates and adhesive layer), while el_y only affects the substrates (because due to its reduced thickness, the adhesive is modelled using a single element along its height). It is visible (Figure 10 (left)) that, for almost all cases, as the number of elements in any direction increases, the failure load tends to a stable/converged value, as would be expected. The exception is the case of one single element for the substrate ($el_y = h_s = 10$ mm), which even with a higher number of elements along the x-axis does not converge. Because of that, $el_y = 1$ mm was chosen as the quickest mesh which provides good results for the comparison on Figure 10 (left), which shows that for the case of $el_x = 1$ mm a curve very close to the experimental one may already be achieved. This means that considerably accurate results may be obtained using element sizes as high as $el_x = el_y = 1$ mm, which translates to relatively fast simulation times.

The geometric and material properties of the specimens (Figure 8) used in the experimental tests [22] is: $a_0 = 20$ mm, $L = 120$ mm, $h_a = 0.2$ mm and $E_s = 71$ GPa, while $h_s = 10$ mm for the specimens used for Nagase XNR 6852-1 and $h_s = 5$ mm for the SikaPower 4720 specimens, which were selected as a function of adhesive toughness (higher toughness means higher stresses on the substrate, meaning the thickness must be increased to guarantee no plasticity in the substrates). The study and selection of substrate thickness is published in the same work [22] and in a previous work [25] devoted to developing reduced specimens for use in environmental degradation studies, needed to reduce the time until moisture saturation is obtained.

For the unaged condition (no relative humidity present on the joint), Figure 11 presents a comparison between experimental results for each adhesive together with numerical curves for each type of traction-separation law implemented in the element code. The analysis was done in 2D using the element size $el_x = el_y = 0.1$ mm, shown in the mesh convergence section to provide a high level of accuracy.
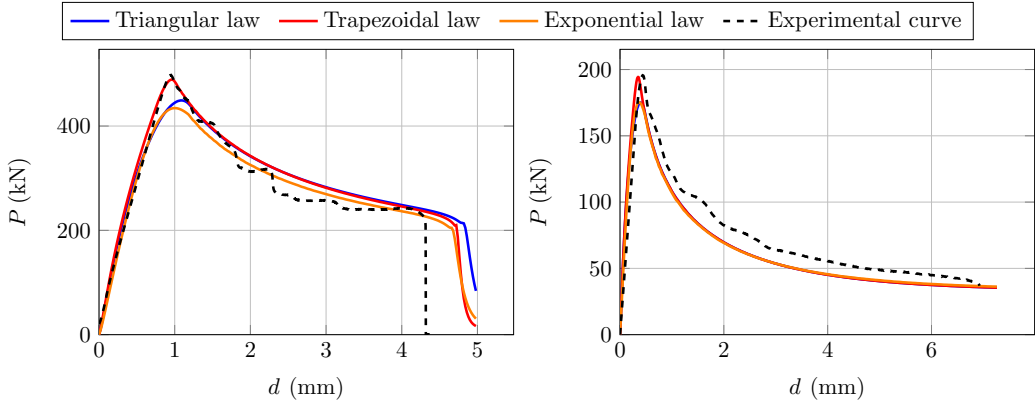

Figure 11: Experimental and numerical results for each type of traction-separation law for the two studied adhesives: Nagase XNR 6852-1 (left), SikaPower 4720 (right).

It can be seen that the numerical results fit the experimental curves, specially for the case of the Nagase XNR 6852-1 adhesive. Some details that are expected when comparing a numerical simulation with an experimental curve are evident: experimental curves usually fail at a displacement lower than the numerical one (due to the inherent microscopic flaws of real world materials), and also the stiffness of the elastic zone of the curve is usually higher in the numerical results (due to numerical modelling considering a perfectly rigid displacement inducement method, which does not happen in reality as test machines have various mechanical components that slightly elastically deform), which is especially visible in the case of SikaPower 4720 but is also present in the case of Nagase XNR 6852-1. Regarding the effectiveness of each type of CZM, the trapezoidal CZM appears to be the best in matching the experimental maximum load for both cases, while both the triangular and exponential CZM result in a slightly lower experimental maximum load. The reason this happens is that the trapezoidal CZM is the one that should be used when more ductile adhesives are

used, which due to its plateau (see Figure 1 (c) for the case of $t_{m_1} = t_{m_2}$ and Figure 7 zone 3) is more appropriate to model the gradual degradation of the adhesive layer of the studied adhesives.

Regarding the tests with moisture degradation, Equation 7 is used together with the values from Table 2 by the element to estimate the degraded CZM properties, such that each type of curve is adapted automatically in the beginning of the simulation to match the degraded stage being modelled. Figure 12 presents the comparison between simulation results and the experimental maximum load, P_{max}, together with the experimental failure displacement, d_{max}, as a function of the adhesive and ageing stage, which are shown in Table 3.

Table 3: Definition of each aged stage for both studied adhesives.

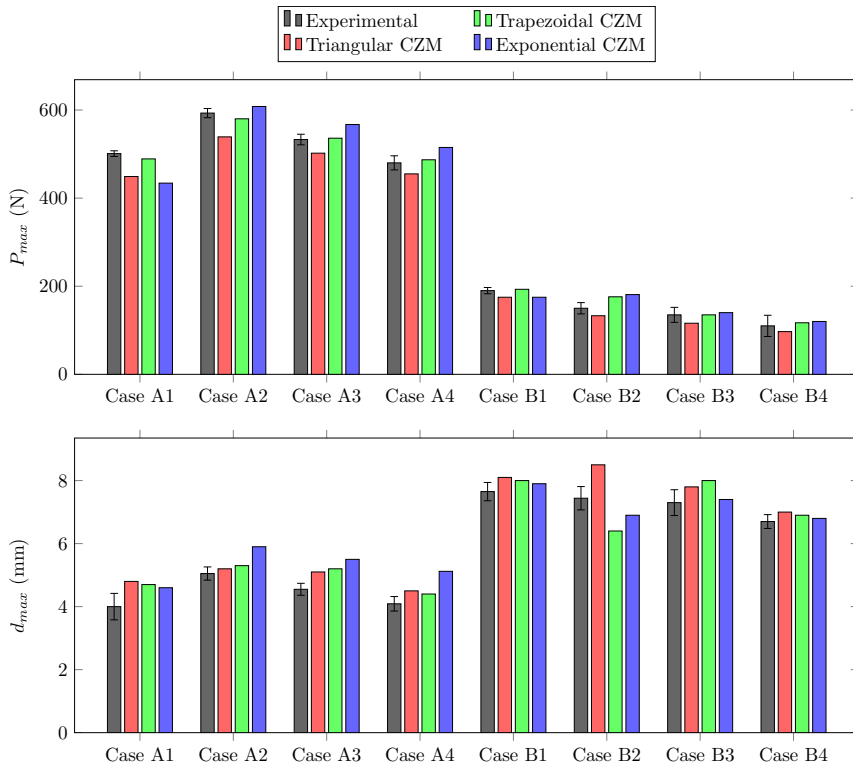|	Nagase XNR 6852-1	SikaPower 4720
RH = 0%	Case A1	Case B1
RH = 25%	Case A2	Case B2
RH = 40%	Case A3	Case B3
RH = 60%	Case A4	Case B4

Figure 12: Comparison between experimental and numerical values of the maximum load and displacement for both adhesives in each aged state.

The Nagase XNR 6852-1 results generally present a higher maximum load than SikaPower 4720, which happens because Nagase XNR 6852-1 has higher mechanical properties and also because the substrate thickness is higher (therefore allowing for less bending in the elastic stage). The maximum displacement is also generally lower for the Nagase XNR 6852-1 adhesive because of the same reason (by bending less, the thicker substrate will force separation for a lower value of displacement, thus breaking the joint sooner). Regarding the ageing stages, it is visible that the maximum load for Nagase XNR 6852-1 increases from the unaged stage (RH = 0%) to 25% relative humidity, which matches the experimental measurements for those two stages [22], and after RH = 25% there is a gradual decrease of the maximum load with an increase in relative humidity. For SikaPower 4720 there is a gradual decrease of the maximum load for all consecutive stages after the unaged stage. As for the results of the numerical simulation for the three types of studied traction-separation laws, the numerical results match the experimental curves in all cases with varying degrees of accuracy, which fluctuates due to the type of CZM being more or less appropriate for the situation. Generally, the trapezoidal CZM is closer to the experimental value than the other two options, but exceptions exist, although in all cases the approximation for any case is acceptably near the experimental values.

4.3. Fatigue tests

Numerical implementation of fatigue phenomena is divided in two parts: crack growth during simulation, and estimation of cycles at failure.

4.3.1. Crack growth simulation

Crack growth is controlled during the numerical simulation by applying Equation 8, which will degrade the traction-separation law as to induce crack propagation as pictured in Figure 5. This will lead to propagation of the crack in an otherwise static simulation, and by adjusting the K constant one can influence the crack propagation behaviour and, specifically, the crack length increases as a function of the number of applied cycles. Figure 13 shows the crack propagation plots (Paris Law) for three different K values.

Altering the value of K has a distinct influence in the Paris Law constants, as an increase in K translates to a decrease in the Paris Law slope, a decrease in G_{th} and an increase in the y-axis intersection value. This makes sense because an increase in K will lead to a quicker decrease in CZM parameters (see Figure 5 (b)), therefore decreasing them faster will result in the crack initiating sooner, thus lowering the value for the crack initiation threshold G_{th}. Furthermore, after the quicker decrease in CZM parameters in the earlier cycles, the parameters will stabilize (gradually halting the decrease), which translates to the crack propagating much more gradually and slower, thus decreasing the slope of the corresponding Paris Law. It is finally concluded that adjusting the K constant has a noticeable influence in the Paris Law parameters, thus K can be chosen as a function of experimental results to closely match the experimental Paris Law curves using the proposed element.
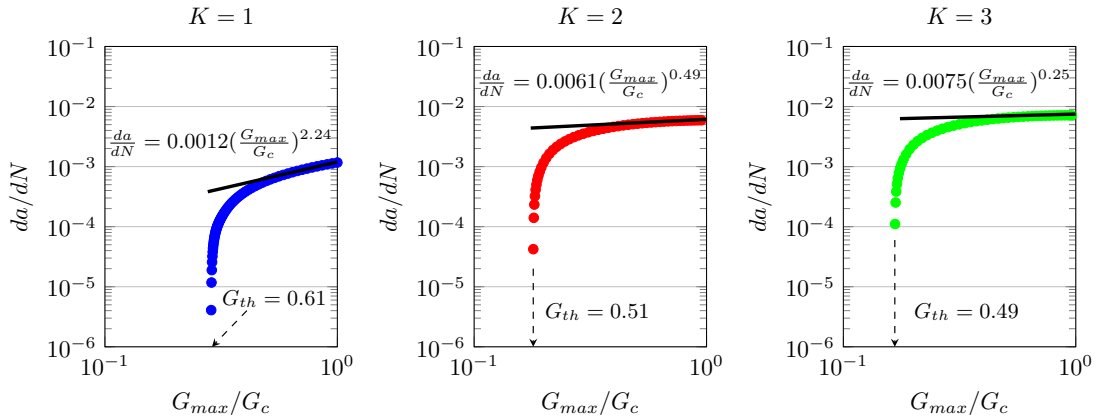
Figure 13: Numerical crack propagation curves for three cases: $K = 1$, $K = 2$ and $K = 3$.

4.3.2. Prediction of failure cycles

Prediction of the number of cycles is based on Equation 9, where an average da/dN value is selected as a function of the experimental Paris Law results for the specific condition [24], with Figure 14 presenting the comparison between experimental and numerical results for the same cases shown in Table 3.
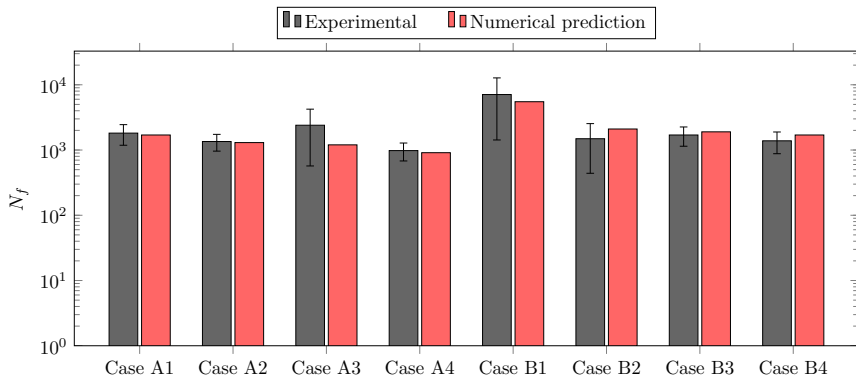

Figure 14: Comparison between experimental and numerical prediction for the number of cycles at failure for each of the studied adhesives and ageing conditions.

It is visible that for almost all cases the predicted number of cycles by the proposed approach is very near the experimental cycles. It is also visible that for all Nagase XNR 6852-1 cases, predicted values are below the experimental results (indicating that they may be trusted and are already affected by a slight safety factor), while SikaPower 4720 aged cases mostly show a predicted value sligthly above the experimental number of cycles, indicating that an extra safety factor should be used for the aged conditions of the least resistant adhesive. In any case, predicted values are in almost all cases very near the experimental average and well within the standard deviation due to experimental scatter, validating their accuracy.

5. Conclusions

A finite element based on the cohesive zone model formulation is proposed. The two main advantages of the element are the ability to model joints degraded by humidity, using degradation formulas based on experimental data that adapt the traction-separation law, and joints subjected to fatigue, using proposed relationships that both damage the bonded area gradually (inducing fatigue crack propagation within the numerical analysis) and predict the number of cycles at failure for the bonded joint. It is shown that the degradation relationships allow for numerical results in both static and fatigue conditions very close to the experimental tests. Additional advantages of this finite element include the implementation of several types of traction-separation laws, such as triangular with exponential softening, trapezoidal, exponential and the possibility to implement a fully customized CZM law. It is shown that the trapezoidal CZM is the one that results in curves and values closer to the experimental tests. Lastly, a MATLAB interface was developed which controls mesh generation for the requested geometry, creation of the input simulation files for ABAQUS$^{\circledR}$, monitoring of the simulation while running, and finally extraction and visualization of results, which has proved to be a useful tool in speeding up the numerical analysis process from start to finish. It is evident that the element shown here presents several advantages over conventional solutions, and will certainly be a valuable tool for any engineer modelling joints subjected to degradation and fatigue, as well as joints that have specific requirements concerning the type of traction-separation law best fit for the situation.

References

[1] L. F. M. da Silva, A. Öchsner, R. D. Adams, Handbook of adhesion technology, Springer Science & Business Media, 2011.

[2] L. F. M. da Silva, D. A. Dillard, B. Blackman, R. D. Adams, Testing adhesive joints: best practices, John Wiley & Sons, 2012.

[3] L. F. M. da Silva, R. D. Campilho, Advances in numerical modelling of adhesive joints, in: Advances in Numerical Modeling of Adhesive Joints, Springer, 2012, pp. 1–93.

[4] G. I. Barenblatt, The mathematical theory of equilibrium cracks in brittle fracture, Advances in applied mechanics 7 (1962) 55–129.

[5] A. Hillerborg, M. Modéer, P.-E. Petersson, Analysis of crack formation and crack growth in concrete by means of fracture mechanics and finite elements, Cement and concrete research 6 (6) (1976) 773–781.

[6] R. D. S. G. Campilho, M. Costa, G. Viana, L. F. M. da Silva, Parameter identification in cohesive zone modelling, Strength Prediction of Adhesively-Bonded Joints (2017) 161.

[7] C. C. R. G. de Sousa, R. D. S. G. Campilho, E. A. S. Marques, M. Costa, L. F. M. da Silva, Overview of different strength prediction techniques for single-lap bonded joints, Proceedings of the Institution of Mechanical Engineers, Part L: Journal of Materials: Design and Applications 231 (1-2) (2017) 210–223.

[8] K. Park, G. H. Paulino, Computational implementation of the ppr potential-based cohesive model in abaqus: educational perspective, Engineering fracture mechanics 93 (2012) 239–262.

[9] R. D. S. G. Campilho, M. D. Banea, J. A. B. P. Neto, L. F. M. da Silva, Modelling adhesive joints with cohesive zone models: effect of the cohesive law shape of the adhesive layer, International Journal of Adhesion and Adhesives 44 (2013) 48–56.

[10] C. D. M. Liljedahl, A. D. Crocombe, M. A. Wahab, I. A. Ashcroft, Modelling the environmental degradation of the interface in adhesively bonded joints using a cohesive zone approach, The Journal of Adhesion 82 (11) (2006) 1061–1089.

[11] K. B. Katnam, J. P. Sargent, A. D. Crocombe, H. Khoramishad, I. A. Ashcroft, Characterisation of moisture-dependent cohesive zone properties for adhesively bonded joints, Engineering Fracture Mechanics 77 (16) (2010) 3105–3119.

[12] A. Mubashar, I. A. Ashcroft, G. W. Critchlow, A. D. Crocombe, Modelling cyclic moisture uptake in an epoxy adhesive, The Journal of Adhesion 85 (10) (2009) 711–735.

[13] M. F. S. F. de Moura, J. P. M. Gonçalves, Cohesive zone model for high-cycle fatigue of adhesively bonded joints under mode i loading, International Journal of Solids and Structures 51 (5) (2014) 1123–1131.

[14] F. Moroni, A. Pirondi, A procedure for the simulation of fatigue crack growth in adhesively bonded joints based on the cohesive zone model and different mixed-mode propagation criteria, Engineering Fracture Mechanics 78 (8) (2011) 1808–1816.

[15] H. Khoramishad, A. D. Crocombe, K. B. Katnam, I. A. Ashcroft, Predicting fatigue damage in adhesively bonded joints using a cohesive zone model, International Journal of fatigue 32 (7) (2010) 1146–1158.

[16] A. Turon, J. Costa, P. P. Camanho, C. G. Dávila, Simulation of delamination in composites under high-cycle fatigue, Composites Part A: applied science and manufacturing 38 (11) (2007) 2270–2282.

[17] O. Nguyen, E. A. Repetto, M. Ortiz, R. A. Radovitzky, A cohesive model of fatigue crack growth, International Journal of Fracture 110 (4) (2001) 351–369.

[18] K. L. Roe, T. H. Siegmund, An irreversible cohesive zone model for interface fatigue crack growth simulation, Engineering fracture mechanics 70 (2) (2003) 209–232.

[19] D. Systèmes, ABAQUS 6.13-4 Documentation, Providence, RI, USA (2013).

[20] B. F. Sørensen, T. K. Jacobsen, Determination of cohesive laws by the j integral approach, Engineering fracture mechanics 70 (14) (2003) 1841–1858.

[21] W. K. Loh, A. D. Crocombe, M. M. A. Wahab, I. A. Ashcroft, Modelling anomalous moisture uptake, swelling and thermal characteristics of a rubber toughened epoxy adhesive, International journal of adhesion and adhesives 25 (1) (2005) 1–12.

[22] M. Costa, G. Viana, L. F. M. da Silva, R. D. S. G. Campilho, Effect of humidity on the mechanical properties of adhesively bonded aluminium joints, Proceedings of the Institution of Mechanical Engineers, Part L: Journal of Materials: Design and Applications (2016) 1464420716645263.

[23] M. Costa, G. Viana, L. F. M. da Silva, R. D. S. G. Campilho, Environmental effect on the fatigue degradation of adhesive joints: a review, The Journal of Adhesion 93 (1-2) (2017) 127–146.

[24] M. Costa, G. Viana, L. F. M. da Silva, R. D. S. G. Campilho, Effect of humidity on the fatigue behaviour of adhesively bonded aluminium joints, Latin American Journal of Solids and Structures 14 (1) (2017) 174–187.

[25] M. Costa, G. Viana, C. Canto, L. F. M. da Silva, M. D. Banea, F. Chaves, R. D. S. G. Campilho, A. A. Fernandes, Effect of the size reduction on the bulk tensile and double cantilever beam specimens used in cohesive zone models, Proceedings of the Institution of Mechanical Engineers, Part L: Journal of Materials: Design and Applications 230 (5) (2016) 968–982.